UNIVERSITY OF

SOUTHERN CALIFORNIA

GEOPHYSICAL LABORATORY

DEPARTMENT OF GEOLOGICAL SCIENCES

A SEISMICITY STUDY FOR PORTIONS OF THE LOS ANGELES BASIN, SANTA MONICA BASIN, AND SANTA MONICA MOUNTAINS, CALIFORNIA

By

James Alexander Buika† and Ta-liang Teng

Technical Report No. 79-9

A Report on Research Project Supported
by the U.S. Geological Survey

Los Angeles, California

September, 1979

†Now at Texaco, Inc., 3350 Wilshire Blvd., Los Angeles, Ca. 90010

EARTHQUAKE HAZARD RESEARCH IN THE LOS ANGELES BASIN AND ITS OFFSHORE AREA

Ta-liang Teng, James Alexander Buika
Thomas L. Henyey, John K. McRaney
Kenneth E. Piper and Richard A. Strelitz

Department of Geological Sciences
University of Southern California
Los Angeles, California 90007

USGS CONTRACT NO. 14-08-0001-16704
Supported by the EARTHQUAKE HAZARDS REDUCTION PROGRAM

OPEN-FILE NO.81-295

TABLE OF CONTENTS

Page

LIST OF ILLUSTRATIONS

LIST OF TABLES

ABSTRACT

Data from seismic station networks in southern California have been collated to relocate 423 earthquakes occurring between January 1, 1973 and December 31, 1976, within the Los Angeles basin, the Santa Monica basin, and the Santa Monica Mountains. From this data set, the seismicity pattern, fault-plane solutions, and compressional stress vectors have been derived and are compared with the most recent known fault displacements in order to determine the casuative fault for some of these earthquakes, the preferred orientation of fault planes and probable focal mechanisms.

The Los Angeles basin region is presently responding to a regional northeast-southwest-oriented compressional stress regime. Earthquakes on the northwest-trending faults of the Newport-Inglewood, Whittier, and Palos Verdes Hills fault zones describe fault-plane solutions dominated by reverse-slip mechanisms. Right-lateral strike-slip is often a secondary component of motion. Focal mechanisms support the concept of convergent right-lateral wrench faulting occurring in the Los Angeles basin.

Seismic activity is concentrated in the Los Angeles and Santa Monica basins rather than within the Santa Monica Mountain block. Most activity appears to terminate at the Santa Monica fault system rather than continue to the north, along the projected trend of the northwest-trending Newport-Inglewood and Palos Verdes Hills fault zones. The western portion of the east-northeast-trending Santa Monica fault system was probably the causative fault for the magnitude 5.9 Point Mugu earthquake of February 21, 1973. Besides reverse faulting, normal faulting appears to be associated with the western portion of the Santa Monica fault system. The eastern portion of the Santa Monica fault, between Hollywood and Glendale has also been the locus for a cluster of microseismicity. Reverse faulting has dominated this eastern cluster. A minor component of left-lateral strike-slip displacement is possible in several fault-plane solutions along the Santa Monica fault system.

INTRODUCTION

General Statement

A seismicity study has been conducted for portions of the Los Angeles basin, the Santa Monica basin, and the Santa Monica Mountains (Figure 1). Bathymetric features for the offshore portion of the study area are shown in Figure 2. The Los Angeles basin, Santa Monica basin, and Santa Monica Mountains are tectonically active structures that have formed at the juxtaposition of three physiographic provinces--the Transverse Ranges, Peninsular Ranges, and California Continental Borderland (Figure 1). These three provinces have a common point at the intersection of the Newport-Inglewood uplift and the Santa Monica fault. The east-west-trending Transverse Ranges, represented at its southern boundary by the Santa Monica Mountains, transects the northwest-trending structural grain associated with the Peninsular Ranges to the south, the Coast Ranges to the north and the San Andreas fault system. Consequently, a complex system of faults has

Figure 1. Physiographic provinces of southern California. Rectangle outlines study area. Geographical boundaries are 118°00'W to 119°15'W longitude and 33°45'N to 34°15'N latitude. The intersection of the Santa Monica fault and the Newport-Inglewood fault (dashed line) is shown. After Yerkes and others (1965) and Junger and Wagner (1977).

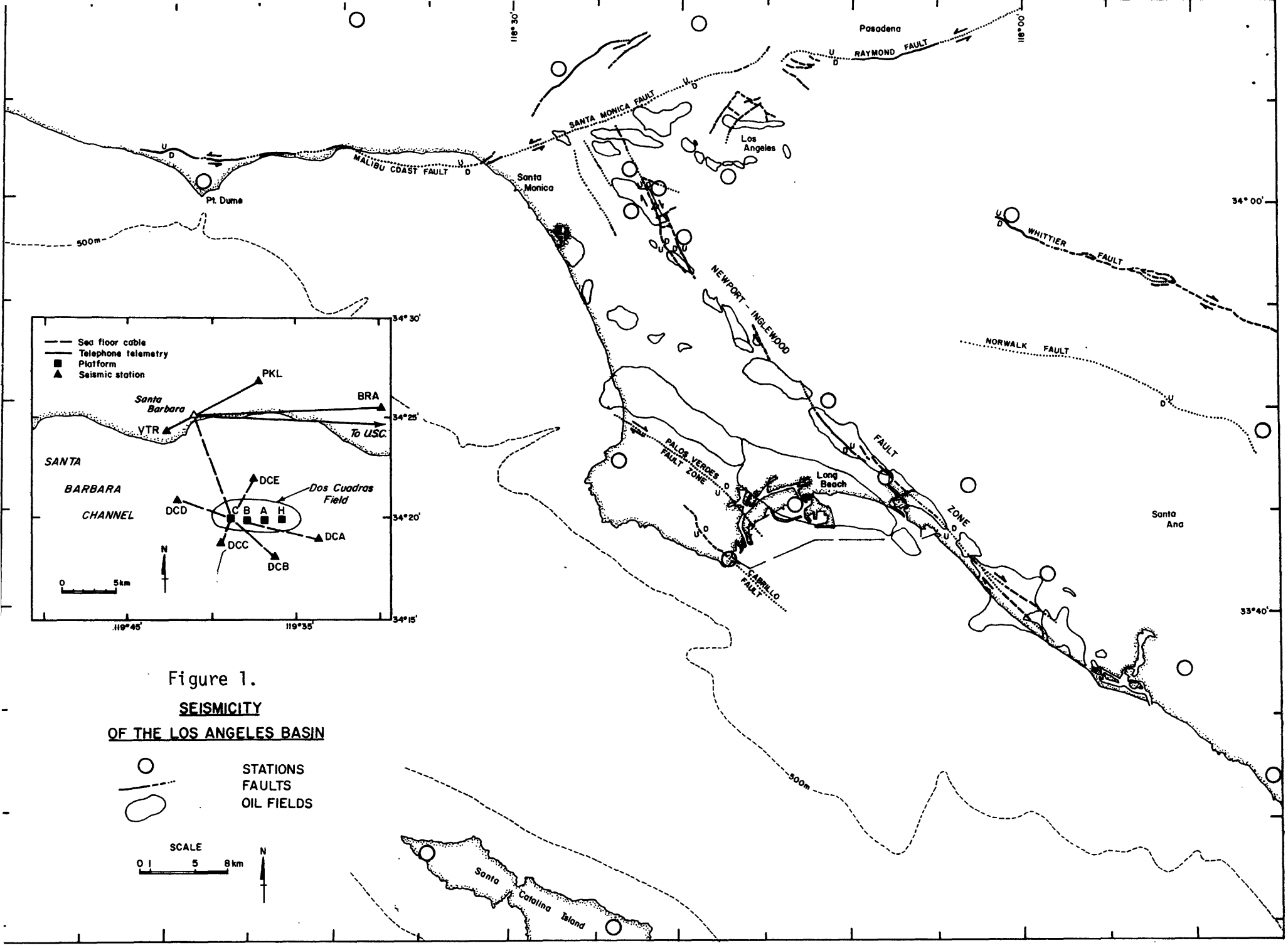

Figure 1.

SEISMICITY

OF THE LOS ANGELES BASIN

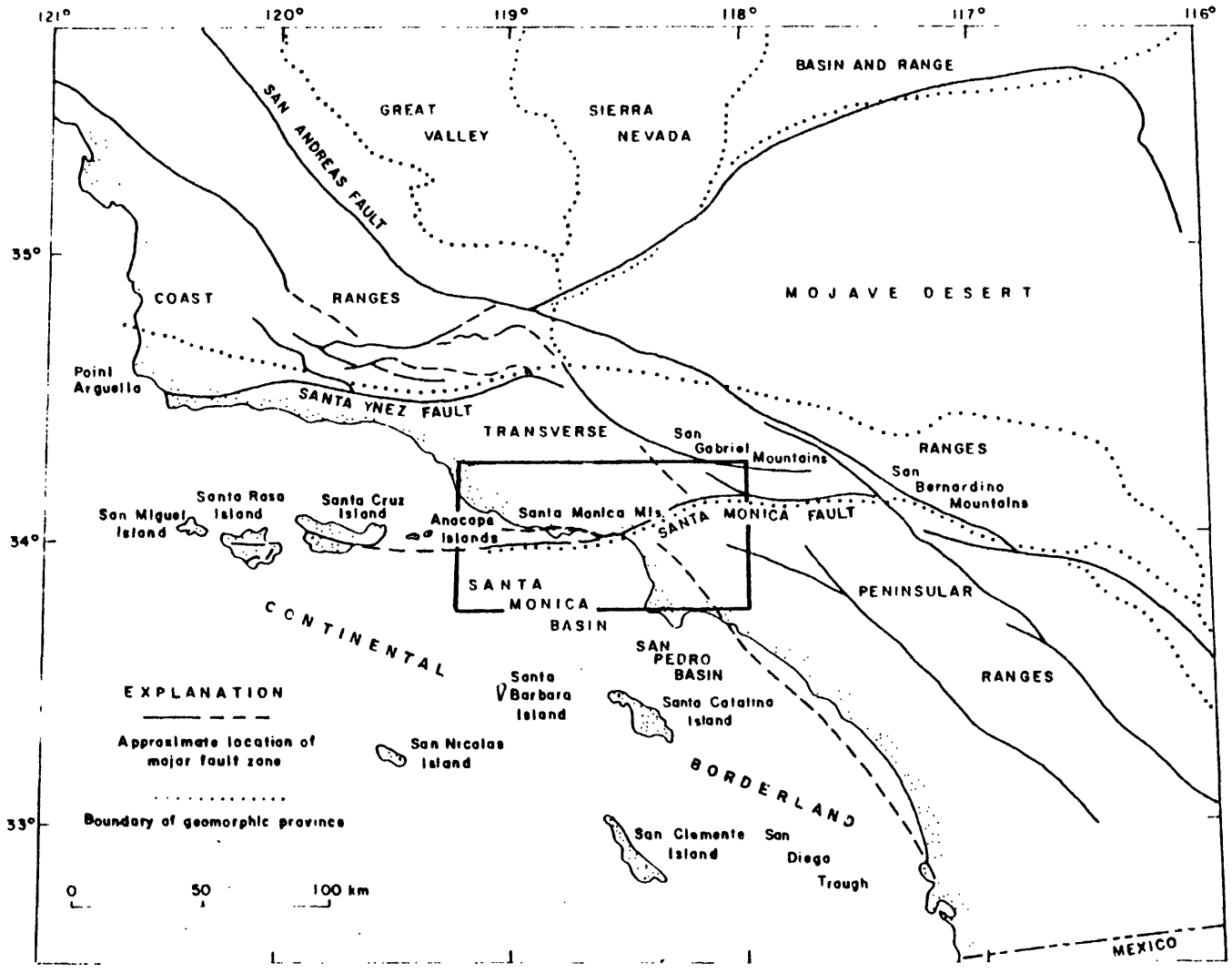
121°
120°
119°
118°
117°
116°
35°
34°
33°
SAN ANDREAS FAULT
GREAT VALLEY
SIERRA NEVADA
BASIN AND RANGE
COAST RANGES
MOJAVE DESERT
Point Arguello
SANTA YNEZ FAULT
TRANSVERSE RANGES
San Gabriel Mountains
San Bernardino Mountains
San Miguel Island
Santa Rosa Island
Santa Cruz Island
Anacapa Islands
Santa Monica Mts.
SANTA MONICA FAULT
SANTA MONICA BASIN
PENINSULAR RANGES
CONTINENTAL BORDERLAND
SAN PEDRO BASIN
Santa Barbara Island
Santa Catalina Island
San Nicolas Island
San Clemente Island
San Diego Trough
EXPLANATION
Approximate location of major fault zone
Boundary of geomorphic province
0
50
100 km
MEXICO

Figure 2. Bathymetric map of the Santa Monica basin and San Pedro basin. After Junger and Wagner (1977).

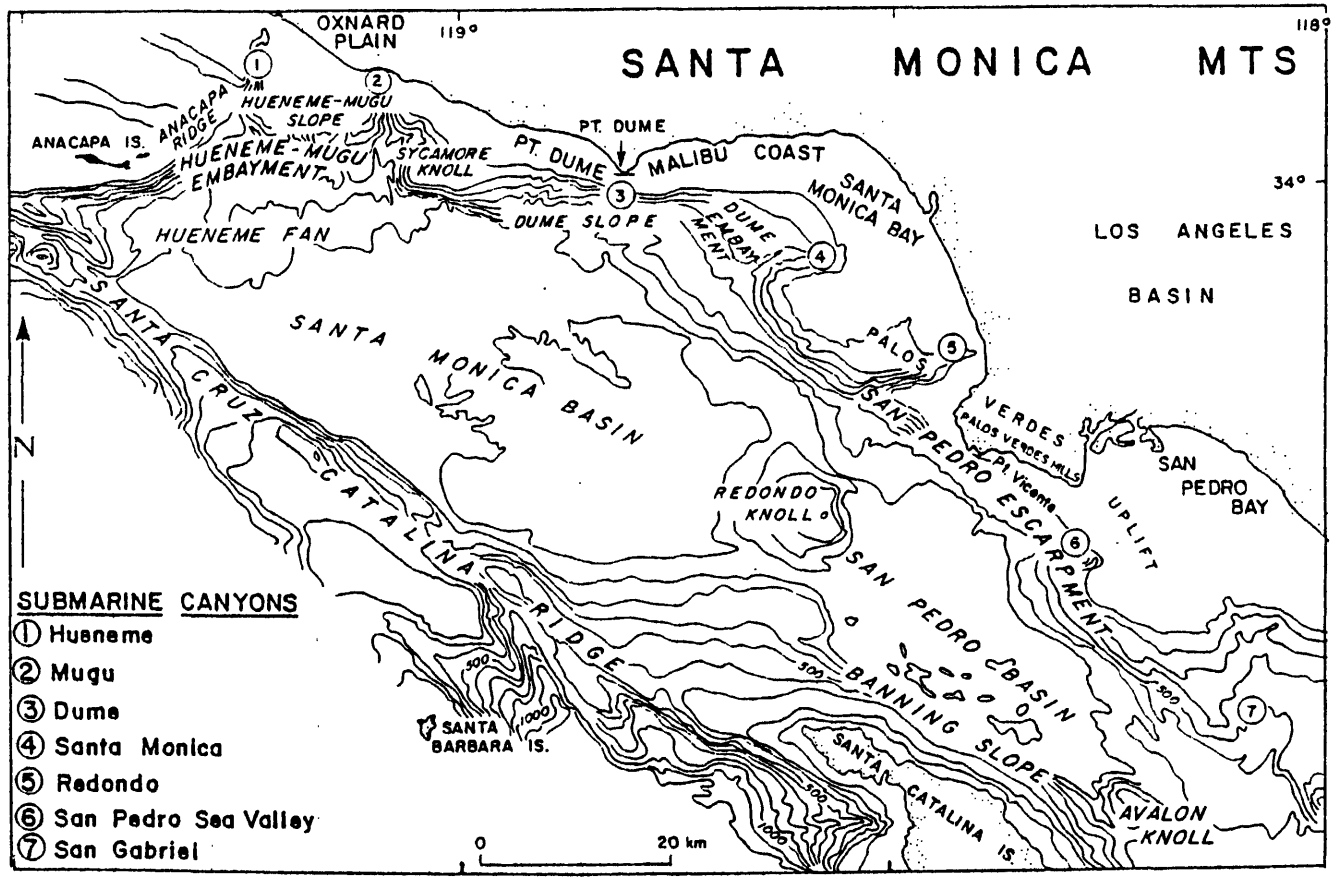
OXNARD PLAIN
119°
118°
SANTA MONICA MTS
ANACAPA IS.
ANACAPA RIDGE
HUENEME-MUGU SLOPE
HUENEME-MUGU EMBAYMENT
SYCAMORE KNOLL
PT. DUME
MALIBU COAST
SANTA MONICA BAY
34°
LOS ANGELES BASIN
HUENEME FAN
DUME SLOPE
DUME EMBAYMENT
SANTA MONICA BASIN
SANTA CRUZ
CATALINA RIDGE
PALOS VERDES
PALOS VERDES HILLS
Pt. Vicente
SAN PEDRO ESCARPMENT
SAN PEDRO BAY
UPLIFT
REDONDO KNOLL
SAN PEDRO BASIN
BANNING SLOPE
SANTA BARBARA IS.
SANTA CATALINA IS.
AVALON KNOLL
N
SUBMARINE CANYONS
① Hueneme
② Mugu
③ Dume
④ Santa Monica
⑤ Redondo
⑥ San Pedro Sea Valley
⑦ San Gabriel
0
20 km

been activated within the wedge of continental landmass lying west of the San Andreas fault in response to a regional NNE-SSW compressional stress regime.

All recorded earthquakes occurring from 1973 through 1976 have been compiled from data received at seismic stations from all seismograph networks operating in southern California and have been located using Lee's and Lahr's (1975) computer program. Epicentral patterns, fault-plane solutions, and compressional stress vectors have been derived from the microearthquake data to determine the causative faults for some earthquakes, the preferred orientations of fault planes, and probably focal mechanisms. These results are discussed in terms of fault displacements and fault geometries.

The objective of this study is to add to the understanding of the contemporary tectonic environment within the Los Angeles basin region by combining known geologic and geomorphic data with recently derived seismic data for this same region. If seismic activity can be associated with a fault or fault zone, then it confirms the active status of that fault. From this relationship, the seismic record can be studied to understand the present tectonic regime. Future earthquake rupture is assumed to occur along pre-existing faults, with the greatest probability of renewed movement on active and potentially active faults, as defined below (Ziony and others, 1973).

Just as the seismic record represents the active tectonic regime, the geologic record represents the past tectonic environment. Fault displacements, measured in the field from geologic relationships, assist in identifying recency of movement along faults. This information can be used to extend the historic and instrumental seismicity records. Since surface rupture can be roughly correlated with a magnitude 6 or greater earthquake (Allen and others, 1965), the youngest preserved stratigraphic or geomorphic evidence for faulting can be used to demonstrate and bracket the time of the latest significant seismic activity. This study compares known Quaternary faulting in the Los Angeles basin region with the 1973-1976 earthquake data set to access similarities and dissimilarities bewteen the present seismic record and the Quaternary geologic record. Geologic and geomorphic evidence, gathered from various published field studies, has been used to document the most recent displacements on known faults in the Los Angeles basin region.

Figure 3 is a fault map for the study area displaying only known or inferred fault displacement of Quaternary to present age. The map was compiled from several sources; onland faults have been adopted from Ziony and others' (1974) comprehensive compilation of recency of fault movements along the southern California coastal area; offshore faults have been compiled from recently interpreted

Figure 3. Fault map showing all faults displaced since at least Quaternary time.

Legend

solid line (or star) - Holocene displacement (<11,000 y.)

long dashed line - Late Quaternary displacement (11,000 - 500,000 y.)

short dashed line - Quaternary displacement (500,000 - 2,000,000 y.)

dotted line (P) - Pliocene (>2,000,000)

star - historic earthquake

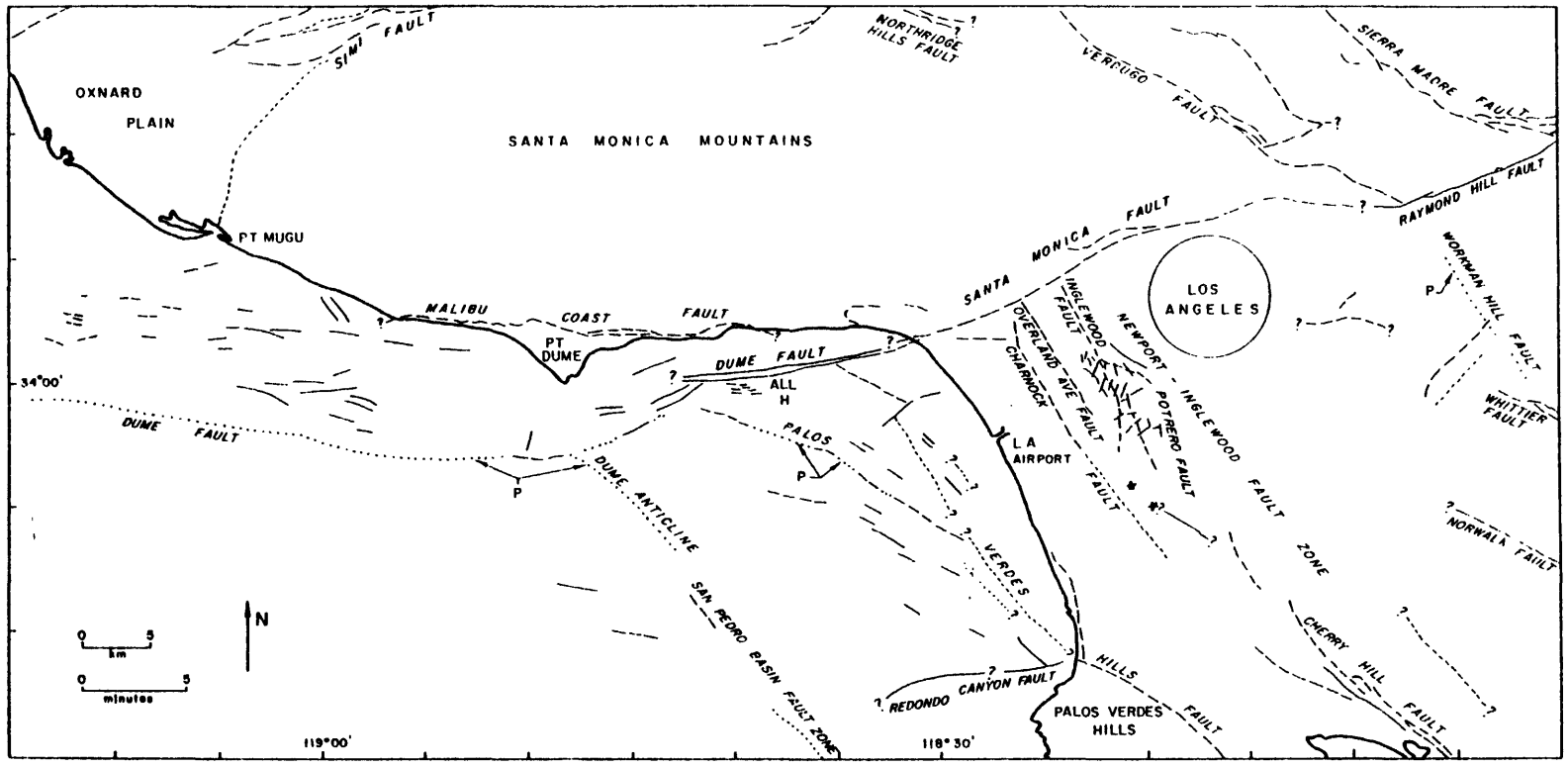
OXNARD
PLAIN
SIMI FAULT
SANTA MONICA MOUNTAINS
NORTHRIDGE HILLS FAULT
VERDUGO FAULT
SIERRA MADRE FAULT
RAYMOND HILL FAULT
PT MUGU
SANTA MONICA FAULT
LOS ANGELES
WORKMAN HILL FAULT
MALIBU COAST FAULT
PT DUME
DUME FAULT
INGLEWOOD FAULT
OVERLAND AVE FAULT
CHARNOCK FAULT
NEWPORT - INGLEWOOD FAULT ZONE
WHITTIER FAULT
34°00'
ALL H
PALOS
LA AIRPORT
DUME FAULT
DUME ANTICLINE
VERDES
NORWALK FAULT
SAN PEDRO BASIN FAULT ZONE
CHERRY HILL FAULT
REDONDO CANYON FAULT
HILLS FAULT
PALOS VERDES HILLS
N
0 5 km
0 5 minutes
119°00'
118°30'

sub-bottom acoustic-reflection profiles by Vedder and others (1974), Green and others (1975), Junger and Wagner (1977), and Nardin and Henyey (1978).

Following Ziony and others (1974), faults demonstrating displacement during the Holocene time (approximately 11,000 y. B.P. to present) have been classified as "active" faults; faults demonstrating displacement since at least Quaternary time (approximately 2-3 m.y. B.P. to present) have been classified as "potentially active" (Figure 4). These criteria have been followed in constructing the active fault map for the study area (Figure 3). The fault classification (Figure 4), used to compose Figure 3, includes four time subdivisions:

(1) Historic - to approximately 200 years before present;

(2) Holocene - to approximately 11,000 years before present;

(3) Late Quaternary - to approximately 500,000 years before present;

(4) Quaternary - to approximately 2-3,00,000 years before present.

Subdivisions (1) and (2) represent active faults while subdivisions (3) and (4) represent potentially active faults (Figure 3).

The important Point Mugu earthquake of February 21, 1973 and its aftershock sequence have not been analyzed

Figure 4. Geologic time scale used to classify fault activity, adopted from Ziony and others, 1974. After Byer (1975).

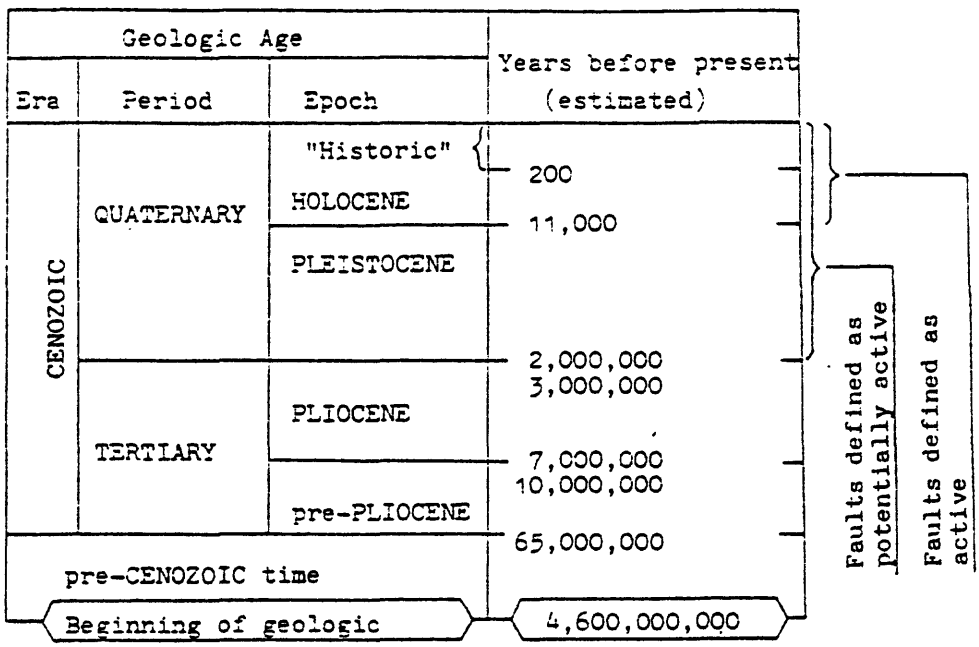
Geologic Age
Era
Period
Epoch
Years before present (estimated)
CENOZOIC
"Historic"
200
QUATERNARY
HOLOCENE
11,000
PLEISTOCENE
2,000,000
3,000,000
TERTIARY
PLIOCENE
7,000,000
10,000,000
pre-PLIOCENE
65,000,000
pre-CENOZOIC time
Beginning of geologic
4,600,000,000
Faults defined as potentially active
Faults defined as active

but are included here to complete a comprehensive earthquake catalog for the study area from 1973-1976.

The Study Area: Major Faults

The study area is delineated by deep-seated, steeply-dipping, and seismically-active faults. Figure 3 shows the portions of these fault traces which have moved during Quaternary time, based on geologic and geomorphic evidence, discussed later.

The Los Angeles physiographic basin is 80 kilometers long and 32 kilometers wide, located along the coast and bounded to the north by the Santa Monica fault system (Figure 3) and to the northeast and east by the Whittier fault zone (Figure 1). The basin's southern and southeastern boundaries are marked by the San Joaquin Hills and the Santa Ana Mountains.

The Santa Monica fault zone is an active north-dipping high-angle reverse fault across which the Santa Monica Mountain structural block has been thrust southward over the alluvial fill of the Los Angeles basin since Pliocene time (Yerkes and others, 1965). This fault continues to the east as the Raymond Hill fault and to the west as the Malibu Coast fault and the offshore Dume fault (Figure 3). Geologic evidence for latest movements

across these fault extensions is north-over-south high-angle reverse displacement.

The only disruption along the east-northeast trending Santa Monica fault zone exists in the Elysian Park-Puente Hills area where sgemented faults comprising the northwestward extension of the Whittier fault zone break the continuity between the Santa Monica fault and the Raymond Hill fault (Figure 5). Since the Los Angeles River flood plain and alluvial deposits have obscured the fault traces at the surface, the crosscutting relationship between these two fault systems is presently subject to debate (Lamar, 1970; 1975).

The north-northwest-trending Whittier fault zone defines the eastern boundary of the Los Angeles basin and is most significantly represented in this study area by its northwesterly extension which intersects the Santa Monica fault zone. It is a continuous fault trace along the southwestern front of the Puente Hills where it has offset Miocene strata up to 4250 meters along a reverse fault dipping 65^{o} to 75^{o} NE (Yerkes and others, 1965).

The Newport-Inglewood fault zone interrupts the otherwise slight seaward grade of the Los Angeles basin and is expressed as a series of low hills extending from Beverly Hills southeast to Huntington Beach. The low hills and mesas within the otherwise expressionless alluviated lowlands are a series of en echelon compres-

Figure 5. Geologic map detailing proposed connections between the Hollywood fault (Santa Monica fault) and the Raymond Hill fault. Generalized from Woodford and others (1954) and Lamar (1970). After Lamar (1975).

Q: alluvium; Tf: Fernando Formation Tp: Puente Formation; Tt: Topanga Formation; Tv: Volcanic rock; Kp: Plutonic + metamorphic rock.

trace 2: Ziony and others (1974)
trace 3: Woodford and others (1954)

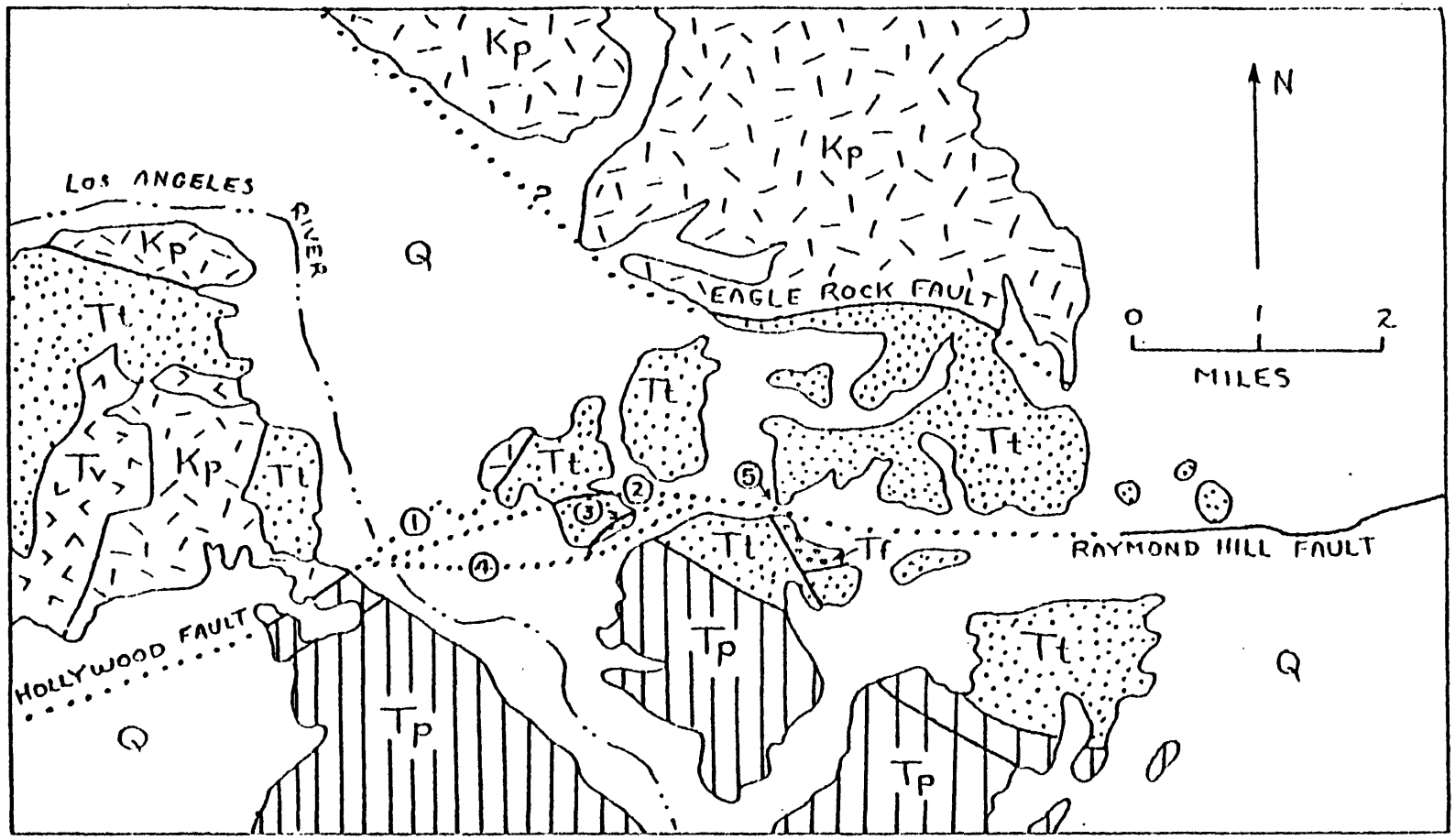
Kp
Kp
N
LOS ANGELES
RIVER
Q
EAGLE ROCK FAULT
0
1
2
MILES
Kp
Tt
Tt
Tv
Kp
Tt
Tt
Tt
Tt
RAYMOND HILL FAULT
HOLLYWOOD FAULT
Tp
Tp
Tp
Tt
Q
Q

sional anticlines which are the result of a deep-seated right-lateral wrench fault process (Wilcox and others, 1973; Harding, 1973).

The Palos Verdes Hills fault (Figure 3) subparallels the Newport-Inglewood fault zone, is seismically active, and displays a deformational mechanism of high-angle reverse faulting. On the Palos Verdes peninsula and to the south, in the San Pedro Bay, the fault dips steeply to the southwest (Woodring and others, 1946; Fischer and others, 1977). The northwesterly trace of the Palos Verdes Hills fault within the Santa Monica Bay, interpreted from subbottom acoustic seismic profiles, terminates against the east-trending Dume fault (Figure 3), where only insignificant amounts of strike-slip displacment are apparent (Greene and others, 1976; Junger and Wagner, 1977; Nardin and Henyey, 1978). Vertical separation appears to terminate at the top of the lower Pliocene strata (Junger, 1976; Nardin and Henyey, 1978).

Southern California Seismic Network

In 46 years, since its inception in 1932, the Southern California Seismic Network has grown to approximately 120 short-period and long-period seismometers. Offshore seismic coverage has been aided by the placement of seismometers on the Channel Islands. Figure 6 shows the

Figure 6. Seismic stations monitored and maintained by the CIT and USGS, as of January 1, 1977. The USGS maintains the stations outlined in the southeastern corner of California.

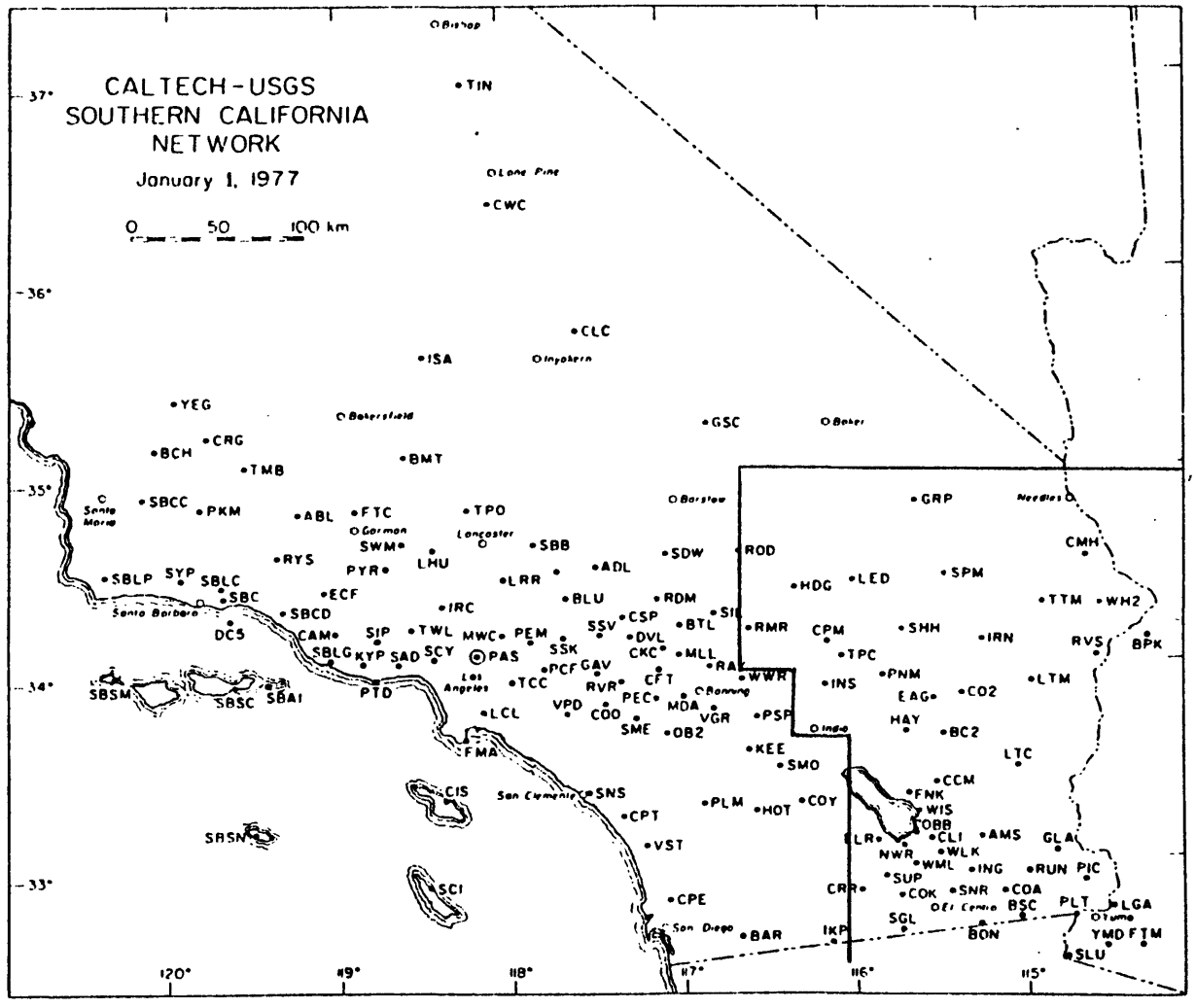
CALTECH-USGS
SOUTHERN CALIFORNIA
NETWORK
January 1, 1977
0 50 100 km
37°
36°
35°
34°
33°
120°
119°
118°
117°
116°
115°
TIN
CWC
CLC
ISA
YEG
CRG
BCH
TMB
BMT
GSC
SBCC
PKM
ABL
FTC
TPO
SWM
LHU
SBB
ADL
SDW
ROD
GRP
CMH
RYS
PYR
LRR
HDG
LED
SPM
SBLP
SYP
SBLC
SBC
ECF
BLU
RDM
TTM
WH2
SBCD
IRC
DC5
CAM
SIP
TWL
MWC
PEM
SSV
CSP
BTL
RMR
CPM
SHH
IRN
RVS
BPK
SBLG
KYP
SAD
SCY
PAS
SSK
DVL
CKC
MLL
RA
TPC
PCF
GAV
WWR
INS
PNM
LTM
SBSM
SBSC
SBAI
PTD
TCC
RVR
CFT
EAG
CO2
LCL
VPD
COO
PEC
MDA
VGR
PSP
HAY
BC2
SME
OB2
KEE
SMO
LTC
FMA
CCM
CIS
SNS
PLM
HOT
COY
FNK
WIS
CPT
OBB
SBSN
VST
CLI
AMS
GLA
ELR
NWR
WLK
WML
ING
RUN
PIC
SUP
SCI
CRR
COK
SNR
COA
CPE
BSC
PLT
LGA
SGL
BAR
IKP
BON
YMD
FTM
SLU

spatial distribution of seismic stations presently monitored by the seismological laboratories at the California Institute of Technology (CIT) and the United States Geological Survey (USGS).

This regional coverage has been augmented, beginning in 1971, by specialty networks set up in the Los Angeles basin by the University of Southern California (USC). In addition, a temporary network to locate and study the aftershocks of the 1973 Point Mugu earthquake was jointly deployed by the USGS and CIT at the western edge of this study area during the months of February, March, and April, following the main shock of February 21, 1973.

Since 1972, USC has established two local seismic networks along the Newport-Inglewood fault zone in the western Los Angeles basin. Stations within the Baldwin Hills Seismic Network (BHSN) and the Long Beach Seismic Network (LBSN) are located in Figure 7 and are listed in Table 1. Both networks serve to study the microearthquake activity associated with the tectonically active Newport-Inglewood fault zone, which is currently subject to substantial oil removal and fluid injection programs. Also shown in Figure 7 and Table 1 are stations located along the periphery of the Los Angeles basin, telemetered to both USC and CIT. This recording overlap provides a cross check on the timing and location of events occurring within the Los Angeles basin. Common

Figure 7. Location map for the Baldwin Hills Seismic Network and the Long Beach Seismic Network. See Table 1 for station coordinates. After Teng and Henyey (1973).

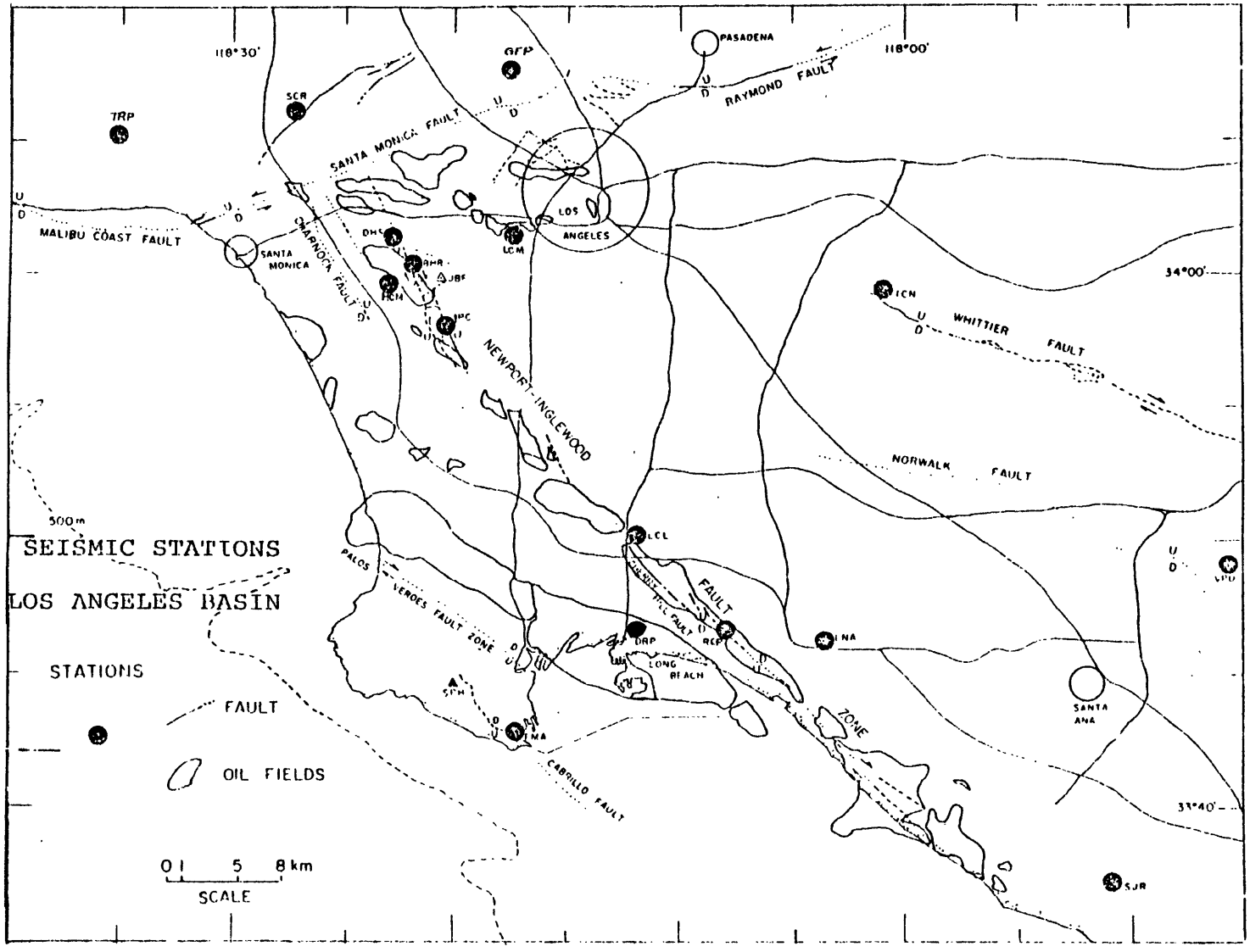
SEISMIC STATIONS
LOS ANGELES BASIN
STATIONS
FAULT
OIL FIELDS
0 1 5 8 km
SCALE
118°30'
118°00'
34°00'
33°40'
PASADENA
RAYMOND FAULT
SANTA MONICA FAULT
MALIBU COAST FAULT
SANTA MONICA
CHARNOCK FAULT
LOS ANGELES
NEWPORT-INGLEWOOD
WHITTIER FAULT
NORWALK FAULT
PALOS VERDES FAULT ZONE
LONG BEACH
SANTA ANA
CABRILLO FAULT
ZONE
TRP
SCR
GFP
DHS
BHR
UBF
HCM
IPC
LCM
ICN
LCL
DRP
RCF
LNA
SPH
SJR
VPU

TABLE 1.

Seismic Network in the Los Angeles basin area.

SEISMIC NETWORK IN THE LOS ANGELES BASIN AREA

Station Code	Latitude, N	Longitude W	Remarks
BHR	34°00.51'	118°21.72'	
HCM	33°59.64'	118°22.98'	
IPC	33°58.24'	118°20.07'	
TPR	34°05.33'	118°35.20'	Began July, 1975
JBF	33°59.58'	118°20.68'	Term. July, 1975
GFP	34°07.76'	118°18.59'	Began Apr., 1975
LCM	34°01.07'	118°17.22'	
DHS	34°01.05'	118°23.13'	Three Components
DHT	33°45.06'	118°13.25'	
DRP	33°46.72'	118°12.27'	
LCL	33°50.00'	118°11.55'	
FMA	33°42.75'	118°17.12'	
LNA	33°47.35'	118°03.27'	
RCP	33°46.66'	118°08.00'	
SCR[a]	34°06.37'	118°27.25'	
SJR[a]	33°37.20'	117°50.70'	
VPD[a]	33°48.90'	117°45.70'	
TCN[a]	33°59.67'	118°00.77'	
CIS[a]	33°24.40'	118°24.40'	
MWC	34°13.40'	118°03.05'	
PAS	34°08.90'	118°10.30'	

After Teng and others (1975).

Superscript a designates stations monitored at both USC and CIT.

seismic records from these overlapping networks permit identification and elimination of nearly all errors involved in the reading, measuring, and recording of daily local seismic events from 1973 to 1976. The cross-over of seismic data between the networks in the Los Angeles basin permits a double check on station polarities, as they are determined from nearby controlled quarry blasts originating in the Mojave Desert.

The BHSN and the LBSN are small-aperture seismic-station clusters employing short-period vertical seismometers (T = 1.0 sec), specifically designed to monitor local microearthquake activity. By combining these local clusters with the peripheral Los Angeles basin seismic stations and the regional CIT-USGS seismic stations, out to a 120 kilometer radius from the Los Angeles basin, every event in the study area with a magnitude, $M_L \gtrsim 2.0$ has been recorded and relocated with improved precision.

Appendix A includes all the stations used in this study. Station installation dates have been variable and many stations have become operable only recently. Enough changes have occurred locally and regionally since 1973 to warrant revising the master list of stations for the 1976 earthquake data set. Table 6 (Appendix A) is a list of stations from which data has been taken to relocate the events occurring from 1973 through 1975;

Table 7 (Appendix A) is a revised master list of stations used to relocate only 1976 events.

Crustal Velocity Model

Since the development of a specific crustal velocity model for the study area is beyond the scope of this project, Healy's (1963) model has been chosen to approximate the crustal velocity structure for the general western Los Angeles basin and the Santa Monica Mountain region (Table 2).

Table 2

Crustal Velocity Structure

Layer	Depth (Km)	P Velocity (Km/sec)
1	0.0 to 2.6	3.0
2	2.6 to 16.7	6.1
3	17.6 to 26.1	7.0
4	below 26.1	8.2

S-wave velocity is assumed to be 0.56 times the P-wave velocity.

Six studies have proposed different crustal velocity structures for southern California. Four models are applicable to travel paths within this study area; the other two velocity structures have been derived for

the Mojave Desert region to the east. Figure 8 shows the basis for the six crustal velocity models for southern California.

The models are compared in Figure 9. All consider the crust to be composed of three layers overlying a uniform half-space (upper mantle). All distinguish a low-velocity surface layer which varies from 3.0 km/sec along the southern California coast to 5.5 km/sec within the Transverse Ranges and Mojave Desert. Each study has established a distinct upper crustal layer, with a velocity of approximately 6.2 km/sec and an intermediate crustal-velocity layer of 6.8-7.0 km/sec, with a low of 6.2 km/sec in the Los Angeles basin (Teng and Henyey; 1973) and a high of 7.66 in the Mojave Desert (Press; 1960). The Pn velocity is typically 8.1 to 8.2 km/sec, at a depth of approximately 30 to 35 km. Hadley and Kanamori (1977) have discovered an anomalously high velocity of 8.3 km/sec for the upper mantle, underlying the Transverse Ranges.

The Los Angeles basin crustal velocity model proposed by Teng and Henyey (1973; Figure 9) is a deriviative of Healy's model for a portion of the Los Angeles basin and thus should not necessarily be extrapolated to a more regional seismic station data base.

Stierman's and Ellsworth's (1976) velocity model, derived from artificial explosion travel-time data for

Figure 8. Plan view of areal extent for each crustal velocity survey conducted in southern California. Shaded area represents study area. Base map after Hileman and others (1973).

H-H' = Healy (1963); R-H = Roller and Healy (1963)

T-T' = Transverse Ranges (Hadley and Kanamori, 1977)

K-K = Mojave Desert (Kanamori and Hadley, 1975)

P-P = Mojave Desert (Press, 1960)

M = Point Mugu (Stierman and Ellsworth, 1976)

L = Los Angeles Basin (Teng and Henyey, 1973)

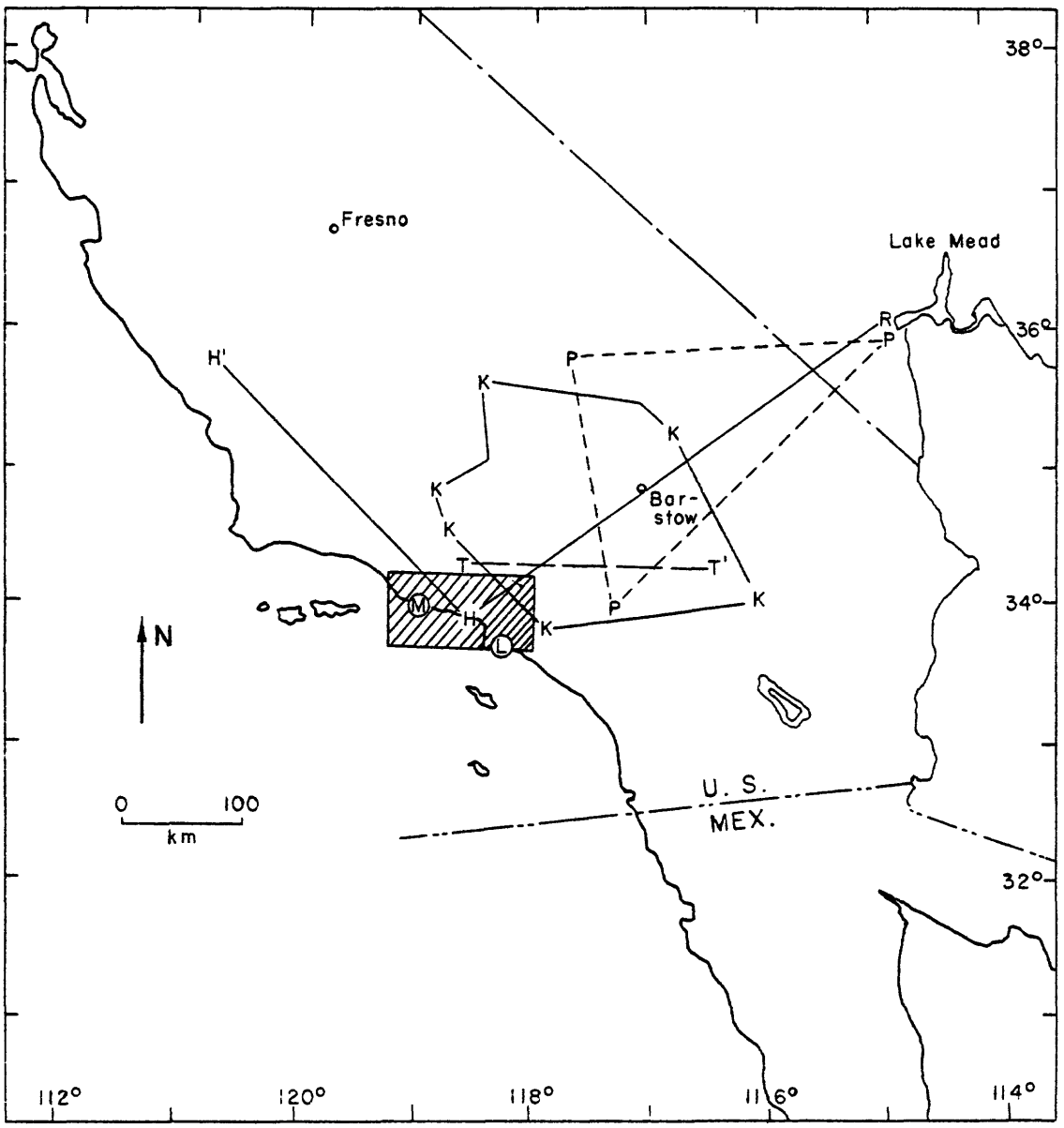
38°
Fresno
Lake Mead
36°
H'
P
R
P
K
K
K
K
Bar-
stow
T
T'
P
K
K
M
H
L
34°
N
0
100
km
U. S.
MEX.
32°
112°
120°
118°
116°
114°

Figure 9. Cross section of the six crustal velocity models proposed for various portions of southern California. Depths and interval thicknesses are in kilometers.

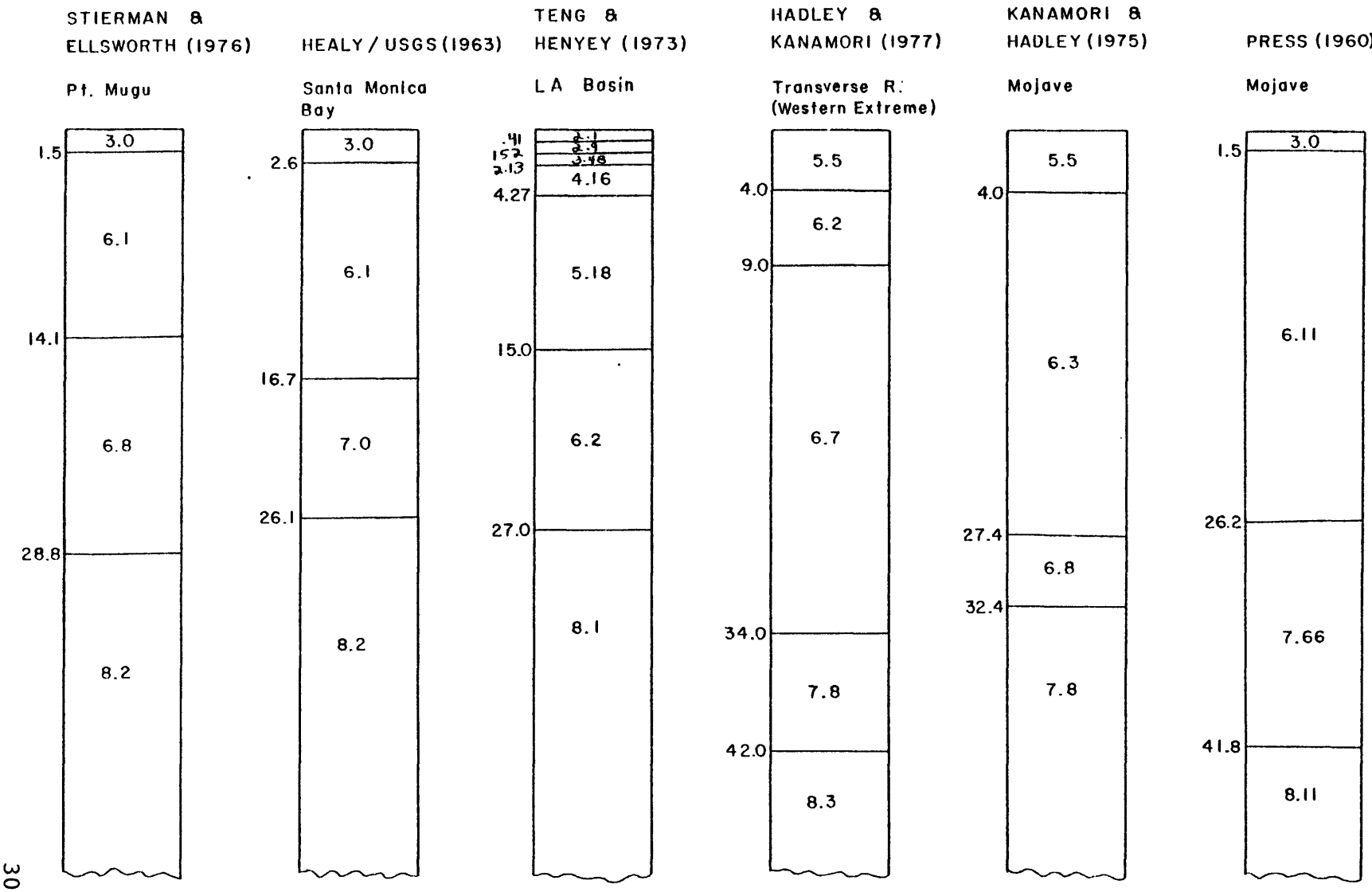
STIERMAN & ELLSWORTH (1976)
Pt. Mugu
1.5
3.0
6.1
14.1
6.8
28.8
8.2
HEALY / USGS (1963)
Santa Monica Bay
2.6
3.0
6.1
16.7
7.0
26.1
8.2
TENG & HENYEY (1973)
LA Basin
.41
1.52
2.13
4.16
4.27
5.18
15.0
6.2
27.0
8.1
HADLEY & KANAMORI (1977)
Transverse R. (Western Extreme)
4.0
5.5
6.2
9.0
6.7
34.0
7.8
42.0
8.3
KANAMORI & HADLEY (1975)
Mojave
4.0
5.5
6.3
27.4
6.8
32.4
7.8
PRESS (1960)
Mojave
1.5
3.0
6.11
26.2
7.66
41.8
8.11

the 1973 Point Mugu earthquake study, should also be discounted as a regional crustal structure due to its localized nature. However, their travel-time plot for the upper crustal region along the coastline supports Healy's model (Figure 9).

Kanamori and Hadley's (1975) Mojave Desert region crustal velocity model is presently used to relocate events within the CIT seismic network. This model assigns a 7.8 km/sec value to the upper mantle. This low value is typical of the Basin and Range structure to the east (Herrin and Taggart, 1962; Cleary and Hales, 1966; Archambeau and others 1969). The existence of such a low Pn velocity for coastal California has not been substantiated elsewhere in the literature. Healy's value of 8.2 km/sec is in closer accordance with Press' (1960) value of 8.1 km/sec and Hadley and Kanamori's (1977) Pn velocity of 8.3 km/sec for the Transverse Ranges. Since both Mojave models (Press, 1960; Kanamori and Hadley, 1975) do not include data within this study area, neither can be as dependable as local models for the Los Angeles basin.

Hadley and Kanamori's (1977) crustal velocity model for the Transverse Ranges describes a locally anomalous velocity pehnomenon occurring strictly beneath this east-west trending structure. Its regional applicability

is doubtful and also should be discounted in terms of a local model.

For a crustal model to be useful it must remain sensitive to the velocity structure within the earthquake focal region while closely approximating travel times at distant seismic stations. Healy's model meets these criteria. Independent crustal velocity studies in coastal southern California, by Teng and Henyey (1973) and Stierman and Ellsworth (1976), have corroborated Healy's choice of surface layer (3.0 km/sec) and upper crustal (6.1 km/sec) velocities as representative of the study area. Healy assigns velocities of 7.0 km/sec to the intermediate crustal layer and 8.2 km/sec to the upper mantle. In light of all six models proposed for southern California (Figure 8), Healy's velocities represent regional averages.

Station Delays

Healy's model has been generalized herein to represent the local velocity structure for the study area as well as the regional velocity structure for southern California. In addition, station delays have been computed and assigned to individual seismic stations. These station delays adjust the arrival time at each seismic station to account for travel paths which are affected by azimuth-dependent and localized velocity variations. The assignments of

individual station delays have been computed using a subroutine from Lee and Lahr's (1975) computer program, HYPO71(REVISED), as outlined below.

Each station correction constant accounts for velocity variations due to: (1) the juxtaposition of differing geologic structures and lithologies resulting from Cenozoic tectonism and recent fault movements, such as the contrasting crystalline basement complexes juxtaposed northeast and southwest of the Newport-Inglewood fault zone in the Los Angeles basin (Woodford, 1924; Bailey and others, 1964; Yerkes and others, 1965); (2) travel-time delays, ranging from 0.3 to 0.7 seconds (Kanamori and Hadley, 1975), for seismic stations in the Los Angeles and Ventura basins, where the sediment pile is estimated to reach 9150 meters (Yerkes and others, 1965; Vedder and others, 1974), (3) P-wave travel-time advances, ranging from 0.1 to 0.3 seconds, as a result of travel paths partly within an anomalously high-velocity upper mantle of 8.3 km/sec which exists beneath the Transverse Ranges (Hadley and Kanamori, 1977); and (4) a minor, yet necessary, elevation correction. Hadley and Kanamori (1977) assume a range of near-surface velocities of 3.0 to 5.0 km/sec to calculate elevation corrections for individual stations within the CIT seismic network. Assuming a maximum travel-time of 3.0 km/sec, the maximum effect of elevation variations between

Table 3. Explanation of earthquake relocation quality rating and data output summary lists found in Appendices C and D. After Lee and Lahr (1975).

Solution Quality	Approximate accuracy	
	Epicenter (km)	Focal Depth (km)
A (excellent)	1	2
B (good)	2.5	5
C (fair)	5	>5
D (poor)	>5	>5

The following data are given for each event:

(1) Origin time in Greenwich Civil Time: date, hour (HR), minute (MN), and second (SEC). If ** precedes the date, it indicates that this event also appeared in the Caltech catalog.
(2) Epicenter in degrees and minutes of north latitude (LAT N) and west longitude (LONG W).
(3) DEPTH, depth of focus in kilometers.
(4) MAG, Richter magnitude of the earthquake.
(5) NO, number of stations used in locating earthquake.
(6) GAP, largest azimuthal separation in degrees between stations.
(7) DMIN, epicentral distance in kilometers to the nearest station.
(8) RMS, root-mean-square error of the time residuals: $RMS = [\Sigma_i(R_i^2/No)]^{\frac{1}{2}}$ where R_i is the observed seismic-wave arrival time minus the computed time at the ith station.
(9) ERH, standard error of the epicenter in kilometers: $ERH = [SDX^2 - SDY^2]^{\frac{1}{2}}$. SDX and SDY are the standard errors in latitude and longitude, respectively, of the epicenter. When $NO \leqq 4$, ERH cannot be computed and is left blank.
(10) ERZ, standard error of the focal depth in kilometers. When $NO \leqq 4$, ERZ cannot be computed and is left blank. If $ERZ \geqq 20$ km, it is also left blank.
(11) Q, solution quality of the hypocenter. This measure is intended to indicate the general reliability of each solution.

Q	*Epicenter*	*Focal Depth*
A	excellent	good
B	good	fair
C	fair	poor
D	poor	poor

Q is based on both the nature of the station distribution with respect to the earthquake and the statistical measure of the solution. These two factors are each rated independently according to the following schemes:

Station Distribution

Q	NO	GAP	$DMIN$
A	$\geqq 6$	$\leqq 90°$	$\leqq$ Depth or 5 km
B	$\geqq 6$	$\leqq 135°$	$\leqq 2 \times$ Depth or 10 km
C	$\geqq 6$	$\leqq 180°$	$\leqq 50$ km

Statistical Measures

Q	RMS (sec)	ERH (km)	ERZ (km)
A	< 0.15	< 1.0	< 2.0
B	< 0.30	< 2.5	< 5.0
C	< 0.50	< 5.0	
D	Others		

Q is taken as the average of the ratings from the two schemes, i.e., an A and a C yield a B, and two B's yield a B. When the two ratings are only one level apart the lower one is used, i.e., an A and a B yield a B.

stations can only account for 0.3 seconds in travel time. The station elevation correction, upper-mantle P-wave advance, basin-alluvial P-wave delay, and lateral velocity variations across faults and structural blocks are statistically combined and smoothed by the calculated station delays, listed in Appendix A.

During the 1970's, southern California's seismic network has increased to over 120 recording sites. This comprehensive coverage, lacking only in the offshore region, affords a statistical advantage for improving the relocation of earthquakes. The scheme utilized here is a least-squares reduction of the travel-time residuals using only good to excellent quality earthquake relocations. For every earthquake, the P and S arrivals from each station list are first routinely edited and weighted, as described in the procedure, using no station delays. From the statistical measures and station distribution, determined from the HYPO71(REVISED) output, each earthquake is quality rated for its hypocentral relocation and placed in a category, "A" through "D," as explained in Table 3. All "A" and "B" quality relocations have an epicentral uncertainty of $\pm$2.5 kilometers and a hypocentral uncertainty of $\pm$5 kilometers. Only "A" and "B" quality locations have then been fitted to the least-squares routine. The least-squares process places each earthquake at the appropriate hypocenter which minimizes the difference

(root-mean-square for all stations) between the actually observed seismic-wave travel time at each station and the travel time calculated for the same travel path using Healy's layered crustal-velocity model. The assigned station delay becomes the average root-mean-square (Table 3) of the residual time difference between the observed and calculated travel times. Appendix B displays the improved quality of hypocentral locations resulting from three iterations of this least squares routine.

PROCEDURE

Data Collection

For every earthquake located within the study area, data from individual seismic stations have been gathered, collated, and merged from all seismic networks in southern California. Station data consist of the P-wave arrival time ($\pm$ .02 sec), its first motion, the S-wave arrival time with its sense of first motion, and the duration of the event ($\pm$ 5 sec). This information from each station has been read directly from records from which a computer-card phase list has been generated.

Initially, USC, CIT, and the USGS had each created a set of preliminary earthquake relocations by only incorporating the station data from their respective seismic networks. From these preliminary earthquake data sets, all earthquakes located within or at the periphery of the study area were considered for subsequent refinement in relocation. These three data sets (USC, CIT, and USCS) were next collated, merged, and then processed by Lee

and Lahr's (1975) computer program, HYPO71(REVISED), to determine the hypocenter, magnitude, and first-motion pattern for these local earthquakes.

Often, seismic records from stations had to be reread to complete the data catalogue for each earthquake. For events through 1975, station data from the USGS Santa Barbara Channel Network had only been catalogued for locations west of longitude 118° 30'W (approximately offshore of Santa Monica). Consequently, station records had to be read for all possible events occurring in the Los Angeles basin, lying to the east of 118° 30'W.

Under the direction of W.H.K. Lee of the USGS National Center for Earthquake Research, I initially assisted in relocating 1972-1975 events for the area bounded by 33° 45'N to 34° 45'N latitude and 118° 30'W to 120° 30'W longitude. The eastern boundary of the above data set overlaps into this study area as outlined in Figure 10. These earthquake relocations are based on station data from the USGS Santa Barbara Channel Network supplemented by data supplied by peripheral USC and CIT seismic stations. Therefore, the 1973-1975 earthquake relocations for the westernmost portions of this study area--to longitude 118° 30'W--are discussed by Lee and others (1979) and are only presented here. This data subset includes the Point Mugu earthquake of February 21, 1973. East of Point Dume, 1973-1976 earthquake relocations

Figure 10. Shaded region represents overlap of 1973-1975 station data between this study and USGS study by Lee and others (1979). Approximate locations for eight-station network installed in the Santa Barbara Channel by USC in August, 1978.

Sm Is. = San Miguel Island

SR Is. = Santa Rosa Island

SC Is. = Santa Cruz Island

A Is. - Anacapa Island

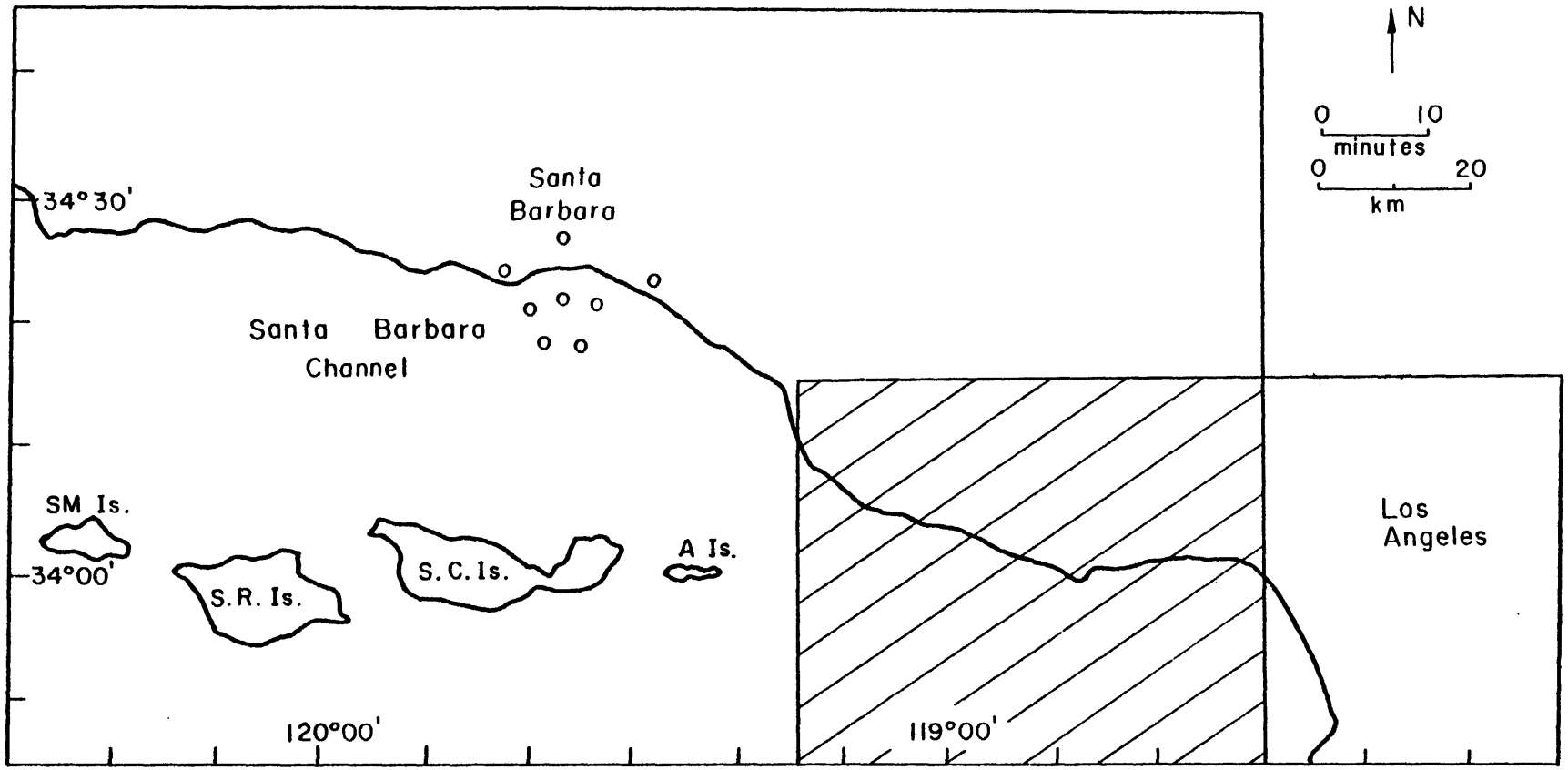
N
0
10
minutes
0
20
km
34°30'
Santa
Barbara
Santa Barbara
Channel
SM Is.
34°00'
S.R. Is.
S.C. Is.
A Is.
Los
Angeles
120°00'
119°00'

are more dependent on the USC and CIT networks, while the USGS Santa Barbara Channel Network assumes a peripheral importance. CIT has assumed operation of the USGS Santa Barbara Channel Network since the beginning of 1976. Consequently, all earthquakes occurring in 1976 near the western boundary of the study area (119° 15'W) are relocated and discussed here.

Data Processing

Seismic station data obtained in this study have been processed by HYPO71 (REVISED), a computer program by Lee and Lahr (1975) which produces an output for each earthquake consisting of its origin time, hypocenter location, magnitude, and plot of the first-motion pattern. Additional statistics, included in the output, described the precision of each earthquake relocation. HYPO71 (REVISED) has been adapted from an earlier version for worldwide data (Lee and Lahr, 1972).

Three forms of input data are required by HYPO71 (REVISED). These are: (1) the geographic coordinates for each seismic station ($\pm$ 0.1 km, whenever possible); (2) a layered, crustal velocity model, preferably controlled by explosion experiments; and (3) precise P-wave ($\pm$ .02 sec) and S-wave ($\pm$ .05 sec) arrival times.

Data Editing and P Residuals

In order to reach its final refined form, the data output from HYPO71 (REVISED) has been subjected to editing and computer processing for five iterations, as outlined by the flow diagram in Figure 11. This editing process, in almost every case, has improved the accuracy of the earthquake epicenters. The computer output for three typical earthquakes, in final form, is shown in Appendix C. An abbreviated explanation of the output, pertinent to this discussion, is included in the appendix.

For every earthquake, each phase list card has been considered individually and edited with respect to four statistical variables in the computer output: (1) the root-mean-square P-wave residual (RMS); (2) the number of seismograph stations recording the event (NO); (3) the maximum azimuthal gap between the recording stations (GAP); and (4) the minimum distance between the trial epicenter and the closest recording station (DM). These variables, as well as the other parameters presented in each output iteration of HYPO71 (REVISED) are explained in Table 3.

Earthquake hypocenters are determined according to Geiger's (1912) method, which minimizes the arrival-time residuals, in a least-squares sense, between the observed

Figure 11. Flow diagram outlining editing procedure.

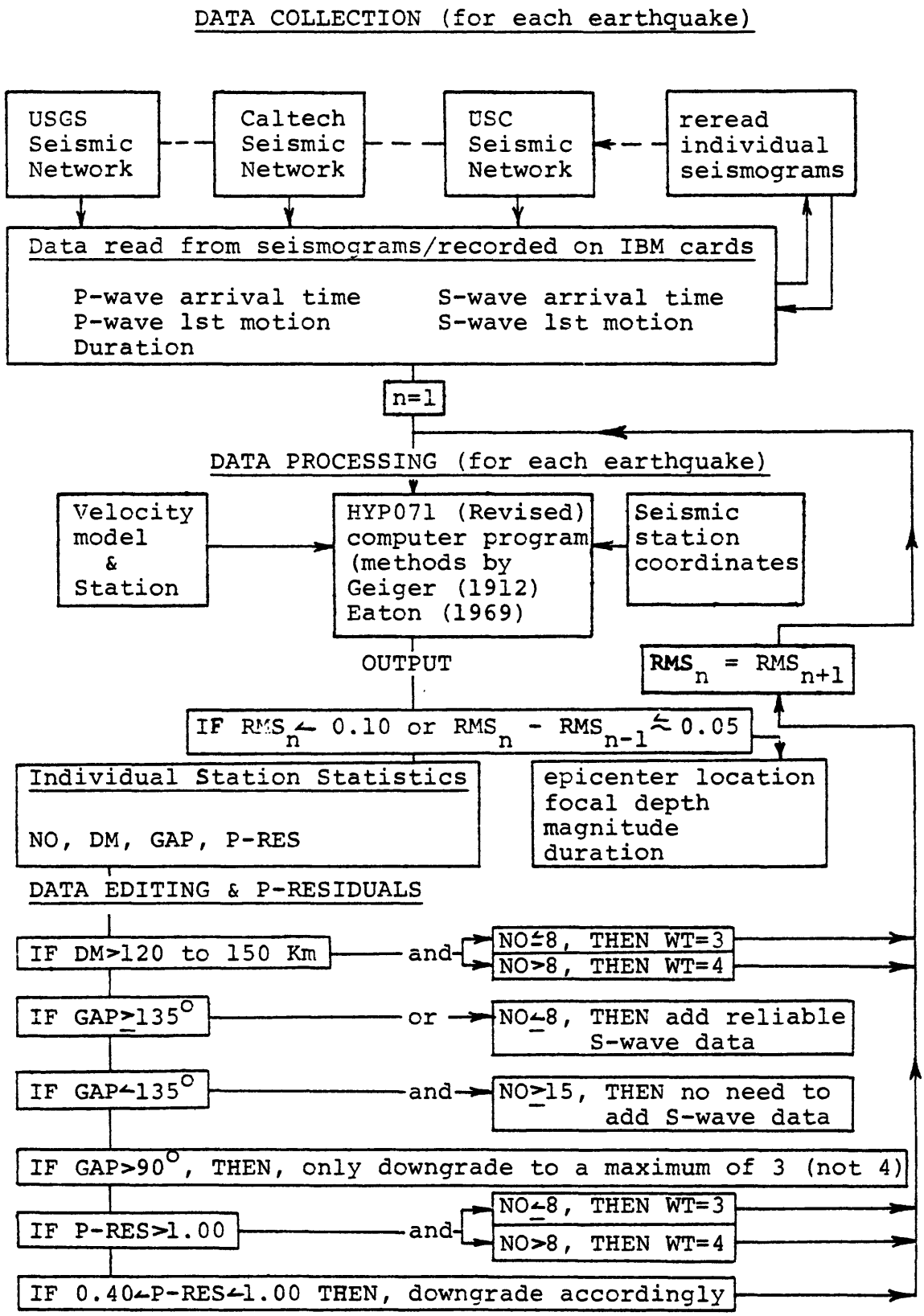
DATA COLLECTION (for each earthquake)
USGS Seismic Network
Caltech Seismic Network
USC Seismic Network
reread individual seismograms
Data read from seismograms/recorded on IBM cards
P-wave arrival time
P-wave 1st motion
Duration
S-wave arrival time
S-wave 1st motion
n=1
DATA PROCESSING (for each earthquake)
Velocity model & Station
HYP071 (Revised) computer program (methods by Geiger (1912) Eaton (1969)
Seismic station coordinates
OUTPUT
RMS_n = RMS_n+1
IF RMS_n ≤ 0.10 or RMS_n - RMS_n-1 ≤ 0.05
Individual Station Statistics
NO, DM, GAP, P-RES
epicenter location
focal depth
magnitude
duration
DATA EDITING & P-RESIDUALS
IF DM>120 to 150 Km
and
NO≤8, THEN WT=3
NO>8, THEN WT=4
IF GAP≥135°
or
NO≤8, THEN add reliable S-wave data
IF GAP<135°
and
NO≥15, THEN no need to add S-wave data
IF GAP>90°, THEN, only downgrade to a maximum of 3 (not 4)
IF P-RES>1.00
and
NO≤8, THEN WT=3
NO>8, THEN WT=4
IF 0.40<P-RES<1.00 THEN, downgrade accordingly

station arrivals and the corresponding calculated station arrivals. Since Geiger's (1912) method, when used for hypocenter relocation, is a summation of least-squares residuals exising at all of the involved seismograph stations, the editing process is actually a weighting process through which the editor can eliminate a station or downgrade a station's influence on the hypocenter relocation. In this manner, editing can eliminate or downgrade the phase list card for any station which may have an incongruent or inconsistent P-arrival reading and which may, in turn, have a strong influence on the least-squares relocation of the event. The weighting options are as follows:

Weighting Symbol	Explanation
0 or "blank"	full weight
1	3/4 weight
2	1/2 weight
3	1/4 weight
4	no weight

The several closest recording stations to an event are usually not downgraded since these stations are critical in determining the focal depth of the earthquake. Only when the distance between the epicenter and the closest recording station is less than the actual focal depth (DM<DEPTH) can the hypocenter be considered to be reliably located. On the other hand, the computer program slightly downgrades the contribution of each station

with increased distance from the trial hypocenter. It is general practice to exclude stations from the phase list which lie more than 120-150 kilometers away from the trial epicenter.

If the number (NO) of seismic stations recording the event is initially small (<8), then the phase list cards are usually only downgraded to a minimum of "3" (¼ weight) rather than to "4" (no weight), since elimination of any stations in this case (NO<8) usually increases the azimuthal gap (GAP) between the remaining recording stations. Ideally, the value of GAP should be less than 90^{o} to properly constrain the hypocenter relocation. If the GAP<135^{o}, the S-wave arrival data from the phase list, if reliable, is considered in the relocation process. If GAP<135^{o} and NO<15, the S-wave arrivals usually will not significantly improve the earthquake relocation.

The root-mean square summation of the P-wave residuals (P-RES) for each phase list card results in the RMS value for each earthquake. In general, the P-RES values for each event have been appropriately weighted such that the resultant RMS value is less than .25 sec (RMS<.25 sec). If P-RES<1.0 sec, the phase list card is excluded from further consideration unless it is critical to the earthquake relocation. In this case, the original seismic record has been reread to determine the exact P-wave arrival time. For the situation 0.4<sec P-RES<1.0 sec,

the phase list card has been appropriately downgraded or eliminated. The final weighting of each phase list card is a combination of the editor's weighting and the computer's distance weighting formula. The resultant of this combination is listed under the heading P-WT, as shown in the three earthquakes in Appendix C, for each phase list card.

RESULTS

Four hundred twenty three earthquakes, occurring between January 1973 and December 1976 in the study area (Figure 12), have been relocated and are summarized in Appendix D. This summary of information for each earthquake includes origin time, epicentral location, focal depth, duration magnitude, number of recording stations, azimuthal gap, distance from epicenter to closest recording station, root-mean-square travel-time residual, epicentral location error, focal depth error, and a statistical quality rating for each earthquake relocation. The complete output summary for each earthquake includes the phase-card list, the iterative step-wise locational procedure used by HYPO71 (REVISED), the statistical information describing the earthquake relocation, and the first-motion plot of the P-wave readings from the phase list. A sampling of the HYPO71 (REVISED) output for three typical earthquakes is provided in Appendix C--the complete listing is on file at USC.

Figure 12. Epicenter plot for all 423 earthquakes relocating in the study area during 1973-1976.

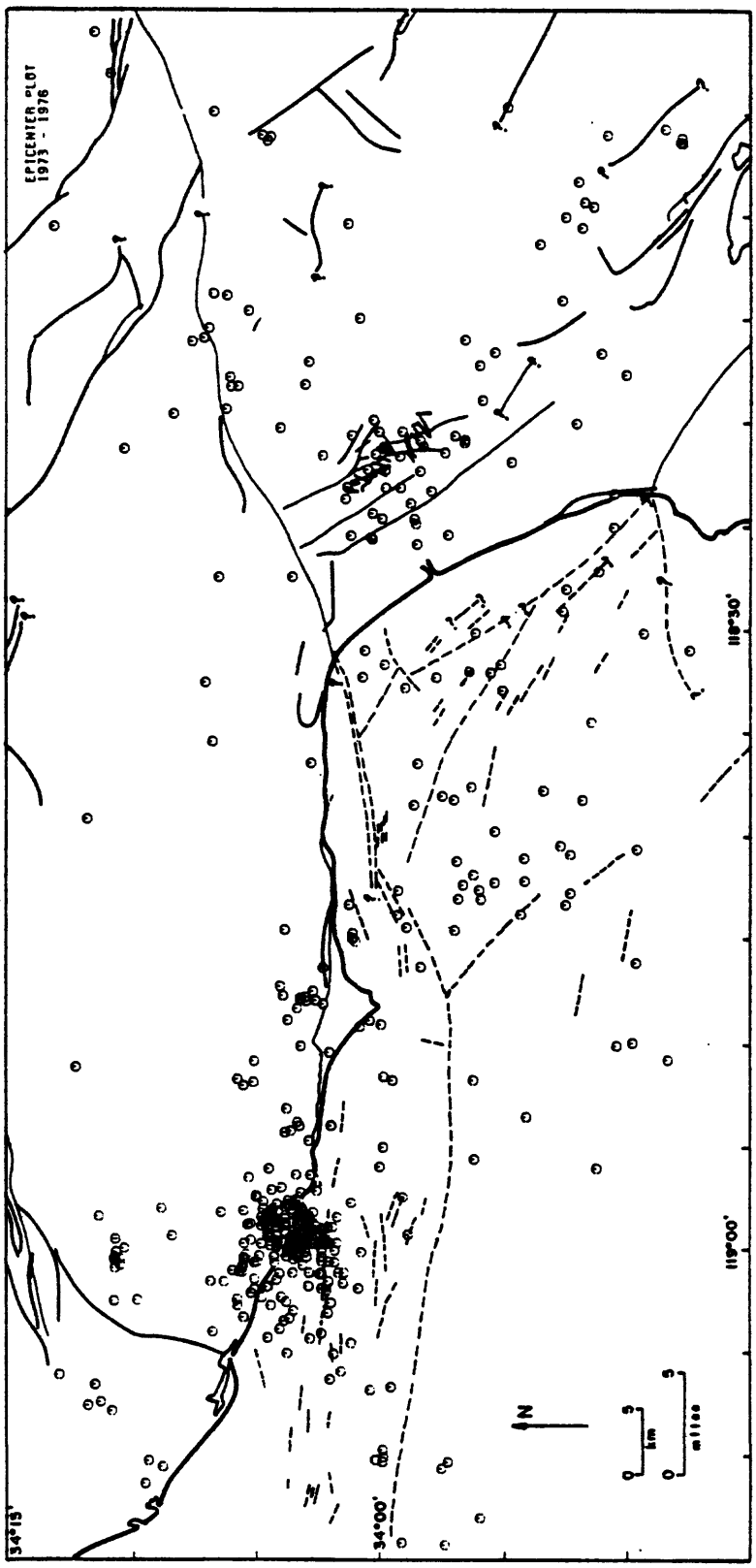
EPICENTER PLOT
1973 - 1976
34°15'
34°00'
118°30'
119°00'
N
0
5
km
0
5
miles

All 423 earthquake epicentral locations are plotted in Figure 12. Also plotted for the 423 events are magnitudes (Figure 13) and focal depths (Figure 14), which correspond to the epicentral locations plotted in Figure 12. Magnitudes are calculated on the basis of the method described by Lee and others (1972) in which the magnitude of an event is considered to be the average of the individual station magnitudes, as determined from their signal durations. The signal duration, tau (τ) is based on the USGS develocorder records. The termination of the signal is defined by an amplitude of less than one centimeter on the develocorder output. The magnitude of an event at a recording station is given by Lee and others (1972):

$$m = -0.87 + 2.00 \log\tau + 0.00035\Delta$$

where

M = magnitude

τ = signal duration in seconds

Δ = epicentral distance in kilometers

Focal depths are plotted in Figure 13 for only "A" and "B" quality relocations. "C" and "D" earthquakes have no defined range of error in focal depth but have been assigned arbitrary focal depths by the computer.

The map size (scale 1:250,000) has been chosen to conform to the size and scale of other published maps

Figure 13. Magnitude plot of 1973-1976 earthquakes

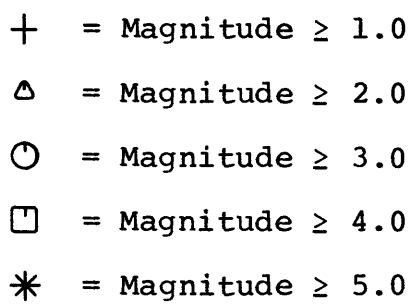

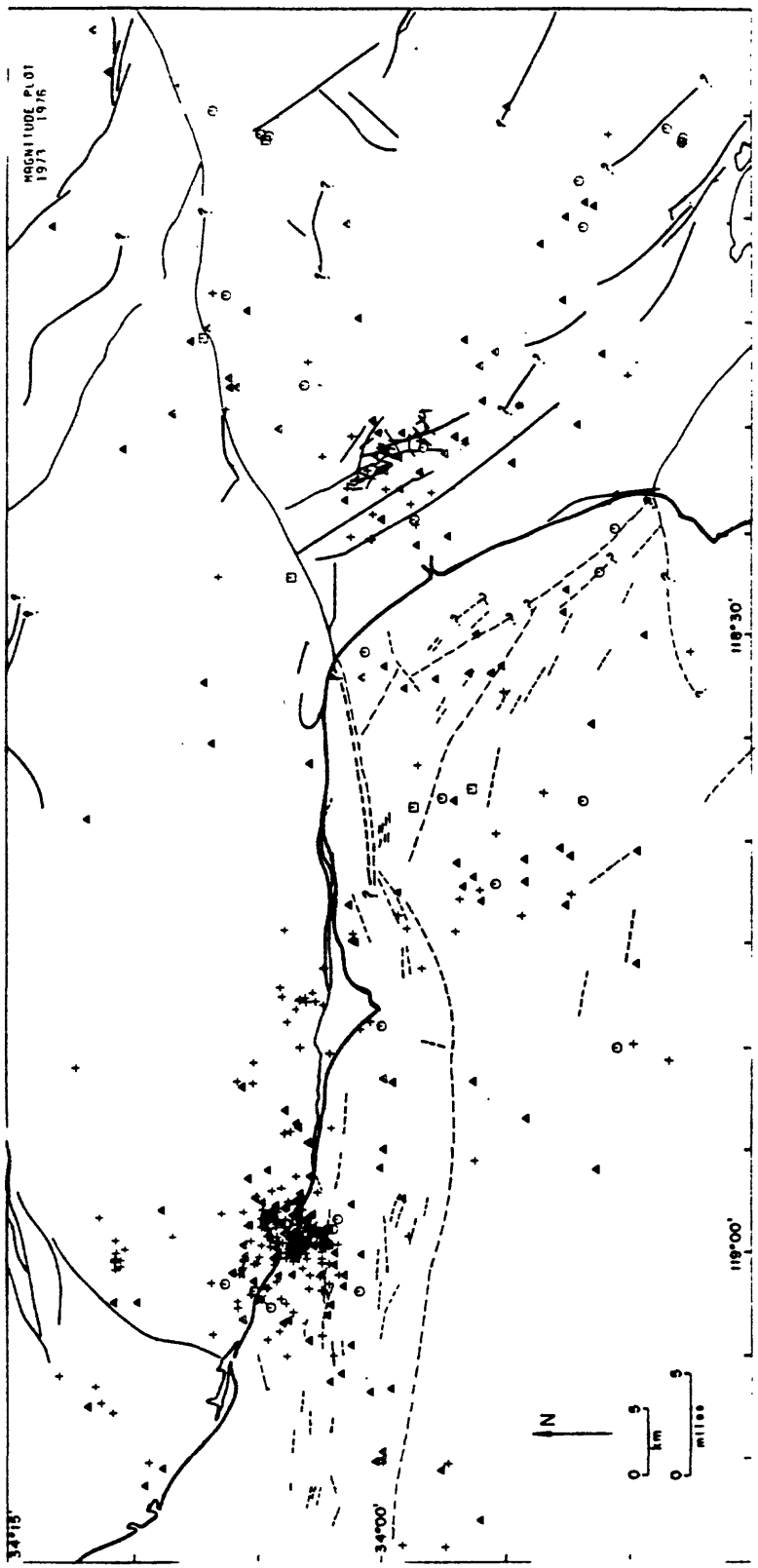
MAGNITUDE PLOT
1973 1976
34°15'
34°00'
118°30'
119°00'
N
0 5
km
0 5
miles

Figure 14. Focal depth plot for 1973-1976 "A" and "B" quality earthquake relocations only.

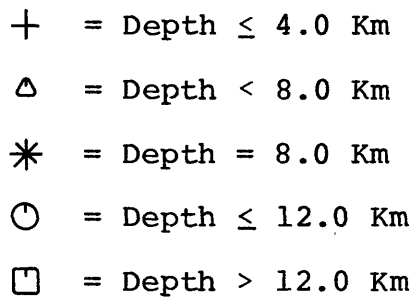

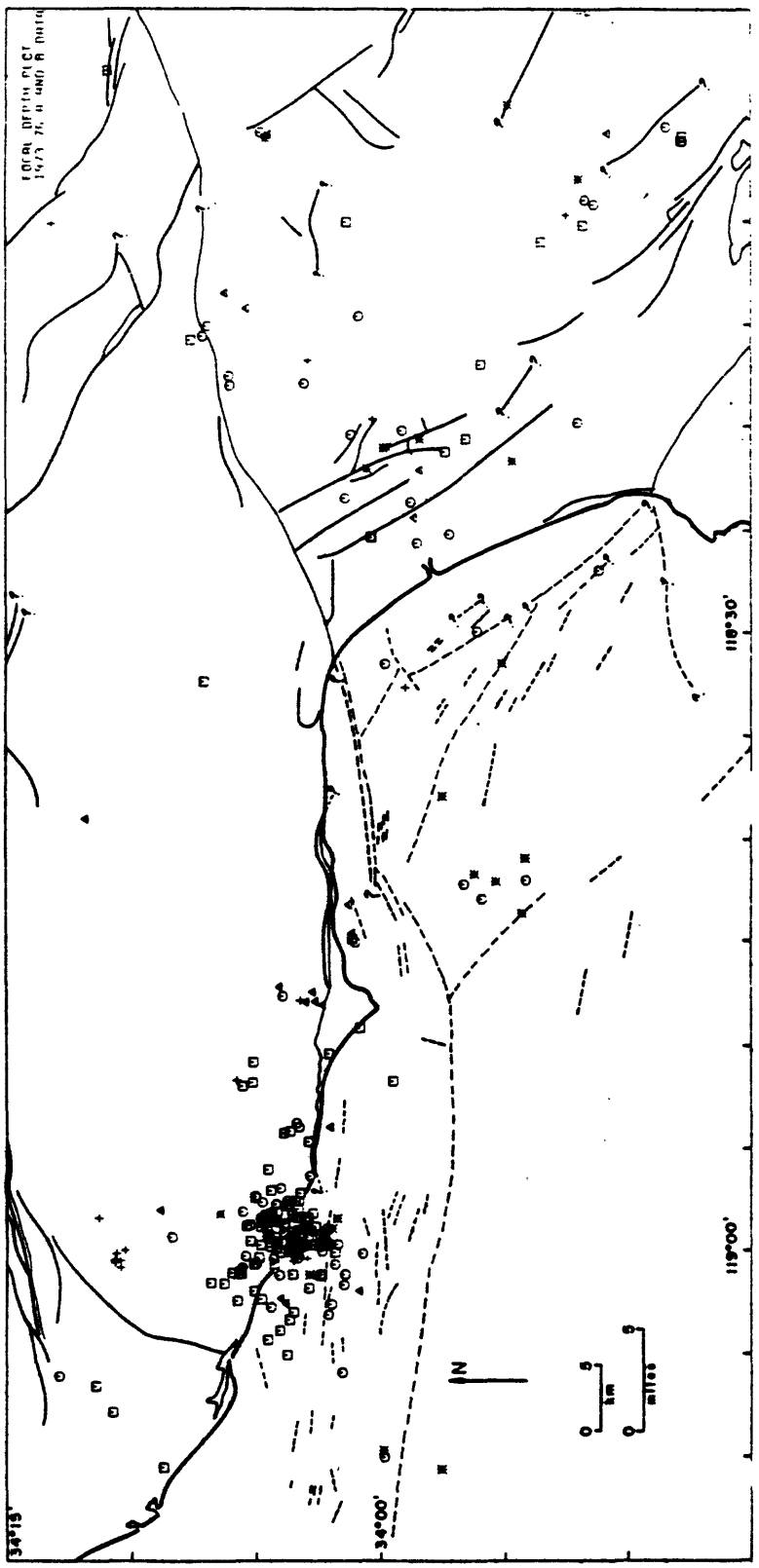
34°15'
34°00'
118°30'
119°00'
N
0
km
0
miles

(e.g., the California Division of Mines and Geology state geologic maps). They are included in Appendix E for reference. Each of these maps has been reproduced at a smaller scale in the text.

The margin of error for "A" quality (Table 3) epicentral locations is $\pm$ 1.0 kilometer; for "B" quality locations, $\pm$ 2.5 kilometers. On a map scale of 1:250,000 (Appendix E) epicenters are plotted as open circles which represent a 3/4 kilometer radius. Therefore, errors in relocation exceed the boundaries of the circles for all events. Fault traces are plotted to within approximately 300 meters (Ziony and others, 1974). The most dependable and accurate relocations, namely "A" and "B" quality events, are plotted in Figure 15. The regional geographical bias of seismic station locations tends to group the more accurate relocations onland rather than offshore.

As shown in Figure 12 (also Appendix E), the 1973 Point Mugu earthquake and its aftershocks cannot be individually deciphered on a plot with a scale of 1:250,000. In order to display these data more meaningfully, the region bounded by 34° 01'N and 34° 07'N latitude and 118°56'W and 119° 04'W longitude has been expanded to a scale of 1:83,333. The same plots as above have been produced for this cluster of events and are presented in Appendix F.

Figure 15. "A" and "B" quality earthquake relocations, 1973-1976.

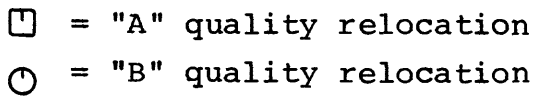

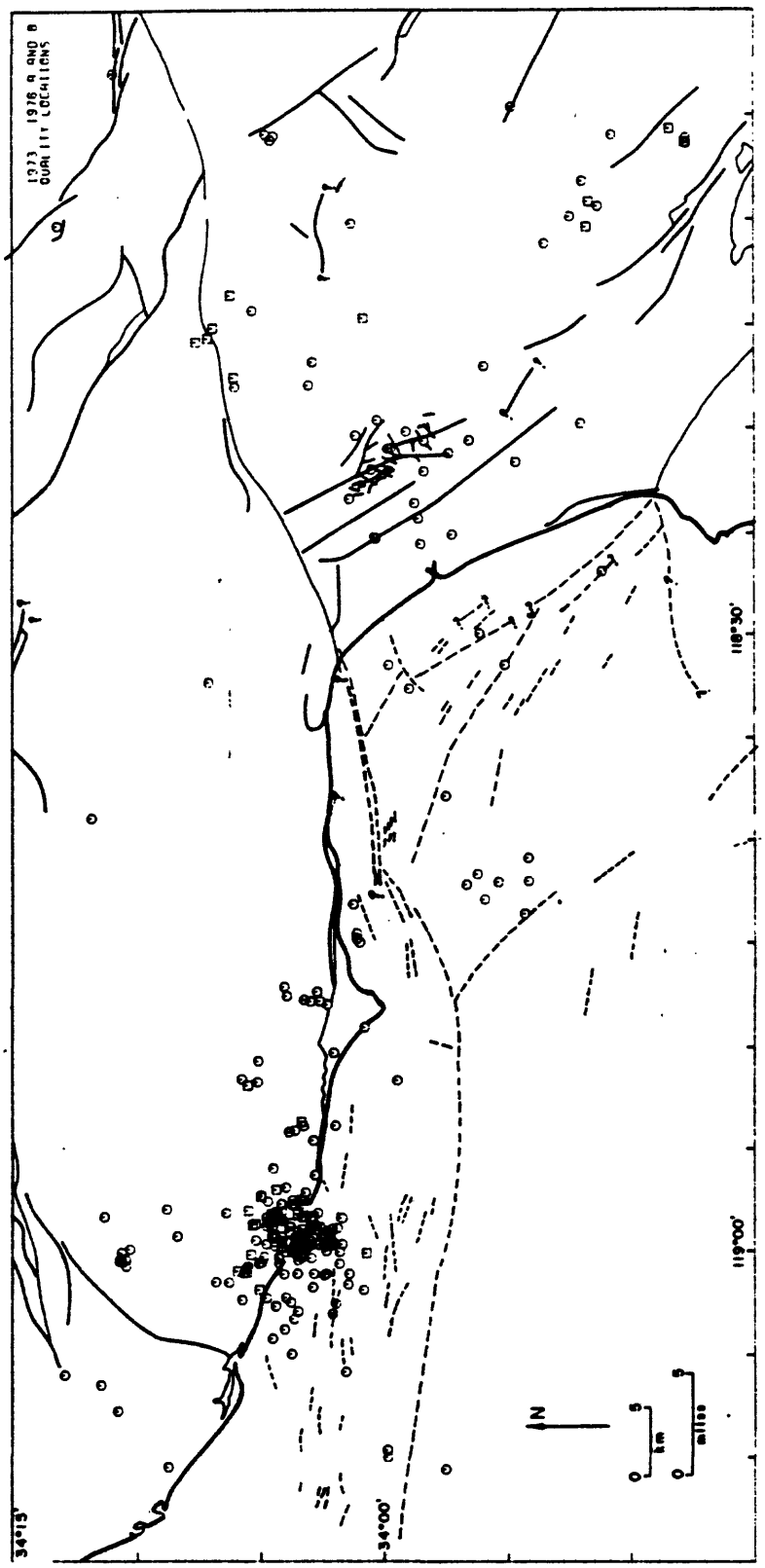
1973 - 1978 A AND B
QUALITY LOCATIONS
g
34°15'
34°00'
118°30'
119°00'
N
0
5
km
0
5
miles

For every earthquake relocation, the HYPO71 (REVISED) output produces a P-wave arrival first-motion plot, which is a lower-hemisphere projection onto the Wulff-net equatorial plane. From the 423 earthquakes, 26 individual solutions were sufficient by themselves to produce enough station control to define a fault plane (Figure 16 and Table 4). In addition, 11 composite fault-plane solutions have been created by combining groups of earthquakes related either in time or space (Figure 17 and Table 5). The choice of fault planes is discussed later in terms of the local geology, structure and seismicity patterns.

The composite fault-plane solutions have been drawn under the assumption that all the earthquakes define the same fault or fault zone and are produced by the same focal mechanism. Due to this assumption, composite fault-plane solutions are more susceptible to error than individual fault-plane solutions. The advantage of the composite fault-plane solution is to incorporate data points from local events into the data set of a well-located earthquake to further constrain the choice of possible fault planes. Combining data from several small events was often sufficient to formulate a consistent first-motion pattern, defining a fault-plane solution.

The focal mechanism for each earthquake is assumed to be a double-couple dislocational model (Stauder, 1962). Thus, the plane of fault movement becomes one of two

Figure 16. Fault-plane solution map for individual earthquakes, 1973-1976. Black quadrants indicate compression; white quadrants indicate dilitation.

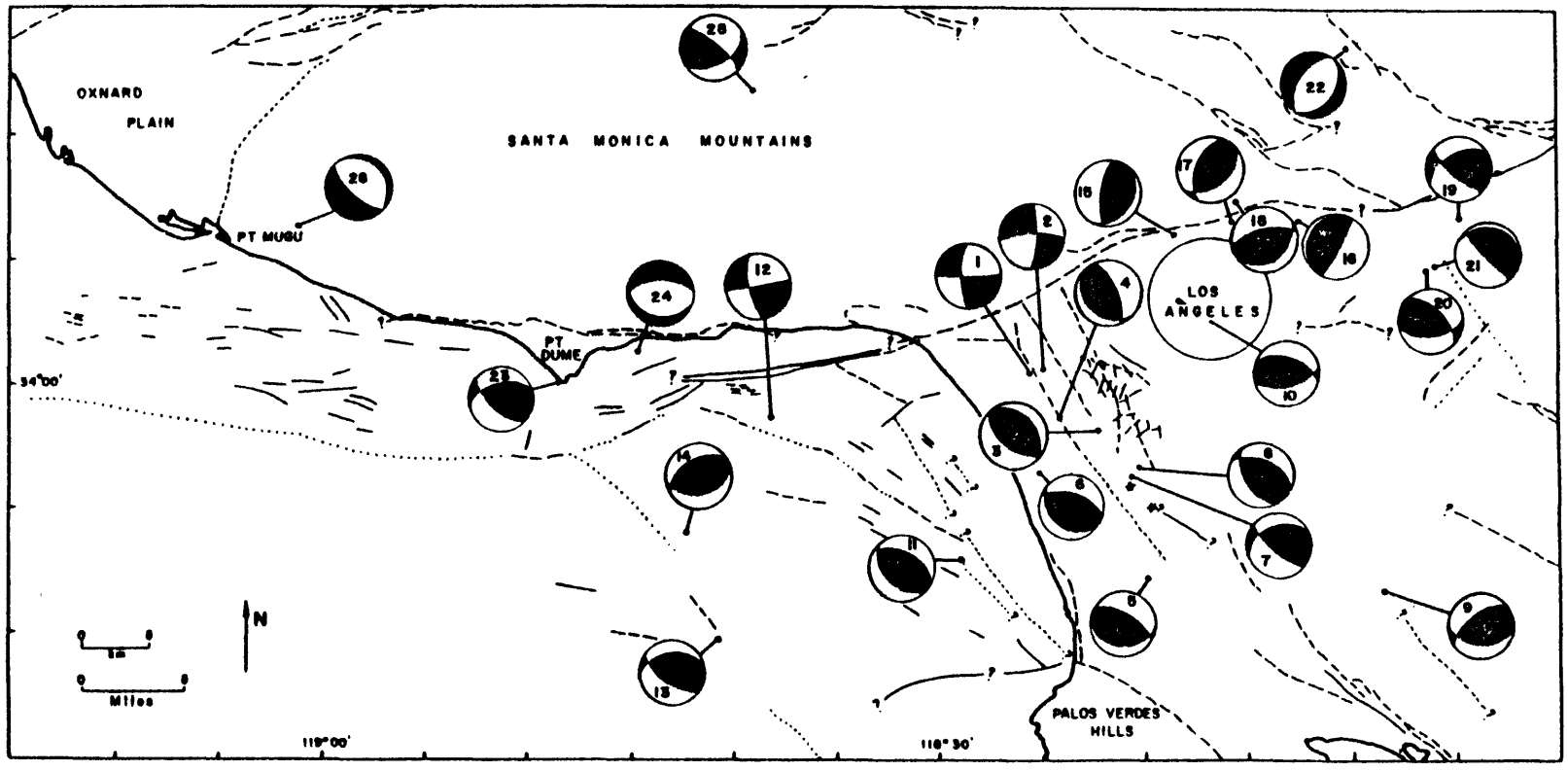
OXNARD
PLAIN
SANTA MONICA MOUNTAINS
PT MUGU
PT DUME
LOS ANGELES
PALOS VERDES HILLS
34°00'
119°00'
118°30'
N
Miles

TABLE 4.

List of individual fault-plane solutions

Solution	Event	YrMonDy	HrMin	Sec	Lat N	Long W
1	179	731129	1125	18.87	34-03.73	119-02.48
2	181	731209	1536	13.69	34-00.33	118-02.48
3	167	731118	0729	59.73	33-58.34	118-25.26
4	255	741022	1213	38.69	33-58.57	118-22.57
5	191	740117	0830	51.05	33-51.99	118-24.97
6	301	750504	2016	33.42	33-57.17	118-19.34
7	124	730520	1808	42.47	33-56.51	118-25.91
8	406	761115	1208	03.77	33-56.49	118-20.75
9	368	760715	0227	39.54	33-51.94	118-20.24
10	367	760627	2211	36.17	34-03.01	118-08.38
11	333	751007	2333	26.69	33-52.55	118-29.03
12	410	761122	1755	11.05	33-56.24	118-37.54
13	084	730308	2349	51.81	33-49.58	118-40.57
14	280	750123	0348	42.42	33-54.09	118-42.08
15	396	760929	0700	51.09	34-06.00	118-18.18
16	205	740312	0735	45.26	34-06.18	118-13.75
17	202	740306	0152	34.01	34-06.89	118-15.34
18	265	741206	1345	13.08	34-07.10	118-15.83
19	334	751011	0655	00.59	34-06.72	118-04.86
20	269	741219	1236	16.58	34-04.57	118-06.27
21	199	740227	0541	17.93	34-04.77	118-05.99
22	257	741106	0038	27.55	34-13.16	118-10.40
23	365	750620	0051	28.91	33-59.88	118-49.07
24	210	740331	1120	46.76	34-01.06	118-44.63
25	358	760504	0055	29.71	34-06.22	119-01.53
26	282	750128	0522	22.85	34-11.77	118-39.07

Figure 17. Composite fault-plane solution map for earthquakes, 1973-1976. Black quadrants indicate compression; white quadrants indicate dilitation.

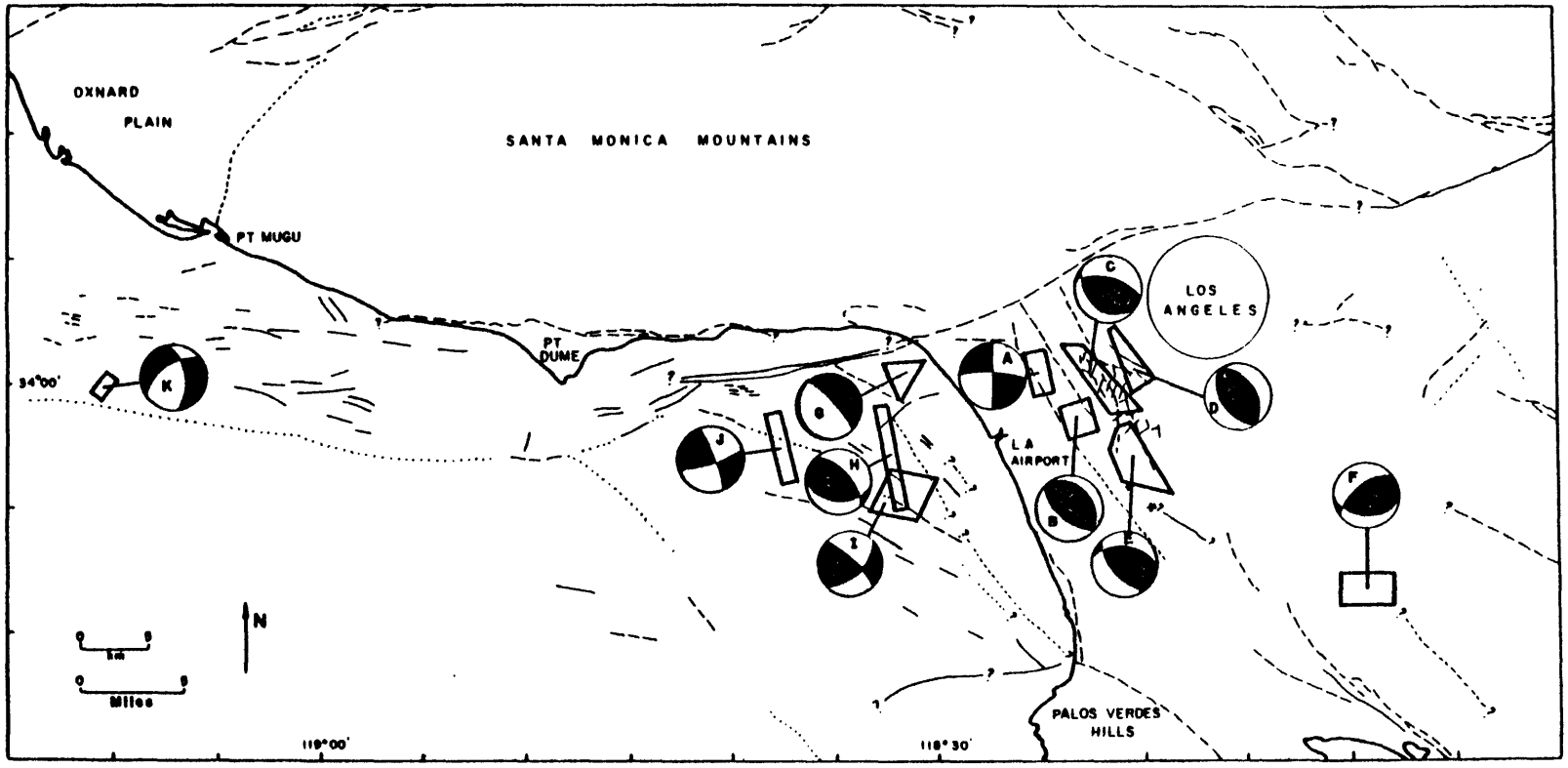
OXNARD
PLAIN
SANTA MONICA MOUNTAINS
PT MUGU
PT DUME
LOS ANGELES
L A AIRPORT
PALOS VERDES HILLS
34°00'
119°00'
118°30'
N
Km
Miles
A
B
C
D
E
F
G
H
I
K

TABLE 5.

List of composite fault-plane solutions

Solution	Event	YrMonDy	HrMin	Sec	Lat N	Long W
A	179	731129	1125	18.97	34-00.27	118-25.54
	181	731209	1536	13.69	34-00.33	118-25.48
	302	750504	2027	16.71	33-58.72	118-23.82
	397	761005	2224	15.48	34-01.15	118-25.37
B	167	731118	0729	59.73	33-58.34	118-22.26
	168	731118	0733	47.62	33-57.88	118-23.23
C	322	750804	0716	15.20	34-01.36	118-23.61
	347	760204	1843	56.26	33-59.80	118-21.18
	349	760207	2018	12.48	33-59.06	118-20.36
	378	760818	1718	57.60	33-00.47	118-22.19
	399	761013	0112	25.87	33-59.82	118-21.09
D	117	730424	1454	57.87	34-00.24	118-19.80
	150	740826	2028	14.15	34-01.12	118-20.54
	348	760206	1844	56.33	34-02.29	118-21.51
	403	761019	1504	16.90	33-60.00	118-20.38
E	124	730520	1808	42.47	33-56.51	118-20.91
	293	750327	0652	49.40	33-58.34	118-20.77
	336	751027	0207	15.92	33-58.21	118-21.09
	338	751125	0236	57.35	33-56.91	118-20.56
	383	760902	0256	46.94	33-55.79	118-18.84
	406	751115	1208	03.77	33-56.49	118-20.75
F	368	76-715	0227	39.54	33-51.94	118-08.24
	369	760716	0327	39.61	33-51.68	118-09.24
G	101	730329	2135	33.96	34-00.67	118-32.23
	291	750307	1629	33.80	34-00.56	118-30.95
	327	750927	1247	33.72	33-59.76	118-31.63
H	81	730306	0627	37.40	33-55.46	118-32.02
	119	730511	0235	36.25	33-58.94	118-32.76
	318	750722	0618	17.76	33-57.67	118-32.24
	373	760727	0900	50.92	33-55.03	118-31.61
	491	761018	0551	15.25	33-56.32	118-31.96
I	81	730306	0627	37.40	33-55.46	118-32.02
	373	760727	0900	50.92	33-55.03	118-31.61
	379	760822	0953	47.24	33-54.98	118-32.87
	401	761018	0551	15.25	33-56.32	118-31.96
	415	761129	0040	01.81	33-56.05	118-30.08

Table 5 (continued)

J	409	761122	1753	10.96	33-58.59	118-38.42
	410	761122	1755	11.05	33-56.24	118-37.54
	411	761122	1806	12.94	33-56.95	118-38.17
	412	761122	1932	36.49	33.57.44	118-37.98
K	407	761121	0009	46.17	33-59.79	119-09.98
	408	761121	1939	44.91	34-01.11	119-10.11

orthogonal nodal planes. This orthogonality criterion, implying equal amounts of dislocation on both sides of a fault, has been shown to deviate from 90^{o} by a maximum of only 10^{o} to 20^{o} (Sykes, 1967). The direction of the inferred axes of maximum compression and tension lie at 45^{o} angles to the nodal planes and in a plane perpendicular to the two nodal planes. The axis of maximum compression bisects the tensional quadrants.

The P-wave first-motion data which have produced reliable fault-plane solutions and accompanying suggested focal mechanisms for each of these events are presented in Figures 20 to 32, in the "Discussion." Appendix G addresses possible problems capable of limiting the reliability of fault-plane solutions. One of these problems, the variance of a fault-plane solution as a function of the crustal velocity model, is investigated for all six possible models presently suggested for southern California.

A local stress pattern, derived from fault-plane solution data, is presented in Figures 18 and 19. The compressional stress direction for each fault-plane solution has been projected onto the horizontal plane; thus, only a component of the true stress direction is shown. The maximum compressive stress is assumed to correspond with the P axis of the fault-plane solution. Azimuthal errors in stress direction determinations have been

Figure 18. Compressive stress pattern for the study area derived from 1973-1976 individual fault-plane solutions. Dots represent epicenters for fault-plane solutions. Lines directed away from each epicenter represent the horizontal projection of the compressional stress vector, derived from the fault-plane solution. The magnitude of the stress is not indicated by the length of the line.

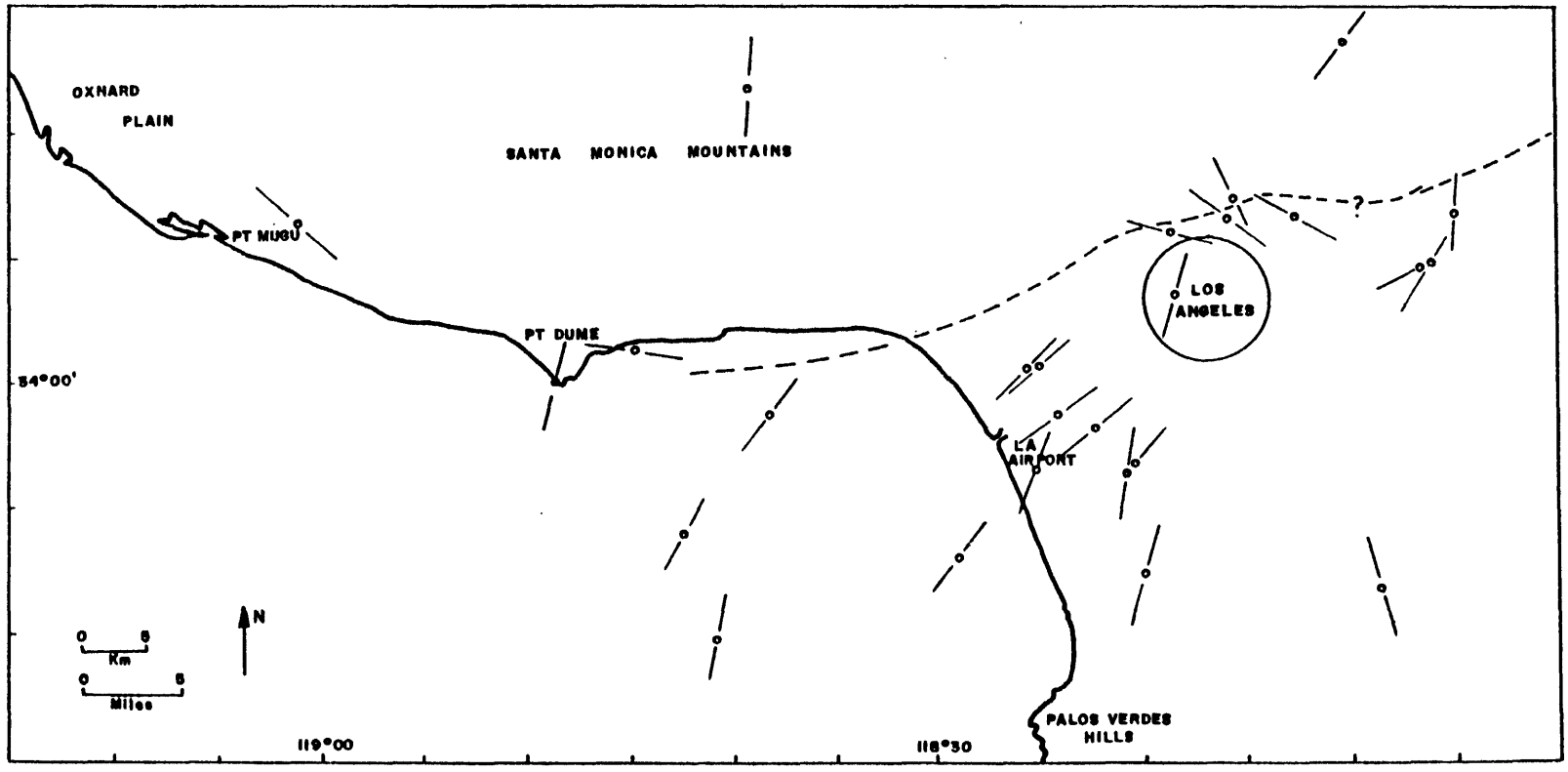
OXNARD
PLAIN
SANTA MONICA MOUNTAINS
PT MUGU
PT DUME
LOS ANGELES
LA AIRPORT
34°00'
0 5
Km
0 5
Miles
N
119°00
118°30
PALOS VERDES HILLS

Figure 19. Compressive stress pattern for the study area derived from 1973-1976 composite fault-plane solutions.

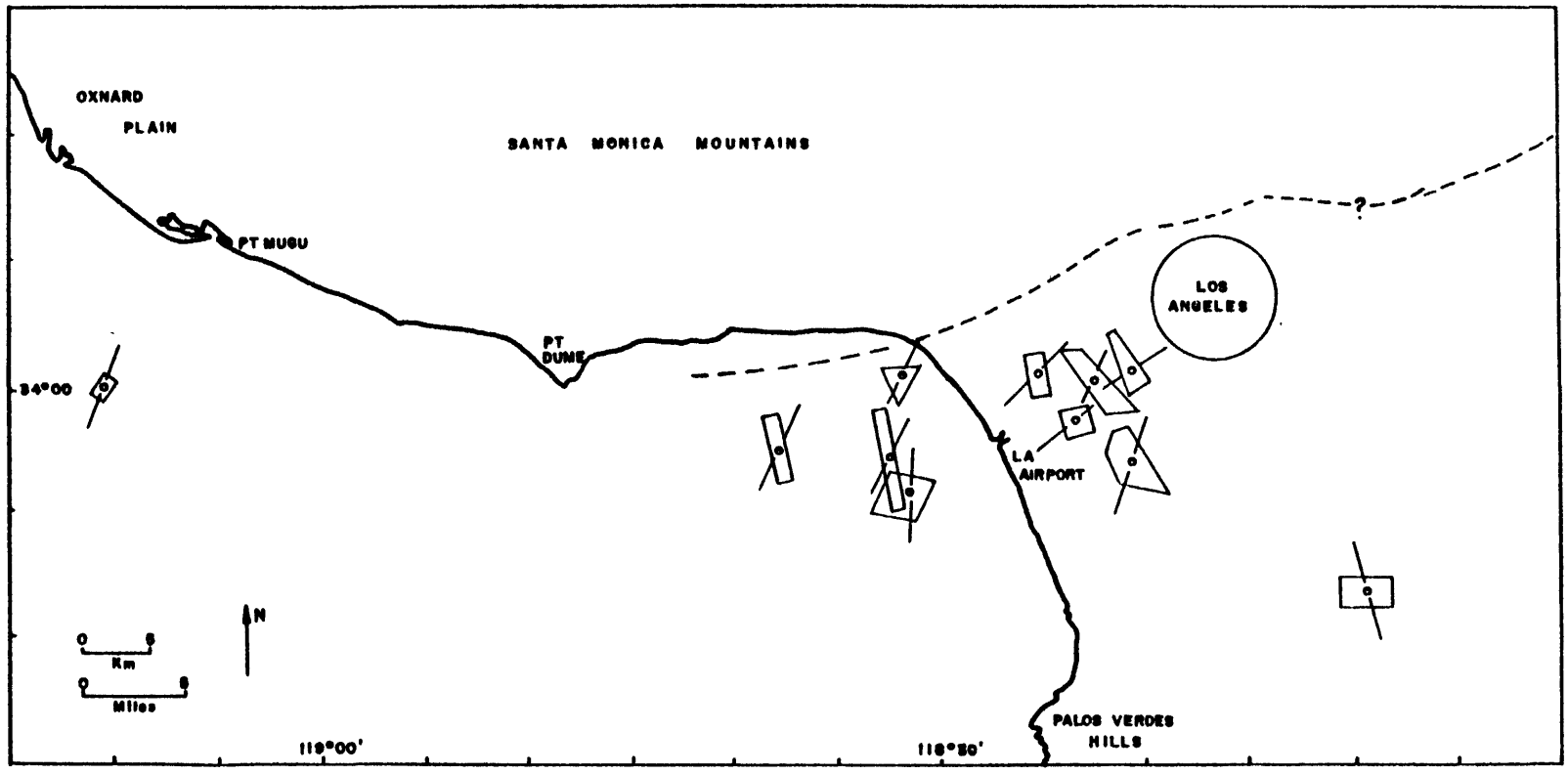
OXNARD
PLAIN
SANTA MONICA MOUNTAINS
PT MUGU
PT
DUME
34°00
LOS
ANGELES
?
LA
AIRPORT
N
0 5
Km
0 5
Miles
119°00'
118°50'
PALOS VERDES
HILLS

reviewed by Sbar and Sykes (1978). This error can reach $\pm$ 40^{o} for strike-slip faulting while it is smaller (<20^{o}) for normal- or reverse-slip faulting (Raleigh, 1972; Sbar and Sykes, 1978). Even though a large margin of error is inherent in the stress directions derived from strike-slip solutions, the large number of measurements (37) and the dominance of reverse-fault mechanisms within this region statistically precludes such a large error from affecting the regional trend of the data. Figure 18 shows variations in derived compressive stress directions of up to 90^{o}. These opposed stress directions appear to be caused by local fault geometries, as discussed below.

LATEST FAULTING: PREVIOUS WORK

Newport-Inglewood Fault Zone

Recent tectonic activity on the Newport-Inglewood fault zone (Figure 3) is marked by a series of en echelon anticlines which have formed in Quaternary basin alluvium. The 1933 Long Beach earthquake, M = 6.3 (Richter, 1958), with an epicenter located offshore of Newport Beach, California, attests to the fault's historic active status. Although no surface faulting has been recognized during historic time, subsurface displacement during the 1920 Inglewood earthquake, M = 4.9 (Tabor, 1920), and during subsequent shocks in the early 1940's, have damaged oil wells in the Dominguez and Rosecrans oil fields (Bravinder, 1942). The sense of shearing, from stratigraphic correlations in oil wells, is right-lateral.

Latest faulting locally cuts upper Pleistocene terrace deposits (Ziony and others, 1974). A similar age for latest faulting also applies to the offshore, southwest extension of the Newport-Inglewood fault zone

where fault-line scarps cut late Plesitocene strata, but nothing younger (Barrows, 1974).

Besides current tectonic evidence, right-lateral slip ranging from 915 meters to several kilometers has been recognized by correlation of offset Pliocene strata (Hill, 1954; Rothwell, 1958). Barrows (1974) also reports right-lateral offsets of 180 meters along the Townsite fault in the Potrero oil field.

Recent studies by Castle and Yerkes (1969) and Jahns and others (1971) acknowledge right-lateral slip of nearly 10,000 meters within Miocene, Pliocene, and Pleistocene strata. Harding (1973) has documented right-lateral offsets of anticlinal axes in the oil fields along the Newport-Inglewood uplift ranging from 180 meters to 760 meters in post-Miocene time.

Hill (1971) cites several reports of apparent normal and reverse faulting observed along this zone (Foster, 1954; Crowder, 1968), but generally discounts these unfavorable observations as only fault separations, rather than fault slips, as defined by Hill (1959). From the results of this study, Hill's (1971) conclusions appear to be suspect.

The Charnock fault and the Overland Avenue fault, which lie west of and parallel to the Newport-Inglewood fault zone in the northern Los Angeles basin (Figure 3), are included in this discussion. Both faults are

considered active (Association of Engineering Geologists, 1973). Faulted rocks of Late Quaternary age (11,000-500,000 m.y. B. P.) are present along both faults. No evidence exists for disturbances since the onset of the Holocene except for one small fault which displaces alluvium between the Charnock and Overland Avenue Faults.

Palos Verdes Hills Fault

The Palos Verdes Hills fault, southwest and sub-parallel to the Newport-Inglewood fault zone, is a southwest-dipping reverse fault marked by late Pleistocene and probable Holocene movement. The onland trace of the fault lies along the northern flank of the Palos Verdes Hills uplift. From well data, offsets in Pleistocene strata mark the latest documented fault movement (Woodring and others, 1946). Displaced upper and lower Pleistocene sediments onland, in the city of Torrance, have been cited in engineering geology reports (Poland and others, 1959).

Offshore seismic profiling has demonstrated that the fault continues northward into Santa Monica Bay, in a segmented fashion, and terminates either at or in the vicinity of the Dume fault (Junger and Wagner, 1977). Portions of the offshore northwest extension of the Palos

Verdes Hills fault have been mapped by Greene and others (1975), Junger and Wagner (1977), and Nardin and Henyey (1978). From published data, this fault appears to branch along two separate courses (Figure 3). Its intersection with the nearly westerly-trending Dume fault is slightly southwest of Point Dume. In the northeastern corner of the Santa Monica Bay, Junger and Wagner (1977) recognize several short, discontinuous, and nearly vertical faults south of the Dume fault which are truncated by a short, recently-active, and westerly-trending fault which cuts the base of the Holocene (Junger and Wagner, 1977). This cross-cutting fault appears to mark the northern truncation of the Palos Verdes Hills fault extension in the Santa Monica Bay (Ziony and others, 1974). Nardin and Henyey (1978) and Greene and others (1975) have also mapped a westerly-trending fault in this vicinity just to the south of the Dume fault. Both studies show evidence of fault movement since at least Pleistocene time.

The southward continuation of the Palos Verdes Hills fault into the San Pedro basin is marked by Holocene faulting (Ziony and others, 1974; Junger, 1976; Fischer and others, 1977; Nardin and Henyey, 1978). From seismic profiles offshore of San Pedro, Junger and Wagner (1977) have interpreted gentle warps in the sea floor as either very late Pleistocene or Holocene.

Santa Monica Fault Zone: East of Beverly Hills

The Santa Monica Mountain structural block has been uplifted along its southern frontal fault system (the Santa Monica fault system) since latest Miocene to early Pliocene time (Yerkes and others, 1965; Yerkes and Wentworth, 1965; Campbell and others, 1970), but geologic evidence does not suggest Holocene displacement except for its easternmost extensions along the Raymond Hill and Sierra Madre-Cucamonga faults.

The Santa Monica fault system extends the length of the study area and for discussion purposes, is divided into recency of faulting east of and west of Beverly Hills. East of Beverly Hills, individual faults within the system are the Santa Monica fault, the Raymond Hill fault, and the Sierra Madre fault. West of Beverly Hills is the continuation of the Santa Monica fault, which bifurcates along the Malibu coast into the Malibu Coast fault and the offshore Dume fault.

Yerkes and others (1965) describe the orientation and displacement across the Santa Monica fault at Beverly Hills. It is a reverse fault dipping approximately 50^{o} to the north. Basement uplift exceeds 2250 meters (Campbell and Yerkes [1976] note 3650 meters of basement

vertical uplift, north side up, indicated in the Beverly Hills oil field). Basal Miocene strata has been uplifted approximately 2000 meters (the base of the Modelo Formation, upper Miocene, is offset vertically a minimum of 450 meters; Lamar, 1961); and the base of the lower Pliocene, approximately 900 meters. To the west, upper Pliocene and Pleistocene marine deposits are locally warped and disrupted, but at Beverly Hills and to the east the base of the upper Pliocene deposits lies unconformably across the uplifted strata (Knapp and others, 1962).

East of the Beverly Hills, the Santa Monica fault trace is inferred from oil well data (Robert Hill, pers. commun., 1978) beneath the alluvium and follows the base of the Hollywood Hills to the vicinity of the Los Angeles River (approximately 118° 18' to 118° 10'), where it is transected by an eight-kilometer-wide zone of northwest-trending faults which likely is the extension of the Whittier fault, located farther to the southeast. Lamar (1961, 1970) has mapped this region of crosscutting faults. No conclusive evidence exists to suggest connection of the Santa Monica fault and the Raymond Hill fault by a fault segment which has demonstrated Quaternary displacement. Figure 5 shows fault traces, proposed from field studies in the Los Angeles River flood plain, which may connect the Santa Monica fault with the Raymond Hill fault.

Between the western banks of the Los Angeles River and the fault scarp marking the western onset of the Raymond Hill fault, at Arroyo Seco, the northwest-trending series of complex faults (the Whittier fault extension) are younger than and offset the east-northeast-trending Santa Monica fault in a right-lateral sense. In the vicinity of the Puente Hills, these faults dip 65^{o} to 75^{o} NE and have displaced Quaternary strata in a reverse sense, northeast side up (Woodford and others, 1954), and also in a right-lateral strike-slip sense (Lamar, 1970). The Workman Hill fault (Figure 3) is considered potentially active by the Association of Engineering Geologists (1973).

Lamar (1970) has noted that only two northwest-trending faults display relatively recent geomorphic features; deflected stream courses and topographic expression are associated with the San Rafael and Eagle Rock faults.

The Raymond Hill fault has been active in recent times. From its western limit at Arroyo Seco, near its obscurred intersection with the San Rafael fault (Lamar, 1970), to its eastern extent, where it merges with the Sierra Madre fault (Figure 3), the Raymond Hill fault can be accurately traced along its 19 kilometer length by a prominent scarp in the Quaternary surface alluvium (Bryant, 1978; Yerkes and others, 1965). It is a reverse

fault, north side up (1060-1220 meters vertical separation) along which the crystalline basement complex (Cretaceous and pre-Cretaceous age) has been juxtaposed against upper Miocene sedimentary rocks (Yerkes and others, 1965). A steep gravity gradient across the Raymond Hill fault suggests approximately 200 meters of displacement in the bedrock, beneath the alluvium (Bryant, 1978).

Latest movement on the Raymond Hill fault has occurred within approximately the last 200 to 3100 years (Payne and Wilson, 1974). Evidence for faulting within this time period includes age dating of carbonaceous sag pond material and fault gouge at 3100 years and a fresh fault scarp; small gullies upslope of this scarp show only minimal erosion. The one sample of crack fill, used in the age dating, is not conclusively fault gouge. Carbonaceous samples in the same area are presently being dated and should provide more reliability and control on dating movement along this fault (Robert Hill, pers. commun., 1978). Bryant (1978) has recently reviewed the Raymond Hill fault. His review includes a generalized geologic map showing the location of the Raymond Hill fault (Bryant, 1978; Plate 1, p. 136-7).

Sierra Madre Fault Zone

Only a minor portion of the Sierra Madre fault system lies wihtin this study area, at its northeastern corner. The fault is of active status and deserves mention here. It is part of the east-trending, north-dipping reverse fault system, which includes the San Fernando fault, lying along the base of the San Gabriel Mountains where granitic and metamorphic basement have been thrust upwards on the north side and juxtaposed against Tertiary and Quaternary nonmarine deposits (Yerkes and others, 1965; Jennings and Strand, 1969). Scarps which offset alluvial deposits are present at several localities along the fault (Wiggins, 1974); two scarps noted by Lamar and others (1973) in the Dry Canyon fan near Cucamonga stand six meters high and 30 meters high, respectively, across the active fan.

Santa Monica Fault Zone: West of Beverly Hills

West of Beverly Hills, the Santa Monica fault is only inferred beneath alluvium from oil company well data (Yerkes and others, 1965; Wiggins, 1974) and nowhere displays any recent geomorphic expression (Yerkes and

Wentworth, 1965). Evidence for at least lower Pleistocene fault displacement has been cited by Hoots (1931) across the mouth of the Potrero Canyon. He has also postulated up to nine meters of movement along a late Pleistocene alluvial fan in this vicinity. East of the mouth of Topanga Canyon, Campbell and others (1966) noted minor faults displaying a maximum of three meters of offset in upper Pleistocene deposits and associate them with the most recent movement along detachment faults active during Miocene thrusting in the central Santa Monica Mountains. The problem of assessing the recency of movement along this segment of the Santa Monica fault system is that Pleistocene and Holocene deposits are only locally exposed and rarely well-preserved (Yerkes and Wentworth, 1965). The Los Angeles Department of City Planning (Wiggins, 1974) classifies this fault as potentially active, showing no movement since late Pleistocene.

The latest evidence for diastrophsim on the Malibu Coast fault, from the city of Santa Monica west to the vicinity of the Point Mugu earthquake, are warped and disrupted late Pleistocene marine terrace platforms and deposits (Yerkes and Wentworth, 1965). Yerkes and Wentworth (1965) note at least seven sites at which late Pleistocene deposits have been offset with up to at least four meters of vertical separation. The age of these marine terrace platforms is bracketed between 35,000

years old and 280,000 years old. Recent deposits, which include nonmarine cover overlying the faulted Pleistocene terraces, flood-plain deposits, and stream deposits, show no signs of geomorphic or geologic disturbance (Yerkes and Wentworth, 1965). Although localized late Pleistocene fault movement is evident, it represents a relatively minor period of tectonism when compared with late Miocene to middle Pleistocene deformation involving displacements of thousands of meters (Campbell and others, 1966).

The offshore continuation of the Malibu Coast fault, near the Point Mugu area, is discussed by Junger and Wagner (1977). From seismic profiles, they interpret a zone of scattered faulting with apparent terminations in Pleistocene sediments to the east of the Hueneme submarine canyon (Figure 2). Most of these faults can be traced to the surface, where they cut the sea floor. These segmented faults, shown in Figure 3, are presented as a broad zone by Junger and Wagner (1977) rather than a continuous and coherent fault, as is the case onshore. Greene and others (1975) have recognized a northwest-trending graben structure on the eastern flank of the Mugu submarine canyon (Figures 2 and 3) which offsets the Holocene basement 15 to 25 meters. This graben locates within the Point Mugu earthquake and aftershock zone.

The Malibu Coast fault is paralleled to the south along the Santa Monica shelf and slope by the active

east-northeast-trending Dume fault which has been mapped by several authors (Vedder and others, 1974; Ziony and others, 1974; Greene and others, 1975; Junger and Wagner, 1977; and Nardin and Henyey, 1978) and has been correlated with the onshore Santa Monica fault. The trace of the Dume fault presented in Figure 3 approximates the trends of Vedder and others (1974), Ziony and others (1974), and Nardin and Henyey (1978), whose maps all agree on its location. A zone of folded, faulted, and sheared slope deposits, up to ten kilometers wide involving Quaternary sediments and upper Pleistocene marine terrace deposits, lies between this offshore fault and the Malibu Coast fault to the north (Birkeland, 1972; Vedder and others, 1974; Ziony and others, 1974; Nardin and Henyey, 1978). The youngest faulting associated with the Dume fault trace is recorded in Holocene shelf sediments. Two parallel west-trending fault traces, from Santa Monica to just east of Point Dume, are approximately one-half kilometer apart, nearly continuous, and form a horst which offsets the Holocene base usually five to ten meters (Greene and others, 1974; plate 10).

From a high resolution profile within the vicinity of Greene and others' interpretation, Nardin and Henyey (1978; Figure 2B) have identified an unconformity, offset by the Dume fault trace with the south side down, which has been interpreted to be approximately 100,000 years old.

FAULT-PLANE SOLUTIONS

General Statement

The fault-plane solutions presented in Figures 16 and 17 are discussed individually, below. The description of each solution includes time of origin of the earthquake and the strike and dip of the suggested fault planes. Closed circles represent compressional onsets and open circles represent dilatational onsets. The smaller circles represent emergent onsets which are either more poorly defined first-motion onsets or onsets lying along the strike of the nodal plane. In a double-couple earthquake radiation pattern the dislocation along the fault plane is nil. Therefore, a pattern of emergent onsets lying along a great circle of the equal-area projection is suggestive of a nodal plane. This guideline was frequently used in deciding upon the orientation of nodal planes. After a set of nodal planes (fault planes) had been chosen which best fit the data points from a first-motion plot, then a preferred fault-plane orientation

was often determined from known geologic field relationships associated with the causative faults.

Three possible problems limiting the precision of a fault-plane solution are addressed in Appendix G. The reliability of a fault-plane solution is dependent upon the choice of a crustal velocity model. Six possible velocity models (Figure 9) were used to determine the fault-plane solutions for five well-located events. Comparing the resultant fault-plane solutions for each event, the standard deviation in strike was 36.5^{o} and dip 27^{o}.

Newport-Inglewood Fault Zone

Fault-plane solutions for the 1973-1976 earthquakes associated with the Newport-Inglewood fault zone describe right-lateral strike slip trending north-south and high-angle reverse slip trending northwest. The preferred focal mechanism for solutions 1 and 2 (Figures 16 and 20) and composite solution A (Figures 17 and 20) is right-lateral strike slip along an approximately vertical fault striking north-south. Events 1 and 2 are spatially and temporally related, occurring along the northern portions of the Charnock and Overland Avenue faults within a ten day period. Data from these and two other spatially related events (7505042027 and 761005224; Table 5) when

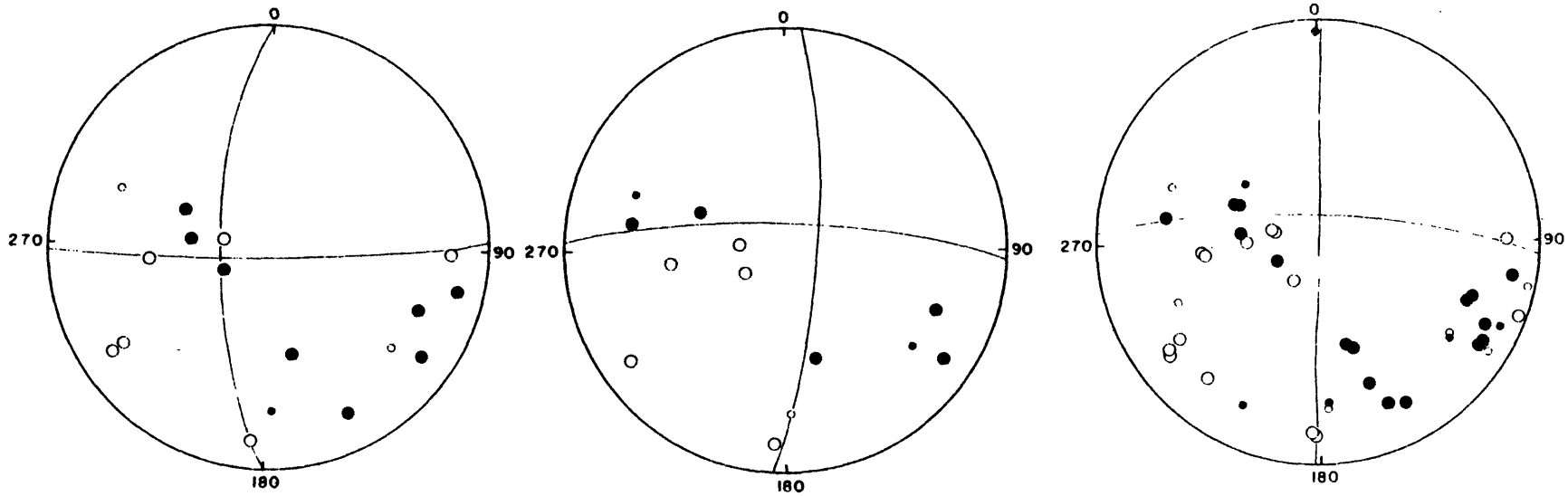

Solution 1: 731129
NS; 72°W
N88°E; 86°S
(N44°E)

Solution 2: 731209
N4°E; 78°E
N88°W; 80°N
(N48°E)

Solution A
N2°E; 90°
N88°W; 80°N
(N45°E)

Figure 20. Fault-plane solutions 1, 2, and A. Solution includes year, month day; strike and dip for both possible fault-plane solutions; and orientation of compressional stress vector (in parentheses).

composited (solution A) lend support to the right-lateral strike-slip fault mechanism for this portion of the Newport-Inglewood fault. Focal depths for solutions 1 and 2 are 14 kilometers and 15 kilometers (± 5 km), respectively. These focal depths locate within the basement rocks and support a steeply-dipping fault surface, suggested by the focal mechanisms.

Fault-plane solution 3 (Figures 16 and 21) and composite fault-plane solution B (Figures 17 and 21) are for events which occurred near the location of the 1920 Inglewood earthquake (Richter, 1958) at the southern termination of the Overland Avenue fault. Solution B is composed of data points from solution 3 and from a sequential event (7311180733; Table 5), triggered approximately four minutes later. The same focal mechanism (from solution 3) satisfies the data points for solution B--reverse slip on a northwest-striking fault plane which dips either to the northeast (32^{o} NE) or to the southwest (58^{o} SW). The focal depth for solution 3 is 6.9 kilometers (± 5 km) which does not preclude either fault plane from consideration.

The epicenter for solution 4 (Figures 16 and 21) lies to the southeast of epicenter for solutions 1, 2, and A, on the surface trace of the Charnock fault. Solution 4 shows reverse slip northwest similar to solutions 3 and B. The orientation of the possible fault

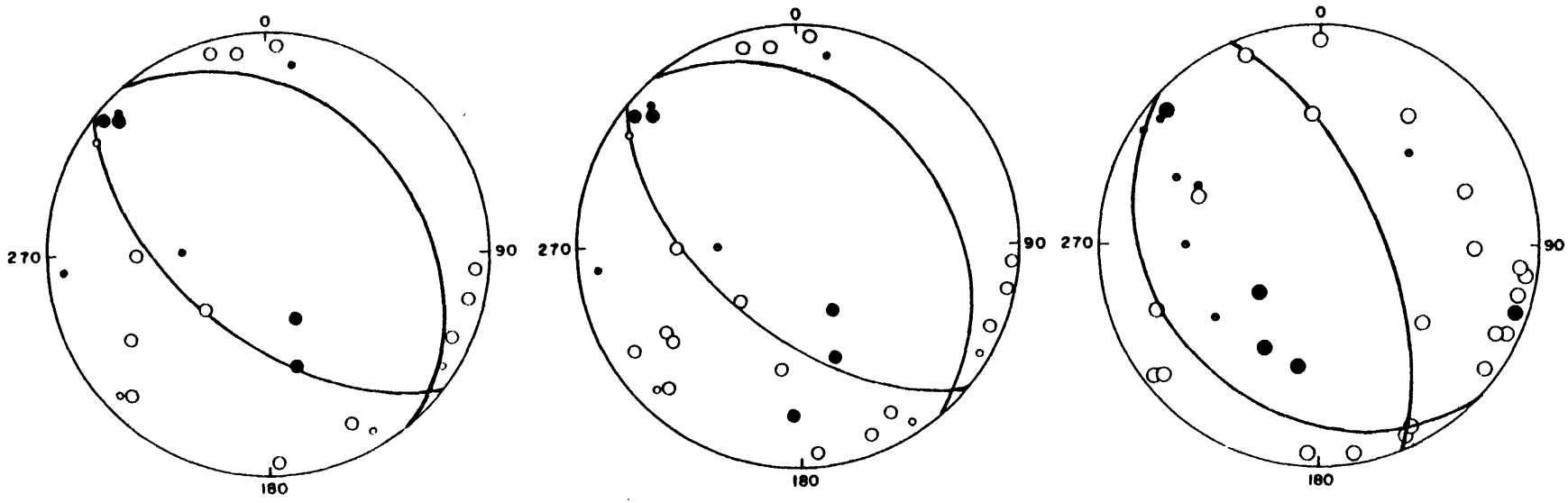

Solution 3: 731118(0729)
N40°W; 32°NE
N50°W; 58°SW
(N50°E)

Solution B
N40°W, 32°NE
N50°W; 58° SW
(N50°E)

Solution 4: 741022(1213)
N24°W; 66°NE
N48°W; 26°SW
(N54°E)

Figure 21. Fault plane solutions 3, B, and 4.

planes are N48° W; 26° SW and N24° W; 66° NE. The calculated focal depth of 7.1 kilometers (± 5 km) does not constrain the choice of fault planes.

Solutions 5 and 6 (Figures 16 and 22) lie west of the trend of the Charnock fault in the vicinity of the city of Hawthorne and the Los Angeles International Airport, respectively. The derived focal mechanism for both events is reverse slip across similarly dipping fault planes with orientations of N87° W; 28° S (solution 5) and N51° W; 30° SW (solution 6) or N62° W; 65° NE (solution 5) and N72°W; 62° NE (solution 6). Either set of fault planes can accommodate reverse slip associated with movement along the Newport-Inglewood fault zone. Focal depths are 10.5 kilometers (± 5 km) and 9.5 kilometers (± 5 km), respectively. Projecting hypocenters for events 5 and 6 on the southwest-dipping fault planes would realign both events within the Newport-Inglewood fault zone, at depth.

Composite fault-plane solutions C (Figures 17 and 23), D (Figures 17 and 23), and E (Figures 17 and 24), compiled from earthquakes in the zone of northwest-trending, en echelon faults and folds associated with the Inglewood and Potrero faults (with the Newport-Inglewood fault zone) support the existence of a large component of reverse faulting in this region. Solution C either strikes N74° W along a steeply-dipping fault plane

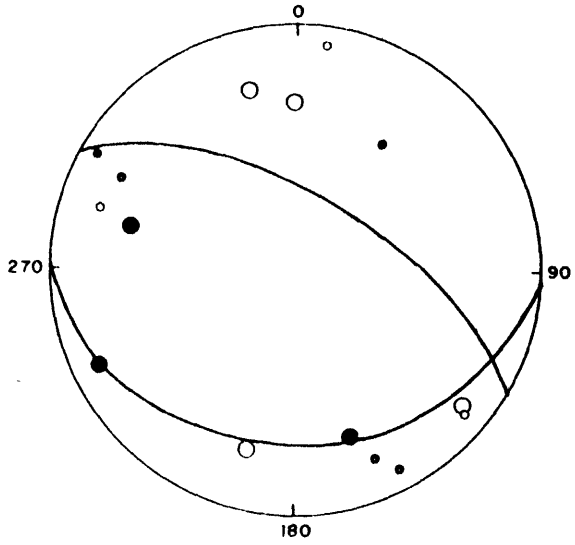

Solution 5: 740117
N62°W; 65°NE
N87°W; 28°S
(N15°E)

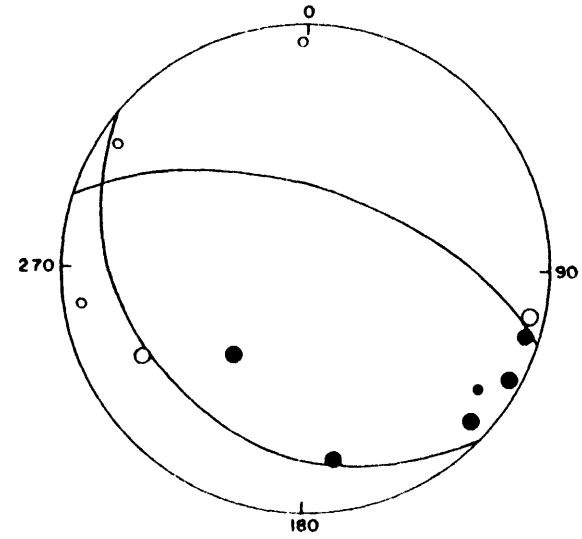

Solution 6: 750504(2016)
N51°W; 30°SW
N72°W; 62°NE
(N21°E)

Figure 22. Fault-plane solutions 5 and 6.

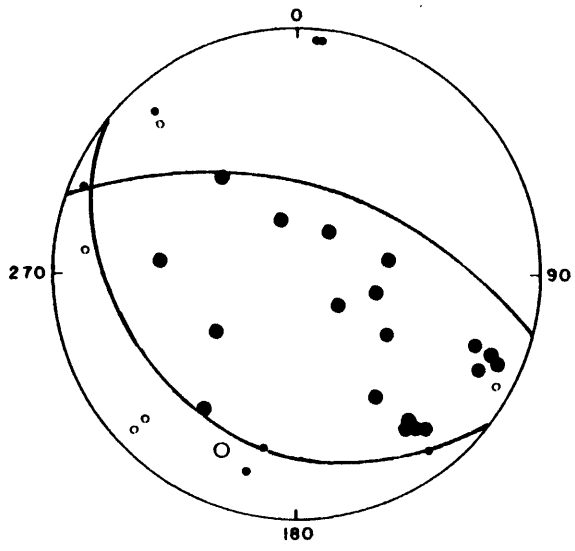

Solution C
N52°W; 32° SW
N74°W 60° NE
(N26°E)

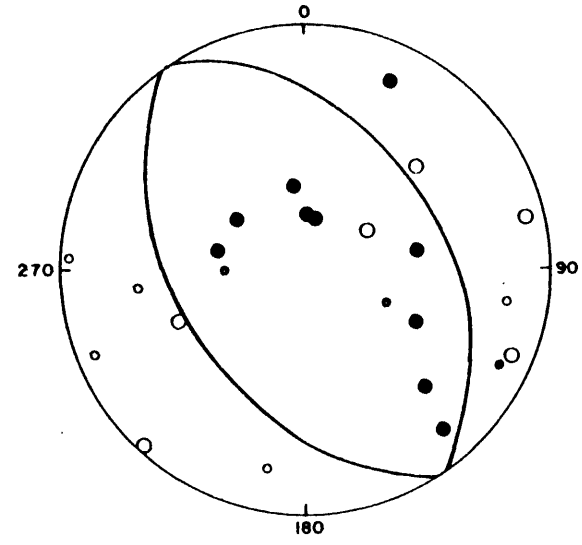

Solution D
N34°W; 44° NE
N34°W; 46° SW
(N56°E)

Figure 23. Fault-plane solutions C and D.

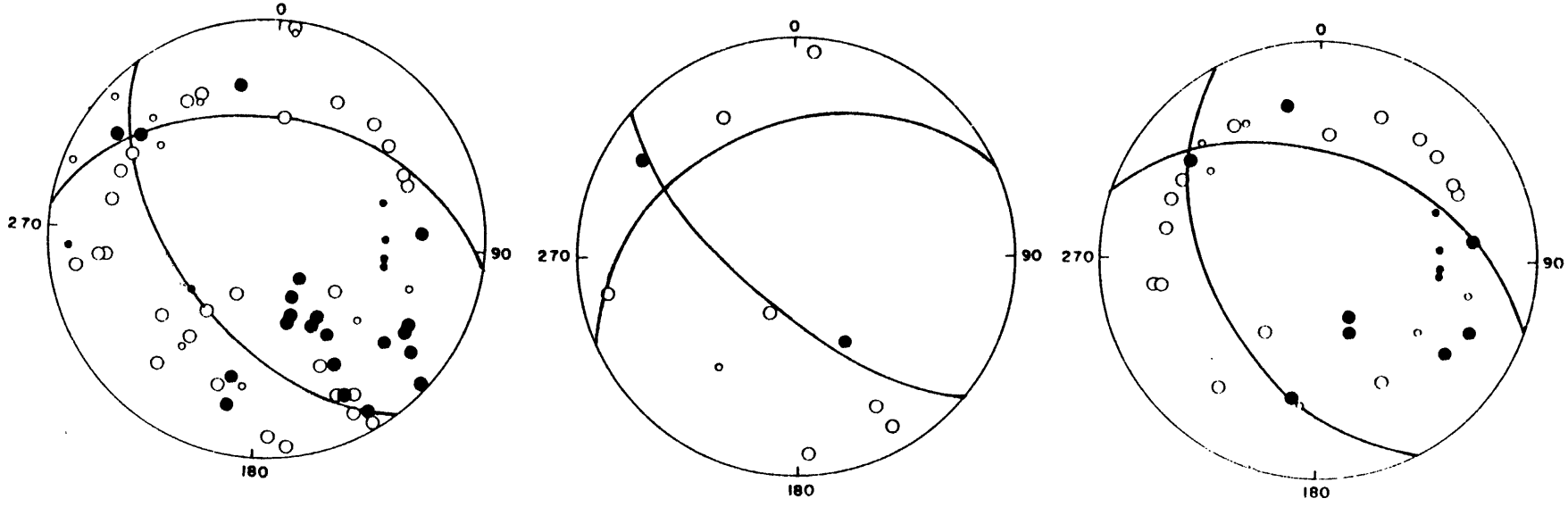

Solution E
N40°W; 56°SW
N83°W; 44°N
(N17°E)

Solution 7: 730520
N48°W; 70°SW
N66°E; 40°NW
(N9°E)

Solution 8: 761115
N30°W; 48°SW
N73°W; 50°NE
(N39°E)

Figure 24. Fault-plane solutions E, 7, and 8.

(60° NE) or strikes N52° W along a shallowly-dipping fault plane (32° SW). The shallowly-dipping fault plane is well defined by emergent P-wave arrivals which, in turn, defines the auxilary fault plane. Focal depths to four of the five events composing solution C all plot between the depths of 8.0 kilometers (± 5 kilometers) and 10.5 kilometers (± 5 kilometers). Data points for solution D constrain the focal mechanism to nearly pure reverse slip although the strike may vary up to 26°, from N26° W to N52° W. Dips of the possible fault planes are 44° NE and 46° SW.

Fault-plane solutions 7 and 8 (Figures 16 and 24) have been combined with four other spatially clustered events to form composite fault-plane solution E (Figures 17 and 24). All three solutions suggest that reverse faulting is also present along the southern portion of the Inglewood and Potrero faults. A minor component of right-lateral strike-slip displacement is present on the preferred fault plane which strikes to the northwest and dips to the southwest. The dips on the various faults range from 48° SW to 70° SW. The data points from the four additional events (7503270652, 7510270207, 7511250236, and 7609020256) comprising part of solution E are also plotted in Figure 24. The preferred focal mechanism for these combined earthquakes is also reverse faulting with a minor component of right-lateral strike-slip

displacement (N40° W; 56° SW). Two events from solution E have reliable focal depths computed at 15.9 and 8.0 kilometers (± 5 kilometers), which is consistent with focal depths computed for other earthquakes associated with this zone of deformation.

Focal mechanisms for solution 9 (Figures 16 and 25) and composite solution F (Figures 17 and 25), derived from a cluster of seven events near the cities of Paramount and Lakewood (Figure 3) demonstrate reverse slip with a large component of strike-slip. Reverse faulting, also present to a significant degree in ten of the thirteen fault-plane solutions (solutions 3, 4, 5, 6, 7, 8, B, C, D, E) presented for the Newport-Inglewood fault zone, appears to be as common and important a faulting mechanism as right-lateral strike-slip faulting. Unlike these same solutions (solutions 3, 4, 5, 6, 7, 8, B, C, D, E), the data points for solutions 9 and F do not suggest a northwest-trending fault plane. For both solutions 9 and F, right-lateral strike-slip motion is accommodated as a component on a reverse fault oriented N86° W; 38° S or left-lateral strike-slip motion is accommodated on a reverse fault oriented N53° E; 60° NW. Thus, neither solution can be preferred to fit the pattern of faulting developed from the previous fault-plane solutions associated with the more northerly portion of the Newport-Inglewood fault zone.

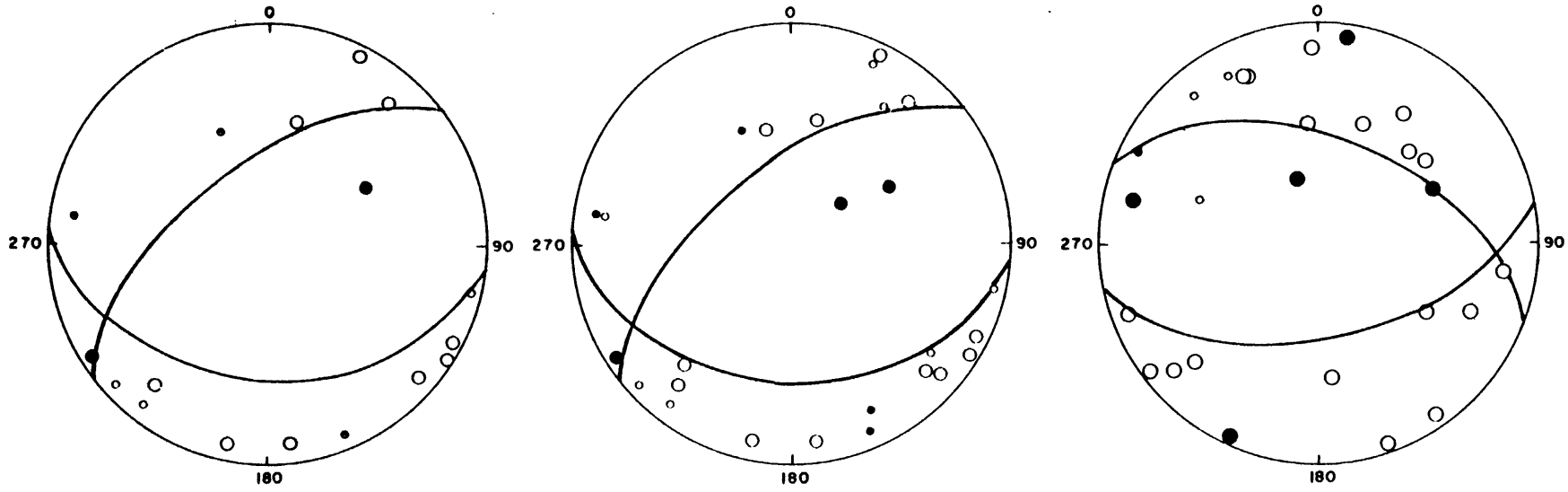

Solution 9: 760715
N53°E; 60°NW
N86°W; 40°S
(N16°W)

Solution F
N53°E; 60°NW
N86°W; 40°S
(N16°W)

Solution 10: 760627
N68°W; 50°NE
N80°E; 54°SE
(N15°E)

Figure 25. Fault-plane solutions 9, F, and 10.

Solution 10 (Figures 16 and 25) occurred to the east of the Newport-Inglewood fault zone and south of the Santa Monica fault zone, within the Los Angeles city limits. The event is not associated with any known active fault. The fault-plane solution indicates reverse slip on a north- or south-dipping fault plane oriented either N68^{o} W; 50^{o} NE or N80^{o} E; 54^{o} SE.

Fault Plane Solutions: Santa Monica Bay

Offshore, in the Santa Monica Bay, six fault-plane solutions, derived from events occurring along faults associated with the northwest extension of the Palos Verdes fault (Figures 16 and 17), reveal that fault movements have probably been restricted to fault planes trending northwest.

Composite fault-plane solution G (Figures 17 and 26), derived from a cluster of three earthquakes (events 7303292135, 7503071629, 7509271247), locates just south of the Santa Monica fault, where it extends offshore to meet the Dume fault, and slightly east of the northwesterly-trending fault which intersects the Dume fault, as mapped by Junger and Wagner (1977). Choosing between the two possible fault planes, movement has most likely occurred in a normal sense along a plane striking N42^{o} W and dipping 79^{o} NE. This fault plane parallels the northwest-trending fault but is inconsistent with its displacement (east

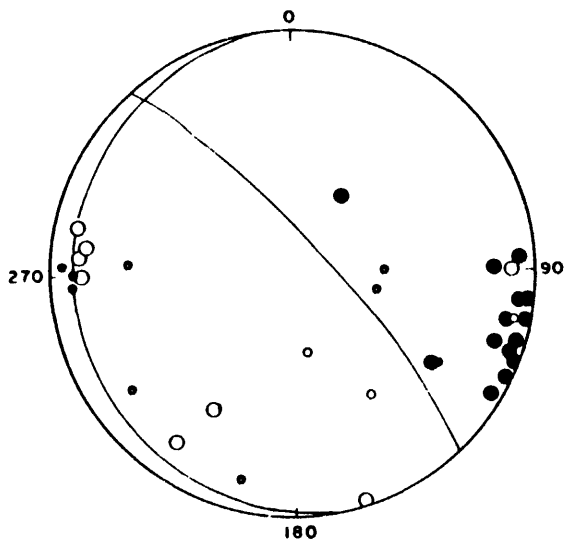

Solution G
N42°W; 79°NE
N9°W; 11°W
(N26°W)

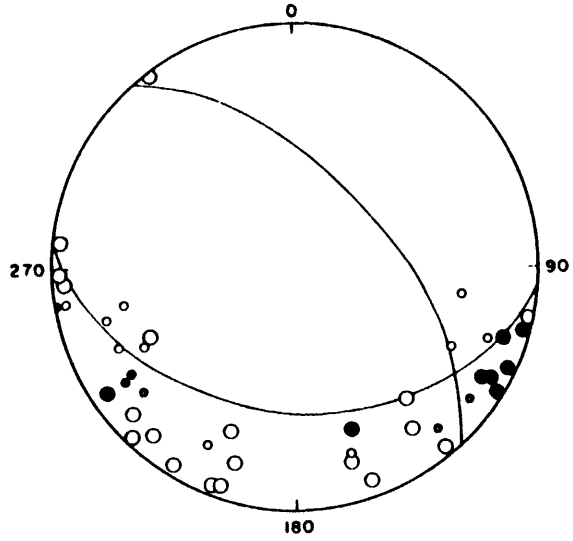

Solution H
N41°W; 60°NE
N85°W; 40°S
(N27°E)

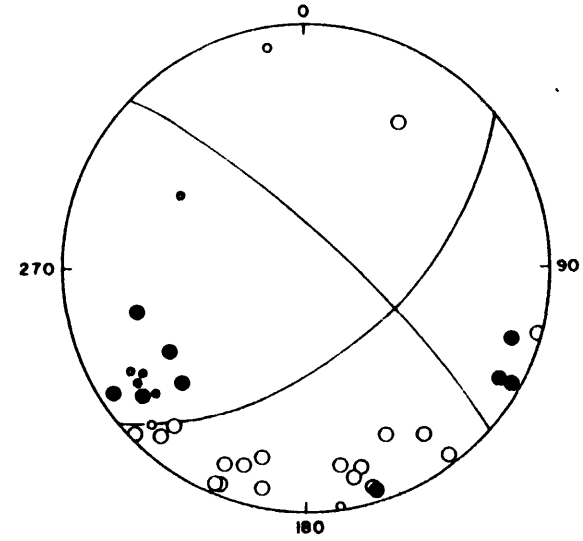

Solution I
N50°E; 60°SE
N46°W; 79°NE
(N2°E)

Solution 11; 751007
N46°W; 40°SW
N61°W; 50°NE
(N37°E)

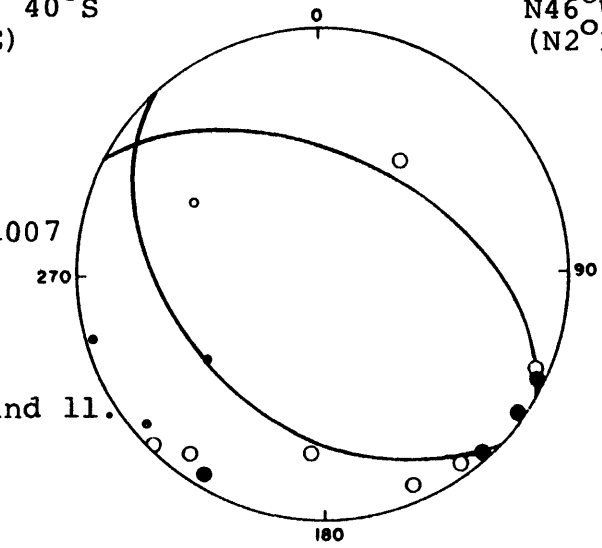

Figure 26. Fault-plane solutions G, H, and 11.

side up) as mapped by Junger and Wagner (1977). Since this fault is truncated by the dominant east-west trending Santa Monica-Dume fault system, constraints are imposed on possible strike-slip movement. Consistent with this condition, the preferred fault plane exhibits only a minor component of right-lateral strike slip.

To the south, focal mechanisms for composite fault-plane solutions H and I (Figures 17 and 26) suggest the presence of an increased right-lateral strike-slip component of displacement with an increased distance, south, away from the east-west trending Dume fault. Solutions G, H, and I have a common fault plane striking approximately northwest and dipping steeply to the northeast (dips of 79°NE, 60°NE, and 79°NE, respectively). This fault plane orientation is contrary to the southwest dip of the onland Palos Verdes fault, further to the south. This same phenon-menon has been observed by Terry and others (1956) in an earlier interpretation of the Palos Verdes Hills fault. They suggest the fault changes from a steep southwesterly dip onland to a steep northeasterly dip in the offshore bay area.

Further south in the Santa Monica Bay, solution 11 (Figures 16 and 26) describes reverse faulting with a minor component of strike-slip displacement. Although motion on either fault plane is possible, the fault plane striking N46° W and dipping 40° SW also accommodates

right-lateral strike-slip displacement and agrees with the orientation of the onland portion of the Palos Verdes fault.

A sequence of four earthquakes occurred on November 22, 1976 in the Santa Monica Bay and trend northwest on the northern flank of the Santa Monica submarine canyon across a portion of the Palos Verdes Hills fault extension, which has moved most recently during the late Pliocene (Figure 2; Junger and Wagner, 1977). The location of these events is outlined in Figure 17 by composite fault-plane solution J (Figure 27). Fault-plane solution 12 (Figures 16 and 27) and solution J both define right-lateral strike-slip motion on a steeply-dipping fault plane which strikes north-northwest. The preferred fault plane for solution 12 is N10^{o} W; 70^{o} W. The preferred fault plane for solution J is N20^{o} W; 80^{o} NE. The data points from solution 12 are incorporated as part of composite solution J.

The sequence of four epicenters align along a trend striking N15^{o}W which also supports the above preferred solutions. The alternative fault planes are both left-lateral strike-slip trending approximately east-northeast, parallel to the Dume fault trace, three kilometers to the north. The location and possible focal mechanisms for solutions J and 12 are similar to solutions A, 1, and 2, which occurred on the Newport Inglewood fault, only several kilometers south of the Santa Monica fault.

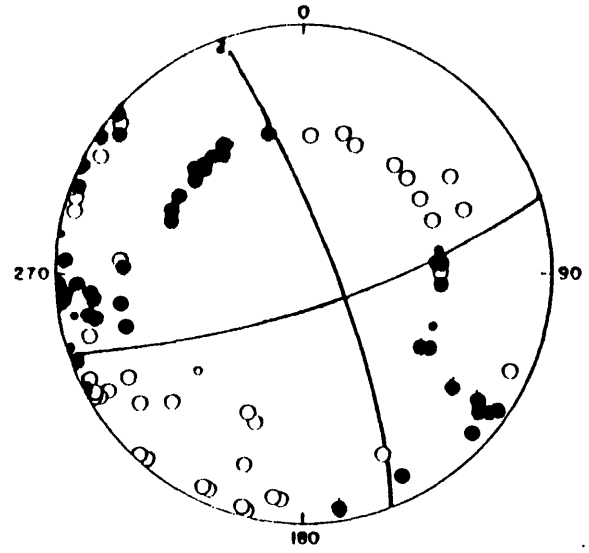

Solution J:
N20°W; 80°NE
N73°E; 78°SE
(N26°E)

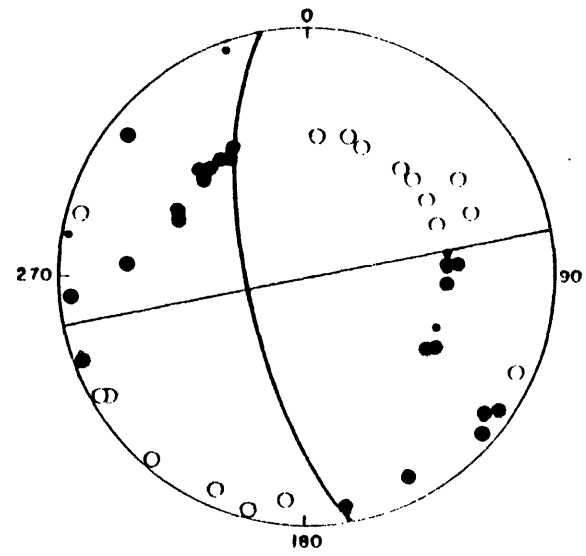

Solution 12:
N10°W; 70°W
N80°E; 90°
(N35°E)

Figure 27. Fault-plane solutions J and 12.

South of this cluster, Nardin and Henyey (1978) have identified a west-northwest-trending fault along the southern flank of the Santa Monica submarine canyon which displaces late Quaternary strata, north side down. This fault dips less than 30° and has been associated with a low-angle slump surface. It is unlikely that this fault was responsible for the strike-slip movement associated with the earthquake sequence to the north.

Further west in the Santa Monica Bay, but east of the Dume anticline, twenty earthquakes align along a broad northwest trend, parallel to the San Pedro escarpment (Figures 3 and 12). Portions of the San Pedro fault zone have moved since Quaternary time, but most of its length has not been active since the Pliocene (Junger and Wagner, 1977). Although seismic activity is high in this portion of the bay, no active faults have been mapped here. The quality of data decreases away from the coast due to less seismic station control over greater distances. Due to this circumstance, only two reliable fault-plane solutions, 13 and 14 (Figures 16 and 28), have been derived from events occurring in the outer Santa Monica Bay. Although neither solution is conclusive, both suggest reverse faulting with a minor component of strike slip.

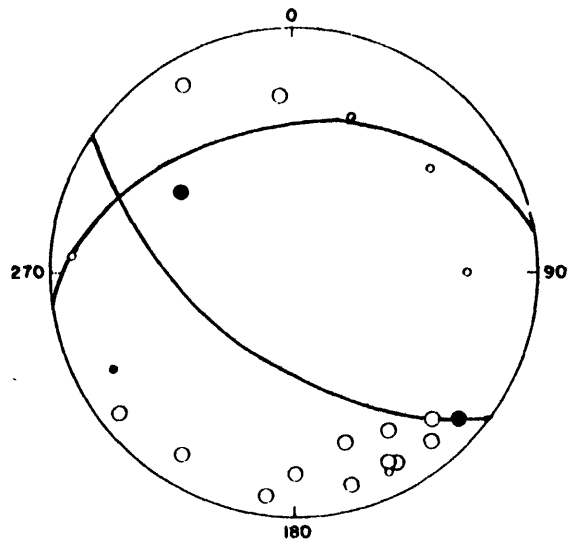

Solution 13: 730307(2349)
N55°W; 50°SW
N79°E; 40°N
(N12°E)

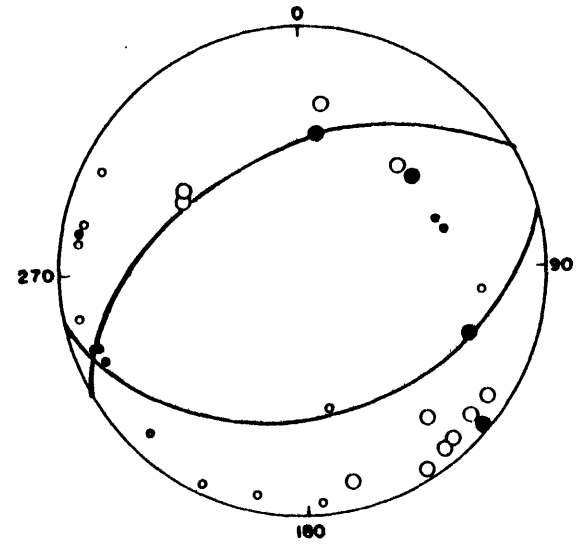

Solution 14: 750123
N61°E; 50°NW
N78°E; 40°SE
(N29°W)

Figure 28. Fault-plane solutions 13 and 14.

Fault Plane Solutions:
Santa Monica Fault, East of Beverly Hills

Four fault plane solutions (15, 16, 17, and 18; Figures 16 and 29) align along the surface traces of the Santa Monica fault between Beverly Hills and Hollywood. In the Hollywood-Los Angeles area, the east-northeast trace of the Santa Monica fault is transected by a zone of northwest-trending faults along the projection of the Whittier and Workman Hill fault (Figures 3 and 5). Three additional fault-plane solutions (19, 20, and 21; Figures 16 and 30) have been derived from earthquakes occurring along this northwest-trending zone of transecting faults, south of the Santa Monica-Raymond Hill fault zone.

Contrary to northwest-trending focal mechanisms for earthquakes occurring south of the Santa Monica fault system, specifically along the Palos Verdes fault extension in the Santa Monica Bay and along the Newport-Inglewood fault zone, fault planes associated with the Santa Monica fault zone generally trend to the northeast. This trend coincides with the east-northeast trend for the surface trace of the Santa Monica fault in this region reverse fault displacement is the dominant fault mechanism for all four solutions (15, 16, 17, and 18). The preferred fault plane for solution 18 is N79^{o}E; 64^{o} N and agrees

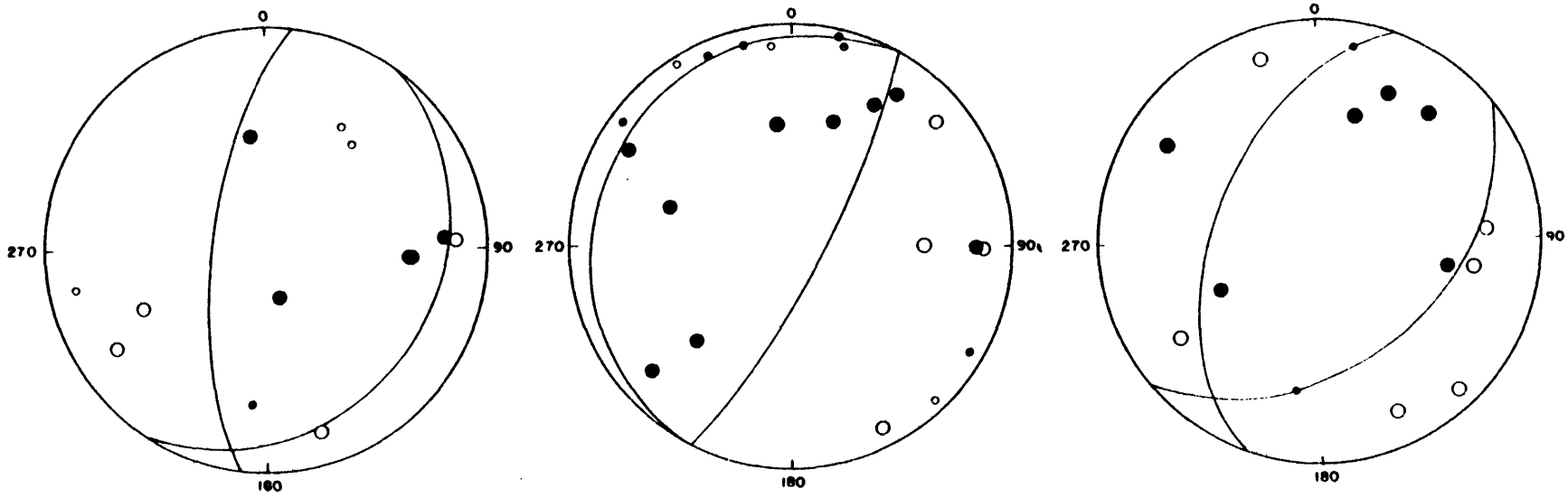

Solution 15: 760929
N6°E; 70°W
N36°E; 24°SE
(N76°W)

Solution 16: 740312(0735)
N29°E; 12°NW
N29°E; 78°SE
(N61°W)

Solution 17: 740306
N21°E; 50°NW
N53°E; 44°SE
(N53°W)

Solution 18: 741206
N49°E; 30°SE
N78°E; 64°N
(N26°W)

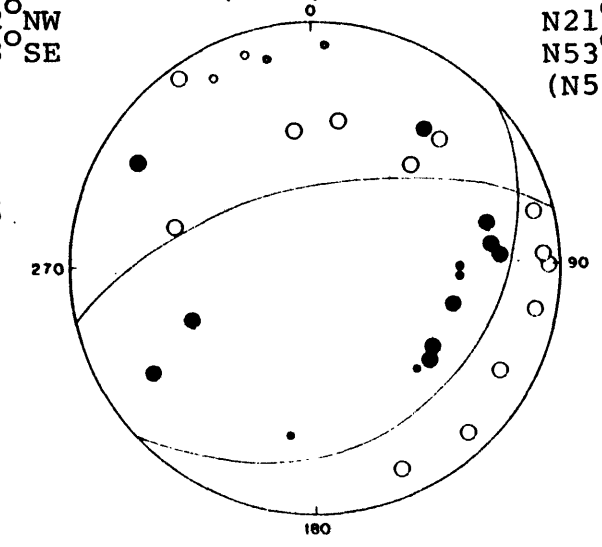

Figure 29. Fault-plane solutions 15, 16, 17, and 18.

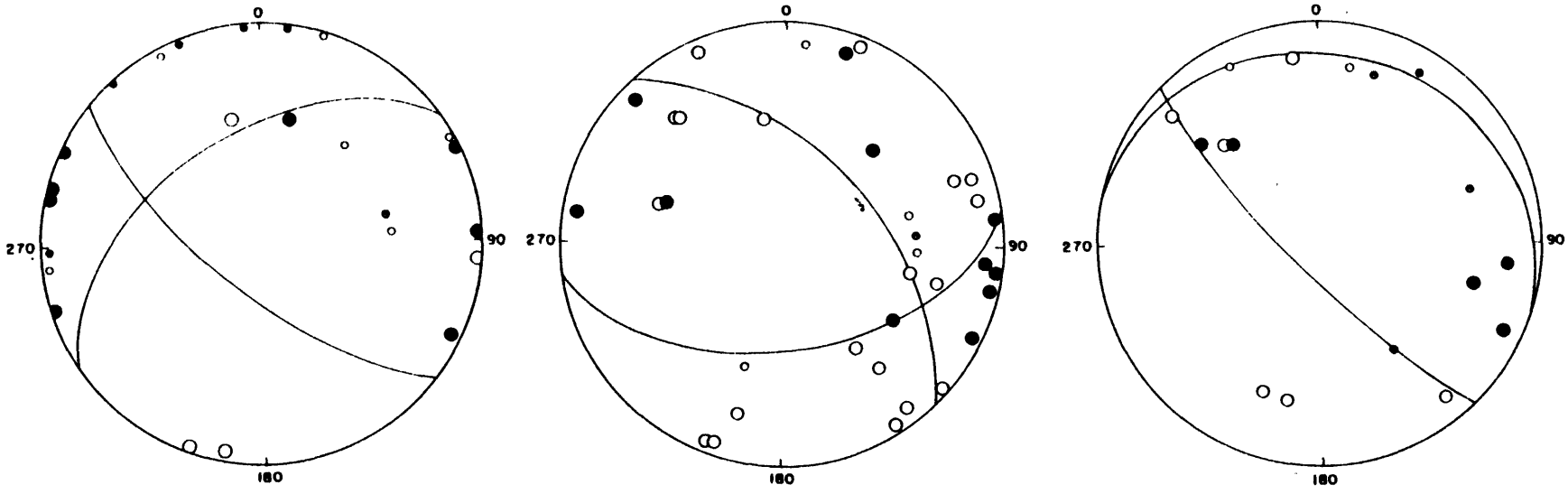

Solution 19: 751011
N50°W; 72°SW
N55°E; 48°NW
(N2°E)

Solution 20: 741219
N42°W; 56°NE
N81°E; 50°S
(N61°E)

Solution 21: 740227
N44°W; 80°SW
N76°W; 16°N
(N30°E)

Figure 30. Fault-plane solutions 19, 20, and 21.

with north-over-south reverse faulting common along the southern frontal fault system of the Santa Monica Mountains. The fault planes for the other three solutions trend more northerly than the trace of the Santa Monica fault zone. The preferred fault plane for solution 17 is N21^{o} E; 50^{o} NW. A preferred fault plane for solutions 15 and 16 is indeterminable with respect to the Santa Monica fault zone.

No fault-plane solutions have been derived for events on or north of the tectonically active Raymond Hill fault. South of the Raymond Hill fault, three solutions (19, 20, and 21; Figures 16 and 30) spatially align within the zone of northwest-trending faults projecting north from the Whittier fault zone. The focal mechanism for solutions 20 and 21 is reverse slip on preferred fault planes striking northwest, parallel to the trend of the fault zone. For solution 20, the fault plane oriented N42^{o} W; 56^{o} NE also exhibits a component of right-lateral strike-slip displacement (besides reverse displacement) which agrees with known displacement along the Whittier fault system. Solution 21 shows only reverse displacement most likely across a steeply-dipping fault plane oriented N44^{o} W; 80^{o} SW.

The possible fault planes for solution 19 satisfy fault displacements for both the northwest-trending fault zone, described above, and the northeast-trending Raymond Hill fault. The northwest-trending fault plane is oriented

N50° W; 72° SW and accommodates right-lateral strike-slip faulting with a component a reverse fault displacement. The alternative fault plane, N55° E; 48° NW, is consistent with the known orientation of young geologic offsets on the Raymond Hill fault but lies south of its surface trace.

Solutions 19 and 20 each have several data points which do not fit the derived fault plane solutions and therefore are less reliable as unique solutions as compared to other solutions in this study. Both are presented here as the best representative fault-plane solutions from the existing data set (1973-1976 earthquakes) for this complex area. As discussed by Lamar (1970) and others, two fault systems with opposing trends (the Santa Monica fault system and the Whittier fault system) intersect in the Los Angeles River floodplain area, within the study area. At the intersection, crosscutting fault relationships are obscured by alluvium. Well-controlled fault-plane solutions would define present-day movement between these two fault systems and lead to an improved tectonic understanding of this complex geometry. Solutions 15, 16, 17, and 18 reveal no evidence for right-slip intervention (due to the Whittier fault system) west of the intersection zone of faults. The two solutions to the south (20 and 21) describe reverse and right-lateral strike-slip displacement on a fault plane striking northwest, which suggests

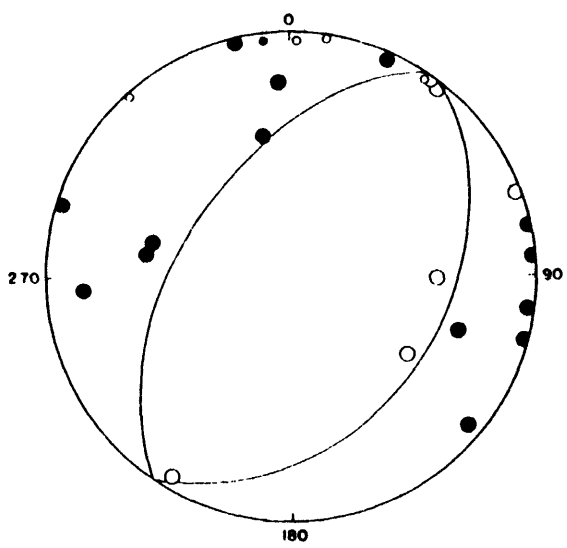

Solution 22: 741106(0038)
N36°E; 54°NW
N36°E; 36°SE
(N36°E)

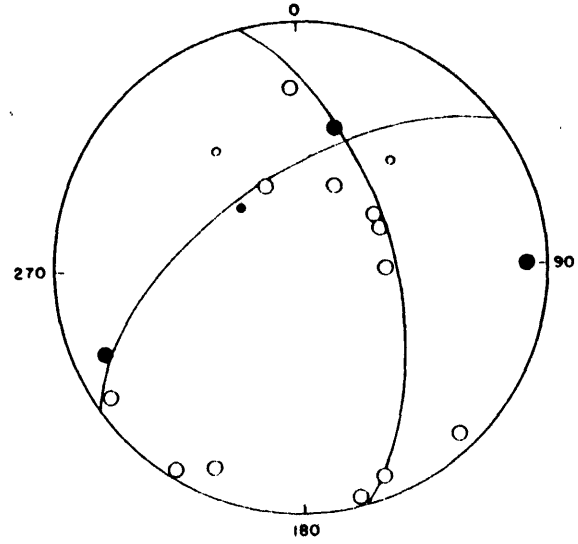

Solution K
N14°W; 58°E
N56°E; 60°NW
(N21°E)

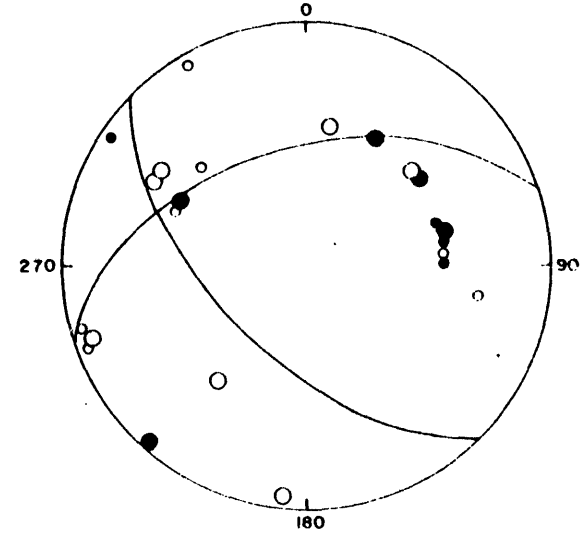

Solution 23: 760620
N46°W; 60°SW
N71°E; 50°NW
(N12°E)

Solution 21: 740331
N74°W; 30°SW
N88°E; 60°N
(N82°W)

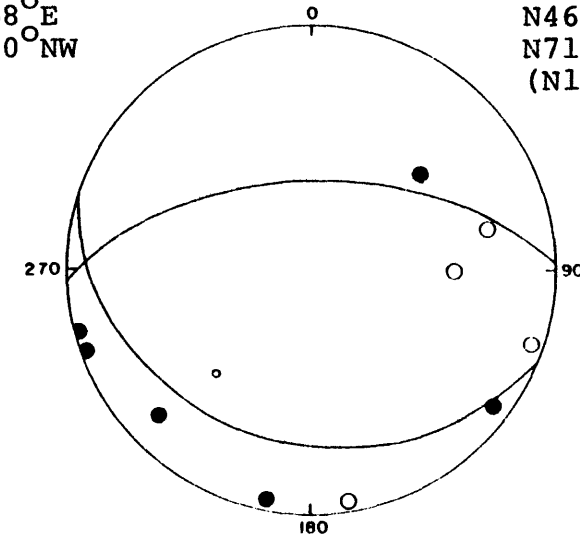

Figure 31. Fault-plane solutions 22, K, 23, and 24.

that the Whittier fault zone extension is the causative fault. Closer to the fault zone intersection, solution 19 describes two possible fault planes which can accommodata displacement occurring on either fault system.

Associated with the Sierra Madre fault, in the northeastern corner of the study area, fault-plane solution 22 (Figures 16 and 31) describes normal displacement across a fault plane striking N36^{o} E and dipping either 54^{o} NW or 36^{o} SE. Normal displacement for this event is contrary to the north-dipping reverse fault documented along this fault zone. Since only one solution is available on this isolated portion of the fault (in this study area) no conclusions have been drawn as to its consequences.

Fault Plane Solutions:
Santa Monica Fault Zone, West of Beverly Hills

In the northwestern Santa Monica Bay, within the Malibu Coast zone of deformation, focal mechanisms for solutions K and 23 (Figures 16, 17, and 31) show a large component of left-lateral strike-slip displacement and solution 24 (Figures 16 and 31) describes normal fault displacement. The preferred fault planes strike to the east and northeast. Even though the fault planes parallel the trend of the Santa Monica fault system, none of these solutions can be spatially assigned to a probable causative fault.

This significant component of left-lateral strike-slip displacement (from solutions K and 23) is also suggested by the alternative focal mechanisms for five solutions (1, 2, A, 12, and J; Figures 16 and 17) which all locate just south of the Santa Monica fault. Although the reverse fault mechanism appears dominant along the Santa Monica fault system, several solutions (1, 2, A, 12, J, 23, and K) suggest that left-lateral strike-slip displacement may also be an active component of faulting along and directly south of this fault system.

In the Santa Monica Mountain structural block, two fault-plane solutions are isolated and cannot be interpreted without additional supporting data. Solution 25 (Figures 16 and 32) defines normal fault movement along a northwest-striking plane. Its location is approximately five kilometers north of the Malibu Coast fault and five kilometers east of the Simi fault extension. The possible faults dip 70° SW and 20° NE.

The only other fault-plane solution, 26, (Figures 16 and 32) locates southwest of the Northridge Hills fault. The possible focal mechanisms are N48° W; 75° NE, reverse-slip with a large component of right-lateral slip or N60° E; 43° SE, left-lateral strike-slip.

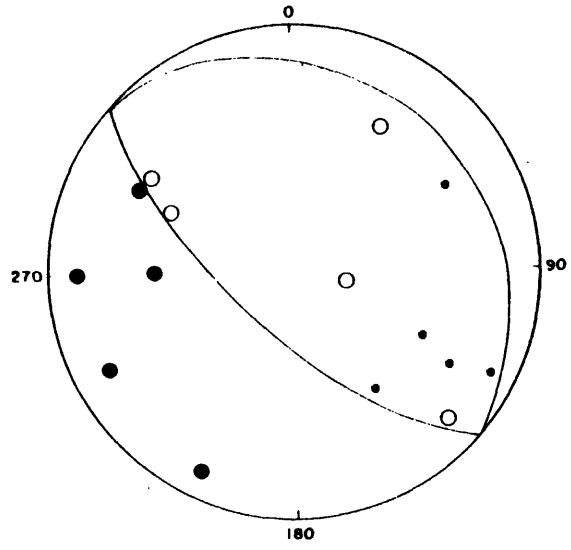

Solution 25: 760504
N48°W; 20°NE
N48°W; 70°SW
(N48°W)

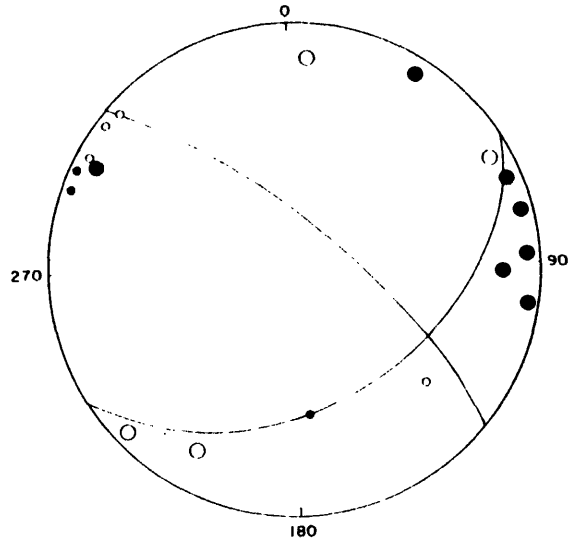

Solution 26: 750128
N48°W; 75°NE
N60°E; 43°SE
(N6°E)

Figure 32. Fault-plane solutions 25 and 26.

SEISMICITY PATTERNS, MAGNITUDES, AND FOCAL DEPTHS

The seismicity patterns and fault-plane solutions derived from four years of data (1973-1976) suggest that present-day tectonic activity is strongly controlled by several pre-existing major fault zones. Diffuse trends of seismicity align parallel, in a northwesterly direction, south of the Santa Monica fault system (Figure 33). Two trends coincide with the Newport-Inglewood fault zone and the Palos Verdes Hills fault extension in the Santa Monica Bay. The third diffuse trend begins north of Point Dume and projects southwestward from the Malibu Coast fault into the Santa Monica Bay, just east and parallel to the San Pedro basin fault zone (Figure 3). No mapped faults are associated with this trend.

Within the study area, the most concentrated group of seismic events occurred as a sequence of aftershocks subsequent to the February 21, 1973 Point Mugu earthquake, located along the westernmost mapped portions of the Malibu Coast fault and extending south, offshore, to the Dume fault (Figure 3). The areal extent of this sequence

Figure 33. Outline of seismicity trends.

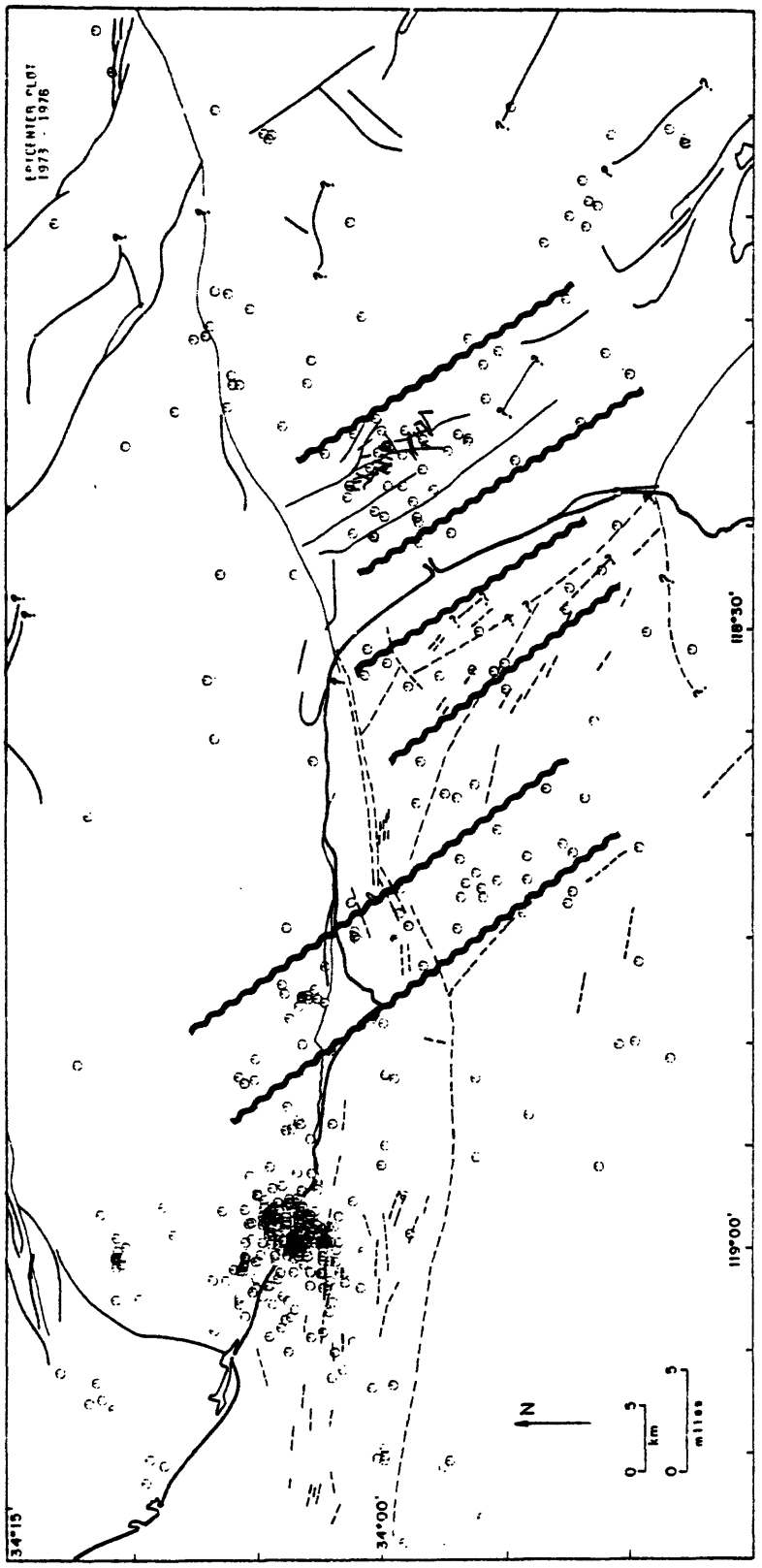
EPICENTER PLOT
1973 - 1976
118°30'
119°00'
34°15'
34°00'
N
0 5 km
0 5 miles

closely corresponds to the Malibu Coast zone of deformation as described by Yerkes and Wentworth (1965) to define the approximately 10 kilometer wide zone of Quaternary deformation south of the Malibu Coast fault and north of the Dume fault.

East of Point Dume, only one earthquake cluster is associated with the Santa Monica fault system. The cluster straddles the fault in the Hollywood area, west of the probable intersection with the Whittier fault zone. Between Point Dume and Hollywood, there is a noticeable lack of seismicity on the Santa Monica fault and to the north, within the Santa Monica Mountain block. The diffuse seismicity trends associated with the Newport-Inglewood and the Palos Verdes Hills fault zones terminate just south of the Santa Monica fault zone. The north-dipping Santa Monica fault is poorly delineated by the scattered epicenter distribution in the Santa Monica Mountain block. The mountain block has been seismically less active (east of Point Dume) than the Newport-Inglewood and Palos Verdes Hills faults. This lack of seismicity associated with the Santa Monica Mountains has also been documented by Lee and others (1979) for the western Santa Monica Mountains (1970-1975 earthquakes) and by Real (1979) for the eastern Santa Monica Mountains (1972-1975 earthquakes). Since the throughgoing Santa Monica fault terminates the northwest-trending structures and also

appears to be the northern boundary for most of the seismicy, part of the crustal shortening may presently be accommodated to the south as folding within the northwest-trending basin structures, as well as thrusting on the Santa Monica fault zone. From the distribution of epicenters, the Santa Monica fault and the northwest-trending faults, including those in the Santa Monica Bay, appear to be the major components of local tectonic deformation. Faults north of the Santa Monica fault have been seismically less active, thus the Santa Monica Mountains appear to remain as a relatively passive and coherent structural block.

The Newport-Inglewood seismicity trend aligns closely with the defined fault zone in the northwestern portion of the Los Angeles basin. The preferred vertical fault planes defined by solutions 1, 2, and A (Figure 20) agree with this alignment. An apparent concentration of events within the Baldwin Hills area represents a bias due to the BHSN's local station coverage.

Further to the southeast, earthquake epicenters continue to parallel the northwest-southeast trend of the Newport-Inglewood fault zone, but group slightly east of the Cherry Hill and Seal Beach faults (Figure 12). Ziony and others (1974) describe a northwest-trending fault in this epicentral area, near the cities of Paramount and Lakewood (Figure 3). Evidence of faulted early Pleistocene (2,000,000 to 500,000 years B.P.) marine terrace

deposits and unfaulted late Pleistocene (500,000-11,000 years B.P.) deposits bracket the latest movement along this fault. The fault is buried beneath Recent deposits and is largely inferred from ground water reports. Seven epicenters, between 1973 and 1976, align along the fault trace and extend beyond its northwest termination, as determined by Ziony and others (1974). If the trend of these epicenters is associated instead with the Newport-Inglewood fault zone, the data would suggest a steep northeasterly dip on the Seal Beach and Cherry Hill faults. Neither focal mechanism (Solutions 9 and F; Figure 25), which have been derived from this cluster, support a northeasterly-dipping fault plane.

On the Santa Monica shelf, seismicity has been concentrated along the length of the Palos Verdes Hills fault extension rather than the more precisely defined Redondo Canyon fault and the Palos Verdes Hills fault, to the south. Seismicity associated with the Whittier fault zone, the Sierra Madre fault and the central Los Angeles basin is marked by only isolated events.

The Point Mugu earthquake, which registered a magnitude of M = 5.9 in this study (Ellsworth and others [1973] estimated M = 6.0), and five other events have occurred of noteworthy magnitude (Figure 13). A sequence of two events (741210[1236] and 741219[1239]; Appendix D) with magnitudes M = 4.3 and 3.8, respectively, occurred in the vicinity

of the Whittier-Santa Monica fault intersection. Along the same trend and to the northwest another well-located event registered M = 4.3 (741206; Appendix D). Several other events with magnitudes $3<M<4$ cluster in this region and mark this zone as one of significant activity. These three events have a focal depth of approximately 8 to 10 kilometers ($\pm$ 5 km). Another sequence of two earthquakes (761122[1753] and 761122[1755]; Appendix D) with magnitudes both greater than 4.0 occurred along the Palos Verdes Hills fault extension just south of the Dume fault. Similar to the above earthquakes, this sequence occurs at the intersection of the two opposing structural regimes. One final event (750512; Appendix D) registers M = 4.8 but is only determined from one duration reading and consequently is suspect.

In general, magnitude 3 or greater earthquakes have grouped along the Santa Monica fault in the Hollywood area; along the Whittier fault, southwest of the Hollywood cluster; along the southern half of the Newport-Inglewood fault zone; and in the Santa Monica Bay near both ends of the Palos Verdes Hills fault trend where it intersects the Dume fault and the Redondo Canyon fault, respectively. This pattern suggests a build-up and release of stress concentrated at the intersections of these cross-cutting fault zones.

Focal depths for relocated "A" and "B" quality earthquakes are generally deeper than eight kilometers but typically less than 12 kilometers. Tectonically, this deep hypocenter bias supports the hypothesis that most of the displacement south of the Transverse Ranges is being accommodated on deep northwest-trending basement faults; this movement is often expressed at the surface as uplifted intervening anticlines.

STRESS REGIME AND PREFERRED FAULT-PLANE SOLUTIONS

From the stress vectors derived in this study (Figures 18 and 19), the Los Angeles basin and the continental borderland of coastal southern California presently appear to be responding to a regional northeast-southwest- to NNE-SSW-trending compressional stress regime. Earthquakes spatially associated with the Newport-Inglewood fault zone and the northwest-trending faults in the Santa Monica Bay predominantly describe stress vectors with this orientation. Similar seismic studies by Yerkes and Lee (1979) and Real (1979) also describe overall compressional stress axes approximately normal to the strike of the San Andreas fault (N24^{o}E). This dominant stress pattern is complicated by an apparent northwest-southeast compressional stress localized along the Santa Monica fault near its intersection with the northeast extension of the Whittier fault zone. From fault-plane solutions, this local change in the stress regime may possibly be caused by geometrical constraints imposed on fault interactions at the intersection of these two opposed structural trends.

The four events (15, 16, 17, and 18; Figure 16) defining northwest-southeast compression have high-angle reverse-fault mechanisms which may be interpreted in terms of north-over-south thrusting across the Santa Monica fault. The extension of the Whittier fault zone intersects the Santa Monica fault to the east of these four solutions. Events 20 and 21 (Figure 16) suggest seismic activity along the Whittier fault system and fault-plane solution 20 supports the notion of right-lateral strike-slip fault displacement. The existence of a local northwest-southeast compressional stress isolated to the west of the fault intersection also supports the notion that right-lateral strike-slip displacement is actively occurring on the Whittier fault extension. In terms of the fault intersection geometry, right-lateral strike-slip along a northwest-trending fault will create a northwest-southeast compressional stress on the western side of an intersection fault (the Santa Monica fault).

Solution 19 (Figure 16), close to the intersection of these crosscutting faults, is transitional in that the possible focal mechanisms described by this solution can fit fault movement along either fault system. The stress information is also transitional, with a compressional stress vector oriented N2^{O}E. Therefore, neither fault can be pinpointed as the more likely causative fault. This transitional solution and stress orientation suggests a

region of interaction at the intersection of the Santa Monica fault and Whittier fault extension.

Besides, evidence for high-angle reverse faulting associated with the Santa Monica fault zone, several events aligning along the northern boundary of the Los Angeles basin (solutions 1, 2, 12, 23, A, J, and K) demonstrate a possible component of left-lateral strike-slip displacement, consistent with the regional compressional stress field. Supporting this sense of displacement is a fault-plane solution from five earthquakes (1972-1976) associated with the Santa Monica-Raymond Hill fault zone which describes oblique left-lateral reverse slip (Real, 1979). West of the study area, fault-plane solutions for earthquakes associated with the Anacapa fault (the westward extension of the Dume fault) show north-over-south reverse slip, consistent with mapped late Quaternary fault displacements in the Santa Barbara Channel (Yerkes and Lee, 1979). Slip vectors analyzed by Yerkes and Lee (1979) for 51 events (1970-1975) demonstrate that the western Transverse Ranges have been dominated by oblique left-lateral reverse slip.

Three of the four normal fault-plane solutions (solutions G, 24, 25; Figures 16 and 17) from this study group are in the vicinity of the Malibu Coast zone of deformation. The only other normal fault-plane solution (solution 22; Figure 16) is on the Sierra Madre fault. Extensional

faulting and left-lateral slip are isolated south of the western Santa Monica Mountains. These fault mechanisms may be due to a clockwise rotation of the east-west-trending structures in response to right-lateral strike-slip motion regionally imposed by the San Andreas fault and locally expressed at the intersection of the opposite-trending structural regimes. The lack of seismicity within the Santa Monica Mountains relative to the concentration of seismicity to the south (Figure 12) suggests that the western Santa Monica Mountains may be decoupled from the Santa Monica basin and are rotating clockwise as a passive and coherent structural block. Paleomagnetic evidence indicates that the Santa Monica Mountains have previously undergone clockwise rotation. Kamerling and Luyendyk (1979) have analyzed paleomagnetic data from Miocene volcanic rocks which suggest that the Santa Monica Mountains have been rotated clockwise approximately 70^{o} and translated northward approximately 10^{o} latitude since middle Miocene time. They suggest clockwise rotation has occurred about a point in the eastern Santa Monica Mountains. Both left-lateral and normal faulting can be accommodated by clockwise rotation. According to a tectonic model derived by Crouch (1979), the translation and rotation of the western Transverse Ranges could have been largely completed by 8 m.y. B.P.

Other than these isolated normal fault-plane solutions, the region has been dominated by compressional tectonics. The 1973 Point Mugu earthquake generated north-over-south reverse slip with a lesser component of left-lateral strike slip (Ellsworth and others, 1973). The preferred fault-plane orientation is N69^{o}E; 49^{o}N. Location of the Point Mugu earthquake (Ellsworth and others, 1973) and its aftershocks (Steirman and Ellsworth, 1976) support the notion derived from the seismicity patterns that interaction between the juxtaposed structural provinces is confined to a transition zone known as the Malibu Coast zone of deformation. Lee and others (1979) have relocated the 1973 Point Mugu earthquake sequence and conclude that the Anacapa fault, a western extension of this zone of deformation, was the causative fault.

For earthquakes south of the Santa Monica fault zone, the preferred focal mechanisms mostly describe high-angle reverse faulting with right-lateral strike-slip as a secondary component of displacement. Reverse faulting is not readily recognized from field data along the Newport-Inglewood fault zone, whereas right-lateral strike-slip offsets are commonly described in the shallow strata and by offset en echelon anticlines, common to this zone (see Latest Faulting: Newport-Inglewood Fault Zone). The focal mechanism descriptions for 1973-1976 earthquakes occurring along the northwest-trending faults support

the concept of small-displacement convergent right-lateral wrench faulting (Harding, 1973; Wilcox and others, 1973; Junger, 1976). Junger (1976) and Wilcox and others (1973) have performed claycake experiments, simulating right-lateral wrench faulting in the continental borderland and the Newport-Inglewood fault zone, which demonstrate that significant amounts of vertical displacement can be accomplished by folding as a result of only limited displacement due to faulting at depth (Garfunkel, 1966). Hypocenters along the Newport-Inglewood fault zone group at depths of approximately eight to ten kilometers. Basement faults may be the source of high-angle reverse focal mechanisms described herein. The northwest strike of the fault planes is in accordance with the described compressional stress regime oriented NNE-SSW.

Although the preferred focal mechanisms for the Newport-Inglewood fault zone suggest northwest-striking fault planes, the data does not describe a consistent dip for this fault zone. Preferred fault planes dip vertically as well as to the northeast, southwest, and south. Real (1979) proposes that the anastomosing nature of fault strands in the fault zone are capable of producing strike-slip, normal, and reverse fault mechanisms. From five earthquakes in this zone, Real has composed a fault-plane solution which shows right-lateral strike-slip accompanied by a secondary component of normal dip slip. The fault

plane dips steeply to the southwest. A similar solution derived by Teng and others (1977) describes a fault dipping steeply to the northeast.

Recent marine geophysical studies by Nardin and Henyey (1978), Junger and Wagner (1977), and Junger (1976) also support the concept of convergent right-lateral wrench faulting for the continental borderland. Vertical uplift in Pliocene and Quaternary time appears not to have been concentrated along the right-lateral wrench faults but rather along the intervening en echelon northwest-trending folds occurring within the continental borderland and the Los Angeles basin.

CONCLUSIONS

Within the study area, field studies describing geologic and geomorphic evidence for Holocene movement reveal the Raymond Hill fault, the Sierra Madre fault, and the Charnock and Overland Avenue faults (within the Newport-Inglewood fault zone) as active faults. Microseismicity during 1973-1976 is spatially associated with the surface traces of the Charnock and Overland Avenue faults as well as with other fault segments comprising the northwesternmost portion of the Newport-Inglewood fault zone. The associated microseismicity supports the active status for this fault zone. The Sierra Madre fault was the locus of three earthquakes during 1973-1976 while the Raymond Hill fault was inactive during the study period.

Marine geophysical seismic profiles interpreted by Greene and others (1975) describe offset Holocene shelf sediments in the vicinity of the 1973 Point Mugu aftershock zone and to the east, on the Dume fault trace. The 1973 Point Mugu earthquake, its aftershocks and subsequent minor activity through 1976, cluster along and just north

of the Malibu Coast zone of deformation and account for the largest concentration of seismic events located in this study. This seismicity confirms the western portions of the Santa Monica fault zone as active.

Several potentially active faults (defined by most recent fault displacements dating between 11,000 years B.P. and 2,000 000 years B.P.) should be classified as active since microseismicity appears to have been caused by these faults. These faults include the intersecting Santa Monica fault and the northwest extension of the Whittier fault, in the vicinity of the Los Angeles River floodplain, and the offshore northwest extension of the Palos Verdes Hills fault, on the Santa Monica shelf. Two clusters of seismic activity have occurred during 1973-1976 which are not spatially associated with any active or potentially active faults. These clusters occur northeast of the Cherry Hill and Seal Beach faults of the Newport-Inglewood fault zone and in the western Santa Monica Bay.

Noticeable seismicity gaps during 1973-1976 exist along fault segments which previously have been subjected to earthquake occurrences or which show Pleistocene and Holocene diastrophism. These faults are the Santa Monica fault, particularly west of Beverly Hills and east of Point Dume; the Raymond Hill fault; the Verdugo fault; the onland portion of the Palos Verdes fault; and the Redondo Canyon fault. Seismic activity is concentrated in the Los

Angeles basin and Santa Monica Bay rather than within the Santa Monica Mountain block. The number of seismic events terminates at the Santa Monica fault system rather than continuing to the north, along the projected trend of the northwest-trending Newport-Inglewood fault zone and the Palos Verdes Hills fault extension. This sharp seismicity decrease corroborates structural evidence which differentiates the Santa Monica Mountains as a separate structural entity from the basins to the south.

Contemporaneous deformation and Neogene evolution of these juxtaposed structures appear to be responding to a regional northeast-southwest compressional stress regime which has been derived from fault-plane solutions for 1973-1976 earthquakes. A combination of high-angle reverse faulting with secondary right-lateral strike slip has been the major deformational mode south of the Santa Monica fault system. Although only insignificant amounts of right-lateral strike-slip have been documented on the Palos Verdes Hills fault northwest extension (Junger and Wagner, 1977), two fault-plane solutions describe a component of right-lateral strike-slip taking place on the Santa Monica shelf.

Concentrations of seismicity, associated with the Newport-Inglewood fault zone and the Palos Verdes Hills fault estension, appear to be originating at depth within the crystalline basement (hypocenters>10 kilometers).

From geologic field evidence, reverse displacement has not been recognized as the major component of faulting, particularly along the Newport-Inglewood fault zone. This reverse displacement is occurring at depth and apparently does not continue to the surface along definitive fault planes. Rather, this motion may be translated into folding of the younger structures associated with these basin fault zones.

Fault-plane solutions along the northern Los Angeles basin suggest that movement across the east-northeast-trending Santa Monica fault system is in a general north-over-south reverse sense accompanied by a secondary component of left-lateral strike-slip displacement. This secondary component of motion is consistent with the expected fault movement in response to a regional northeast-southwest compressional stress regime.

Isolated on the eastern portion of the Santa Monica fault, in the Hollywood area, are reverse fault mechanisms, striking northeast-southwest, in response to a local northwest-southeast-oriented compressional stress field. This isolated northwest-southeast compressional stress is most likely due to geometrical constraints created at the intersection of the east-northeast trending Santa Monica fault and the northwest-trending Whittier fault.

Three normal focal mechanisms have occurred along the Malibu Coast zone of deformation and may be in response

to a regional clockwise rotation of the Transverse Ranges, motivated by right-lateral strike slip along the San Andreas fault. These normal solutions suggest decoupling between the Transverse Ranges and the northwest-trending structural provinces to the south.

REFERENCES

Allen, C. R., Amand, P. S., Richter, C. F., and Nordquist, J. M., 1965, Relationship between seismicity and geologic structure in the southern California region: Bull. Seismol. Soc. Am., v. 55, p. 753-797.

Archambeau, C. B., Flinn, E. A., and Lambert, D. G., 1969, Fine structure of the upper mantle: Jour. Geophys. Research, v. 74, p. 5825-5865.

Association of Engineering Geologists, 1973, Geology and earthquake hazards--Planners guide to seismic safety element: AEG, Southern California Section, 44 p.

Bailey, E. H., Irwin, W. P., and Jones, D. L., 1964, Franciscan and related rocks and their significance in the geology and western California: California Div. Mines and Geology Bull. 183, 177 p.

Barrows, A. G., 1974, A review of the geology and earthquake history of the Newport-Inglewood structural zone, southern California: California Div. Mines and Geology Special Rept. 114, 115 p.

Birkeland, P. W., 1972, Late Quaternary eustatic sea-level changes along the Malibu Coast, Los Angeles County, California: J. Geology, v. 80, p. 432-448.

Bravinder, K. M., 1942, Los Angeles basin earthquake of October 21, 1941, and its effect on certain producing wells in Dominquez field, Los Angeles County, California: Am. Assoc. Petroleum Geologists Bull., v. 26, p. 388-399.

Bryant, W. A., 1978, The Raymond Hill fault--an urban geological investigation: California Geology, v. 31, p. 127-142.

Byer, J. W., field trip chairman, 1975, Association of Engineering Geologists Field Trip Guide Book, Sycamore Canyon Fault, Verdugo Fault, York Boulevard Fault, Raymond Fault, and Sierra Madre Fault zones, 68 p.

Campbell, R. H., and Yerkes, R. F., 1976, Cenozoic evolution of the Los Angeles basin area--relation to plate tectonics: in Aspects of the geologic history of the California continental borderland: Am. Assoc. Petroleum Geologists Pacific Sec. Misc. Pub. 24, p. 541-557.

Campbell, R. H., Yerkes, R. F., and Wentworth, C. M., 1966, Detachment faults in the central Santa Monica Mountains, California: U. S. Geol. Survey Professional Paper 550-C, p. C1-C11.

Campbell, R. H., Blackerby, B. A., Yerkes, R. F., Schoellhamer, J. E., Birkeland, P. W., and Wentworth, C. M., 1970, Preliminary geologic map of the Point Dume quadrangle, Los Angeles County, California: U. S. Geol. Survey, open-file map, scale 1:12,000.

Castle, R. O., and Yerkes, R. F., 1969, Recent surface movements in the Baldwin Hills, Los Angeles County, California: U. S. Geol. Survey, open-file rept., 300 p.

Cleary, J. R., and Hales, A. L., 1966, An analysis of travel times of P waves to North American stations, in the distance range 32^{o} to 100^{o}; Bull. Seismol. Soc. Am., v. 56, p. 452-489,

Crouch, J. K., 1979, Neogene tectonic evolution of the California Continental Borderland and western Transverse Ranges: Geol. Soc. America Bull., v. 90, p. 338-345.

Crowder, R. E., 1968, Cheviot Hills oil field: California Div. Oil and Gas, California Oil Fields--Summ. Operations, v. 54, p. 17-22.

Eaton, J. P., 1969, Hypolayer--a computer program for determining hypocenters of local earhtquakes in an earth consisting of uniform flat layers over a half-space: U. S. Geol. Survey, open-file rept., 155 p.

Ellsworth, W. L., Campbell, R. H., Hill, D. P., Page, R. A., Alewine, R. W. III, Hanks, T. C., Heaton, T. H., Hileman, J. A., Kanamori, H., Minster, B., and Whitcomb, J. H., 1973, Point Mugu, California, earthquake of 21 February 1973 and its aftershocks: Science, v. 182, p. 1127-1129.

Fischer, P. J., Parker, J., and Farnesworth, R., 1977, Beta platform site evaluations; geophysical and geotechnical evaluations of platform site areas on OCS tracts 35-261 and 35-262 (Shell Oil Company, et al., OCS-P0300 and OCS-P0301), San Pedro Bay, California Continental Borderland: Dept. of Geosciences, California State University, Marine Studies, 77-2, 60 p.

Foster, J.F., 1954, Rosecrans and South Rosecrans oil field: California Div. Oil and Gas, California Oil Fields,--Summ. Operations, v. 40, p. 1-15.

Garfunkel, Z., 1966, Problems of wrench faults: Tectonophysics, v. 3, p. 457-473.

Geiger, L., 1912, Probability method for the determination of earthquake epicenters from the arrival time only (translated from Geiger's 1910 German article): Bulletin of St. Louis University, v. 8, p. 56-71.

Greene, H. G., Clarke, S. H., Jr., Field, M. E., Linker, F. I., and Wagner, H. C., 1975, Preliminary report on the environmental geology of selected areas of the southern continental borderland, U. S. Geol. Survey open-file report. 75-596, 70 p., 16 pls.

Hadley, D., and Kanamori, H., 1977, Seismic structure of the Transverse Ranges, California: J. Geophys. Res., v. 88, p. 1469-1478.

Harding, T. P., 1973, Newport-Inglewood trend, California--an example of wrenching style of deformation: Am. Assoc. Petroleum Geologists Bull., v. 57, p. 97-116.

Healy, J. H., 1963, Crustal structure along the coast of California from seismic refraction measurements: J. Geophys Res., v. 68, p. 5777-5787.

Herrin, E., and Taggart, J., 1962, Regional variations in Pn velocity and their effect on the location of epicenters: Bull. Seism. Soc. Am., v. 52, p. 1037-1046.

Hileman, J. A., Allen, C. A., and Nordquist, J. M., 1973, Seismicity of the southern California region 1 January 1932 to 31 December 1972: Contribution No. 2385, Div. of Geological and Planetary Sciences, CIT.

Hill, M. L., 1954, Tectonics of faulting in southern California, in Jahns, R. H., (ed.), Geology of Southern California: California Div. Mines, Bull., 170, ch. 4, p. 5-13.

Hill, M. L., 1959, Fault names and symbols: Geol. Soc. America Bull. Abstracts, v. 69, p. 1582-1583.

Hill, M. L., 1971, Newport-Inglewood Zone and Mesozoic subduction, California: Geol. Soc. America Bull., v. 82, p. 2957-2962.

Hoots, H. W., 1931, Geology of the eastern part of the Santa Monica Mountains, Los Angeles County, California: U. S. Geol. Survey Prof. Paper 165-C, p. 83-134.

Jahns, R. H., Hill, M. L., LeConte, J. , Moore, D. G., Scott, R. F., Smith, J. L., and Smith, S. W., 1971, Geologic structure of the continental shelf off San Onofre, regional relationships and influence on seismicity: Report to Southern California Edison Co. and San Diego Gas and Electric Co. for consideration in earthquake-resistent design of Units 2 and 3 of the San Onofre Nuclear Generating Station, San Clemente, Ca., 55 p.

Jennings, C. W., and Strand, R. G., 1969, Geologic map of California, Los Angeles sheet: California Div. Mines and Geology, scale 1:250,000.

Junger, A., 1976, Tectonics of the southern California borderland; in Aspects of the geologic history of the California continental borderland: AAPG Pacific Sec. Misc. Pub. 24, p. 418-426.

Junger, A., and Wagner, H. C., 1977, Geology of the Santa Monica and San Pedro Basins, California Continental Borderland: U. S. Geol. Survey Map MF-820, 10 p.

Kamerling, M. J. and Luyendyk, B. P., 1979, Tectonic rotations of the Santa Monica Mountains region, western Transverse Ranges, California, suggested by paleomagnetic vectors: Geol. Soc. America Bull., v. 90, p. 331-337.

Kanamori, H. and Hadley, D., 1975, Crustal structure and temporal velocity change in southern California, Pageoph., v. 113, p. 257-280.

Knapp, R. R., chairman, and others, 1962, Cenozoic correlation section across Los Angeles basin from Beverly Hills to Newport, California: Am. Assoc. Petroleum Geologists, Pacific Section (chart).

Lamar, D. L., 1961, Structural evolution of the northern margin of the Los Angeles basin: unpublished Ph. D. dissertation on file at Univ. of Calif., Los Angeles, 142 p.

Lamar, D. L., 1970, Geology of the Elysian Park-Repetto Hills area, Los Angeles, California: California Div. Mines and Geology Spec. rept. 101, 45 p., map scale 1:24,000.

Lamar, D. L., 1975, Relationship between Hollywood and Raymond Hill faults; in Assoc. of Eng. Geologists Field Trip Guidebook, Sycamore Canyon fault, Verdugo fault, and Sierra Madre fault zone, John W. Byer, field trip chairman, p. 43-47.

Lamar, D., Merifield, F., and Proctor, R., 1973, Earthquake recurrence intervals on major faults in southern California: in Proctor, R. J. (ed.), Geology, Seismicity and Environmental Impact, AEG Spec. Pub.

Lee, W. H. K., and Lahr, J. C., 1975, HYPO71(REVISED): A computer program for determining hypocenter, magnitude, and first motion pattern of local earthquakes: U. S. Geol. Survey open-file rept. 75-311, 114 p.

Lee, W. H. K., Bennett, R. E., and Meagher, K. L., 1972, A method of estimating magnitude of local earthquakes from signal duration: U. S. Geol. Survey open-file rept., 28 p.

Nardin, T. R., and Henyey, T. L., 1978, Pliocene-Pleistocene diastrophism of Santa Monica and San Pedro shelves, California continental borderland: Am. Assoc. Petroleum Geologists Bull., v. 62, p. 247-271.

Payne, C. M., and Wilson, K. L., 1974, Age dating recent movement on the Raymond fault Los Angeles County California (abstract): Geological Society of America Abstract with Programs, Cordilleran section, v. 6, p. 234.

Poland, J. F., Garrett, A. A., Sinnott, A., 1959, Geology, hydrology, and chemical character of ground waters in the Torrance-Santa Monica area, California: U. S. Geol. Survey Water Supply Paper 1461, 425 p.

Press, F., 1960, Crustal structure in the California-Nevada Region: J. Geophys. Res., v. 65, p. 1039-1051.

Raleigh, C. B., Healy, J. H., and Bredehoeft, J. D., 1972, Faulting and crustal stress at Rangely, Colorado, in Heard, H. C., J. Y. Borg, N. L. Carter, and C. B. Raleigh, (eds.) Flow and Fracture of Rocks, Geophys. Monogr. Ser., v. 16, AGU, Washington D. C., p. 275-284.

Real, C. R., 1979, Seismicity and tectonics of the Santa Monica-Hollywood-Raymond Hill fault zone and northern Los Angeles basin, Los Angeles County, California: California Div. Mines and Geology (in press).

Richter, C. F., 1958, Elementary Seismology: San Francisco, W. H. Freeman and Company, 768 p.

Roller, J. C., and Healy, J. H., 1963, Seismic-refraction measurements of the crustal structure between Santa Monica Bay and Lake Mead: J. Geophys. Res.,v. 68, p. 5837-5849.

Rothwell, W. T., Jr., 1958, Western Los Angeles basin and harbor area, in A guide to the geology and oil fields of the Los Angeles and Ventural regions: Am. Assoc. Petroleum Geologists, Ann. Mtg., March 1958, p. 65-73.

Sbar, M. L. and Sykes, L. B., 1977, Seismicity and lithospheric stress in New York and adjacent areas: J. Geophys. Res., v. 82, p. 5771-5786.

Stauder, W. S. J., 1962, The focal mechanism of earthquakes: Advances in Geophysics, v. 9, p. 1-76.

Stierman, D. J., and Ellsworth, W. L., 1976, Aftershocks of the February 21, 1973 Point Mugu, California earthquake: Bull. Seis. Soc. Am., v. 66, p. 1931-1952.

Sykes, L., 1967, Mechanism of earthquakes and nature of faulting on the mid-oceanic righes: J. Geophys. Res., v. 72, p. 2131-2152.

Tabor, S., 1920, The Inglewood earthquake in southern California: Bull. Seismol. Soc. America, v. 10, p. 129-145.

Teng, T. L., and Henyey, L. T., 1973, Microearthquake monitoring in the city of Long Beach area for the year 1972: USC Geophysical Laboratory Technical Report No. 73-2.

Teng, T. L., Henyey, T. L., and Manov, D. V., 1975, Research on earthquake prediction control in Los Angeles basin: USC Geophysical Laboratory Technical Report No. 75-3, 42 p.

Teng, T. L., Henyey, T. L., Manov, D., and Lo, C., 1977, Seismic network development and monitoring in the greater Los Angeles basin and its offshore area: Summaries of Technical Reports, v. 4, U. S. Geol. Survey, p. 195-199.

Terry, R. D., Keesling, S. A., and Uchupi, E., 1956, Submarine geology of Santa Monica Bay, California: Final Report to Hyperion Engineers, Inc. by the Geology Dept., University of Southern California, 177 p.

Vedder, J. G., Beyer, L. A., Junger, A., Moore, G. W., Roberts, A. E., Taylor, J. C., and Wagner, H. C., 1974, Preliminary report on the geology of the continental borderland of southern California: U. S. Geol. Survey Misc. Field Study 624, 34 p.

Wiggins, J. H., 1974, Seismic safety analysis, City of Los Angeles (draft): Department of City Planning, Los Angeles.

Wilcox, R. E., T. P. Harding, and D. R. Seely, 1973, Basic wrench tectonics: Am. Assoc. Petroleum Geologists Bull., v. 57, p. 74-96.

Woodford, A. O., 1924, The Catalina metamorphic facies of the Franciscan series: California Univ. Pubs. Geol. Sci., Berkeley, Calif., v. 15, p. 49-68.

Woodford, A. O., Schoellhamer, J. E., Vedder, J. G., and Yerkes, R. F., 1954, Geology of the Los Angeles basin: in Jahns, R. H. (ed.), Geology of southern California, California Div. Mines Bull. 170, p. 65-82.

Woodring, W. P., Bramlette, M. N., and Kew, W. S. W., 1946, Geology and paleontology of Palos Verdes Hills, California: U. S. Geol. Survey Prof. Paper 207, 145 p.

Yerkes, R. F., and Lee, W. H. K., 1979, Late Quaternary deformation in the western Transverse Ranges, California: in, Earthquake activity and Quaternary deformation in the western Transverse Ranges, California: U. S. Geol. Survey circular 799-B., p. 27-37.

Yerkes, R. F., and Wentworth, C. M., 1965, Structure, Quaternary history and general geology of the Corral Canyon area, Los Angeles County: U.S. Geol. Survey rept. prepared on behalf of U. S. Atomic Energy Comm., 215 p.

Yerkes, R. F., McCulloh, T. H., Shoellhamer, J. E., and Vedder, J. G., 1965, Geology of the Los Angeles basin, California--an introduction: U. S. Geol. Survey Prof. Paper 420-A, 55 p.

Ziony, J. I., Wentworth, C. M. and Buchana, J. M., 1973, Recency of faulting; a widely applicable criterion for assessing the activity of faults: Fifth world conference on earthquake engineering, Rome, Italy, p. 1680-1583.

Ziony, J. I., Wentworth, C. M., Buchanan-Banks, J. M., and Wagner, H. C., 1974, Preliminary map showing recency of faulting in coastal southern California: U. S. Geol. Survey Map MF-585, 14 p.

APPENDIX A: List of seismic stations used for recording and relocating 1973-1976 earthquakes.

Table 6. List of seismic stations used for recording and relocating 1973-1975 earthquakes. The three DELAY columns represent successive refinements in the staion delay constant (in seconds) as applied to each corresponding station. The last column represents the correction factor used in the final relocation for 1973-1975 earthquakes. Asterisk indicates USC station.

	STN	LAT	LONG	ELV	DELAY	DELAY (1)	DELAY (2)	DELAY (FINAL)
1	PNM	3850.84N	12256.78W	785	0.0	0.0	0.0	0.0
2	JAS	3756.80N	12026.30W	457	0.0	0.0	0.0	0.0
3	SAO	3645.90N	12126.70W	350	0.0	0.0	0.0	0.0
4	PRI	36 8.50N	12039.90W	1187	0.0	0.0	0.0	0.0
5	MNV	3825.93N	118 9.26W	1507	0.0	0.0	0.0	0.0
6	MHC	3720.50N	12138.50W	1282	0.0	0.0	0.0	0.0
7	EHC	4048.10N	12359.10W	610	0.0	0.0	0.0	0.0
8	BLU	3424.32N	11743.52W	0	0.0	0.0	0.0	0.0
9	CKC	34 8.18N	11710.48W	0	0.0	0.0	0.0	0.0
10	SME	3349.36N	11721.32W	0	0.0	0.0	0.0	0.0
11	LED	3428.06N	11556.19W	0	0.0	0.0	0.0	0.0
12	SDW	3436.55N	117 4.45W	0	0.0	0.0	0.0	0.0
13	CKC	34 8.18N	11710.48W	0	0.0	0.0	0.0	0.0
14	DB2	3344.10N	117 3.72W	0	0.0	0.0	0.0	0.0
15	KEE	3338.30N	11639.19W	0	0.0	0.0	0.0	0.0
16	CPE	3252.80N	117 6.00W	0	0.0	0.13	0.20	0.23
17	IRN	34 9.60N	11511.04W	980	0.0	0.0	0.0	0.0
18	CPM	34 9.24N	11611.80W	937	0.0	0.0	0.0	0.0
19	WWR	3359.51N	11639.36W	0	0.0	0.0	0.0	0.0
20	MLL	34 5.48N	11656.18W	0	0.0	0.01	-0.02	-0.03
21	DVL	3411.99N	11719.69W	0	0.0	-0.19	-0.23	-0.23
22	BC2	3339.42N	11527.67W	0	0.0	0.0	0.0	0.0
23	CO2	3350.83N	11520.68W	0	0.0	0.0	0.0	0.0
24	SHH	3411.26N	11539.27W	1122	0.0	0.0	0.0	0.0
25	INS	3356.14N	11611.66W	1700	0.0	0.0	0.0	0.0
26	RMR	3412.77N	11634.52W	1702	0.0	0.0	0.0	0.0
27	BMM	3345.40N	11435.14W	564	0.0	0.0	0.0	0.0
28	CFT	34 2.11N	117 6.66W	0	0.0	0.0	0.0	0.0
29	WIND	34 5.15N	119 2.20W	0	0.0	0.0	0.0	0.0
30	TPNG	34 6.47N	11836.34W	0	0.0	0.0	0.0	0.0
31	SYCA	34 8.37N	11858.06W	0	0.0	0.0	0.0	0.0
32	SQPT	34 3.37N	11855.94W	0	0.0	0.0	0.0	0.0
33	SIMI	3414.81N	11848.28W	0	0.0	0.0	0.0	0.0
34	SHER	34 7.44N	11851.57W	0	0.0	0.0	0.0	0.0
35	SBOB	34 2.20N	119 1.00W	0	0.0	0.0	0.0	0.0
36	POTR	34 9.37N	11859.33W	0	0.0	0.0	0.0	0.0
37	NIDO	34 3.45N	11840.84W	0	0.0	0.0	0.0	0.0
38	MUGU	34 6.87N	119 4.00W	0	0.0	0.0	0.0	0.0
39	LONG	3419.77N	11856.82W	0	0.0	0.0	0.0	0.0
40	LEMN	3410.79N	119 1.57W	0	0.0	0.0	0.0	0.0
41	EGGR	34 7.87N	119 8.82W	0	0.0	0.0	0.0	0.0
42	DUME	34 0.25N	11848.38W	0	0.0	0.0	0.0	0.0
43	DEER	34 4.02N	11859.20W	0	0.0	0.0	0.0	0.0
44	CLEF	3414.07N	11854.64W	0	0.0	0.0	0.0	0.0
45	CAMH	3415.19N	119 2.28W	0	0.0	0.0	0.0	0.0
46	AGOR	34 0.52N	11844.52W	0	0.0	0.0	0.0	0.0
47	TRP	34 4.33N	11834.20W	0	0.0	0.14	0.16	0.15

48	SCY	34 6.37N	11827.25W	287	0.0	-0.19	-0.21	-0.23
49	SBB	3441.30N	11749.50W	850	0.0	-0.11	-0.15	-0.17
50	PVR	3045.50N	11821.40W	0	0.0	0.0	0.0	0.0
51	*GFP	34 7.76N	11818.59W	0	0.0	-0.10	-0.19	-0.23
52	*DRP	3346.70N	11824.20W	0	0.0	-0.77	-0.80	-0.85
53	*DHB	34 1.05N	11823.13W	0	0.0	-0.06	-0.07	-0.08
54	BOL	3344.50N	11812.27W	0	0.0	0.0	0.0	0.0
55	FRI	3659.50N	11942.50W	119	0.0	0.0	0.0	0.0
56	PYR	3434.08N	11844.46W	1247	0.0	0.26	0.31	0.33
57	PEC	3353.52N	117 9.64W	616	0.0	0.03	-0.01	-0.05
58	MRD	3420.57N	11714.46W	975	0.0	0.0	0.0	0.0
59	CSL	3414.94N	1171.68W	1490	0.0	0.0	0.0	0.0
60	CSP	3417.88N	11721.45W	1268	0.0	-0.12	-0.15	-0.17
61	*RCP	3346.66N	118 8.00W	0	0.0	0.02	0.02	0.03
62	ORP	3346.72N	11812.04W	0	0.0	0.0	0.0	0.0
63	*LNA	3347.35N	118 3.27W	0	0.0	0.11	0.15	0.16
64	*LCL	3350.32N	11811.55W	0	0.0	0.04	0.08	0.10
65	*FMA	3342.92N	11817.12W	0	0.0	-0.09	-0.12	-0.13
66	TCN	3359.67N	118 0.77W	0	0.0	0.02	0.01	0.01
67	SCR	34 6.37N	11827.25W	0	0.0	-0.18	-0.23	-0.25
68	*LCM	34 1.07N	11817.22W	0	0.0	0.10	0.16	0.20
69	SJR	3337.20N	11750.70W	0	0.0	-0.05	-0.06	-0.06
70	*JBF	3359.58N	11820.68W	0	0.0	0.04	0.10	0.14
71	*IPC	3358.24N	11820.07W	0	0.0	0.05	0.11	0.15
72	HCC	3359.64N	11822.98W	0	0.0	0.0	0.0	0.0
73	*HCM	3359.64N	11822.98W	0	0.0	0.12	0.16	0.18
74	*BHR	34 0.51N	11821.72W	0	0.0	0.10	0.16	0.19
75	VPD	3348.96N	11745.73W	183	0.0	-0.12	-0.15	-0.16
76	TWL	3416.70N	11835.67W	390	0.0	0.27	0.28	0.28
77	TPC	34 6.35N	116 2.92W	720	0.0	0.0	0.0	0.0
78	TCC	3359.67N	118 0.77W	299	0.0	0.01	-0.02	-0.03
79	SJQ	3337.20N	11750.70W	165	0.0	0.01	0.00	-0.02
80	TIN	37 3.30N	11813.70W	1195	0.0	0.0	0.0	0.0
81	SWM	3443.10N	11834.90W	1220	0.0	-0.17	-0.15	-0.12
82	SYP	3431.60N	11958.70W	1305	0.0	0.0	0.0	0.0
83	SPM	3344.80N	11820.08W	445	0.0	-0.02	-0.04	-0.04
84	SCI	3258.80N	11832.80W	219	0.0	0.06	0.09	0.12
85	SBC	3426.50N	11942.80W	90	0.0	0.35	0.47	0.48
86	RVR	3359.60N	11722.50W	260	0.0	-0.01	-0.02	-0.02
87	PLM	3321.20N	11651.70W	1692	0.0	0.15	0.22	0.26
88	PAS	34 8.90N	11810.30W	295	0.0	-0.10	-0.13	-0.14
89	MWC	3413.43N	118 3.46W	1730	0.0	0.11	0.11	0.10
90	LGC	3350.15N	118 9.02W	17	0.0	0.05	0.07	0.09
91	ISA	3539.80N	11828.40W	835	0.0	0.58	0.83	0.97
92	IRC	3423.40N	11824.00W	580	0.0	0.09	0.10	0.09
93	IKP	3238.93N	116 6.48W	957	0.0	0.0	0.0	0.0
94	HAY	3342.50N	11538.30W	439	0.0	0.0	0.0	0.0
95	GSC	3518.10N	11648.30W	990	0.0	0.0	0.0	0.0
96	GLA	33 3.15N	11449.59W	627	0.0	0.0	0.0	0.0
97	CWC	3626.30N	118 4.70W	1620	0.0	0.0	0.0	0.0

98	CLC	3549.00N	11735.80W	766	0.0	0.37	0.60	0.74
99	CIS	3324.40N	11824.20W	485	0.0	-0.05	-0.05	-0.04
100	BAR	3240.80N	11640.30W	510	0.0	-0.10	0.04	0.09
101	WKR	3548.87N	12030.67W	503	0.0	0.0	0.0	0.0
102	TAY	3556.73N	12028.45W	552	0.0	0.0	0.0	0.0
103	SHG	3624.83N	12115.22W	192	0.0	0.0	0.0	0.0
104	PTV	36 6.50N	12043.27W	506	0.0	0.0	0.0	0.0
105	PNC	3633.73N	12128.18W	403	0.0	0.0	0.0	0.0
106	PKF	3552.91N	12024.81W	469	0.0	0.0	0.0	0.0
107	JOL	36 5.02N	12110.15W	336	0.0	0.0	0.0	0.0
108	GDH	3549.86N	12021.17W	433	0.0	0.0	0.0	0.0
109	CAS	3555.90N	12020.22W	1189	0.0	0.0	0.0	0.0
110	SUF	3424.58N	11912.15W	0	0.0	0.0	0.0	0.0
111	PTD	34 0.25N	11848.37W	41	0.0	0.12	0.10	0.08
112	KYP	34 6.10N	11852.77W	701	0.0	-0.17	-0.21	-0.23
113	SIP	3412.26N	11846.92W	701	0.0	-0.12	-0.14	-0.16
114	SAD	34 4.88N	11839.90W	727	0.0	-0.06	-0.09	-0.12
115	EGG	34 7.95N	119 8.85W	0	0.0	0.0	0.0	0.0
116	ECF	3427.48N	119 5.44W	1005	0.0	0.55	0.72	0.77
117	CLP	34 5.33N	11857.85W	549	0.0	-0.16	-0.22	-0.26
118	CJP	3410.92N	11859.21W	317	0.0	-0.16	-0.25	-0.28
119	CAM	3415.27N	119 1.99W	271	0.0	0.28	0.33	0.34
120	SBSN	3314.70N	11930.40W	259	0.0	-0.09	-0.08	-0.09
121	SBSM	34 2.25N	12020.99W	172	0.0	0.10	0.37	0.46
122	SBSC	3359.68N	11937.99W	457	0.0	0.08	0.13	0.21
123	SBLP	3433.62N	12024.03W	134	0.0	0.0	0.0	0.0
124	SBLG	34 6.57N	119 3.85W	415	0.0	-0.19	-0.25	-0.27
125	SBLC	3429.79N	11942.81W	1190	0.0	0.16	0.24	0.26
126	SBCD	3422.12N	11920.63W	213	0.0	0.25	0.38	0.43
127	SBCC	3456.48N	12010.32W	610	0.0	0.0	0.0	0.0
128	SBAI	34 0.79N	11926.23W	104	0.0	0.0	0.0	0.0
129	OCB	34 2.20N	119 1.00W	-75	0.0	0.26	0.31	0.30

TABLE 7. List of seismic stations used for recording and relocating 1976 earthquakes. The last column represents the station delay factor used in the final relocation for 1976 earthquakes.

	STN	LAT	LONG	ELV	DELAY (1)	DELAY (2)	DELAY FINAL
1	BLU	3424.32N	11743.52W	0	0.0	-0.11	-0.18
2	SME	3349.36N	11721.32W	0	0.0	-0.09	-0.12
3	SDW	3426.55N	117 4.45W	0	0.0	0.0	0.0
4	CKC	34 8.18N	11710.48W	0	0.0	0.20	0.29
5	DB2	3344.10N	117 3.72W	0	0.0	0.09	0.08
6	KEE	3338.30N	11639.19W	0	0.0	0.0	0.0
7	BC2	3339.42N	11527.67W	0	0.0	0.0	0.0
8	CO2	3350.83N	11520.68W	0	0.0	0.0	0.0
9	SHH	3411.26N	11539.27W	1122	0.0	0.0	0.0
10	INS	3356.14N	11611.66W	1700	0.0	0.0	0.0
11	RMR	3412.77N	11634.52W	1702	0.0	0.0	0.0
12	BMM	3345.40N	11435.14W	564	0.0	0.0	0.0
13	CFT	34 2.11N	117 6.66W	0	0.0	0.07	0.14
14	TPR	34 5.33N	11835.20W	0	0.0	0.03	0.01
15	SCY	34 6.37N	11827.25W	287	0.0	-0.03	-0.04
16	SBB	3441.30N	11749.50W	850	0.0	0.10	0.10
17	GFP	34 7.76N	11k1k.59W	0	0.0	-0.07	-0.11
18	DHB	34 1.05N	11823.13W	0	0.0	-0.14	-0.18
19	PYR	3434.08N	11844.46W	1247	0.0	0.17	0.22
20	PEC	3353.52N	117 0.64W	616	0.0	0.08	0.11
21	CSP	3417.88N	11721.45W	1268	0.0	-0.03	-0.05
22	RCP	3346.66N	118 8.00W	0	0.0	0.14	0.22
23	LNA	3347.35N	118 3.27W	0	0.0	0.05	0.07
24	LCL	3350.32N	11811.55W	0	0.0	0.06	0.14
25	FMA	3342.92N	11817.12W	0	0.0	-0.10	-0.12
26	TCN	3359.67N	118 0.77W	0	0.0	0.12	0.19
27	SCR	34 6.37N	11827.25W	0	0.0	-0.06	-0.08
28	LCM	34 1.07N	11817.22W	0	0.0	0.20	0.36
29	SJR	3337.20N	11750.70W	0	0.0	-0.05	-0.08
30	IPC	3358.24N	11820.07W	0	0.0	0.10	0.17
31	HCM	3359.64N	11822.98W	0	0.0	0.24	0.30
32	BHR	34 0.51N	11821.72W	0	0.0	0.88	0.82
33	VPD	3348.96N	11745.73W	183	0.0	-0.05	-0.08
34	TWL	3416.70N	11835.67W	390	0.0	0.02	0.02
35	TPC	34 6.35N	116 2.92W	720	0.0	0.0	0.0
36	TCC	3359.67N	118 0.77W	299	0.0	0.13	0.17
37	SJQ	3337.20N	11750.70W	165	0.0	0.0	0.0
38	SWM	3443.10N	11834.90W	1220	0.0	-0.15	-0.16
39	SYP	3431.60N	11958.70W	1305	0.0	0.02	0.05
40	SCI	3258.80N	11832.80W	219	0.0	0.0	0.0
41	RVR	3359.60N	11722.50W	260	0.0	0.0	0.0
42	PLM	3321.20N	11651.70W	1692	0.0	0.0	0.0
43	PAS	34 8.90N	11810.30W	295	0.0	-0.13	-0.17
44	NWC	3413.43N	118 3.46W	1730	0.0	0.0	-0.02
45	ISA	3539.80N	11828.40W	835	0.0	0.0	0.0
46	IKP	3238.93N	116 6.48W	957	0.0	0.0	0.0
47	GSC	3518.10N	11648.30W	990	0.0	0.0	0.0
48	CLC	3549.00N	11735.80W	766	0.0	0.0	0.0

49	CIS	3324.40N	11824.20W	485	0.0	0.0	0.00
50	PTD	34 0.25N	11848.37W	41	0.0	0.11	0.12
51	KYP	34 6.10N	11852.77W	701	0.0	-0.12	-0.12
52	SIP	3412.26N	11846.92W	701	0.0	-0.08	-0.11
53	SAD	34 4.88N	11839.90W	727	0.0	0.01	0.01
54	ECF	3427.48N	119 5.44W	1005	0.0	0.23	0.31
55	CAM	3415.27N	119 1.99W	271	0.0	0.17	0.21
56	SBSN	3314.70N	11930.40W	259	0.0	-0.08	-0.13
57	SBSM	34 2.25N	12020.99W	172	0.0	0.11	0.16
58	SBSC	3359.68N	11937.99W	457	0.0	-0.12	-0.17
59	SBLP	3433.62N	12024.03W	134	0.0	0.0	0.0
60	SBLG	34 6.57N	119 3.85W	415	0.0	-0.09	-0.11
61	SBLC	3429.79N	11942.81W	1190	0.0	-0.01	-0.00
62	SBCD	3422.12N	11920.63W	213	0.0	0.12	0.19
63	SBCC	3456.48N	12010.32W	610	0.0	0.0	0.0
64	IRC	3423.40N	11824.00W	580	0.0	0.04	0.03
65	PSP	3347.63N	11632.93W	195	0.0	0.0	0.0
66	TMB	35 5.24N	11932.08W	0	0.0	0.0	0.0
67	ABL	3451.05N	11913.25W	0	0.0	-0.07	-0.03
68	RYS	3438.60N	11921.10W	0	0.0	0.30	0.32
69	CRG	3514.53N	11943.40W	0	0.0	0.0	0.0
70	LHU	3440.26N	11824.68W	0	0.0	-0.08	-0.11
71	LRR	3431.50N	118 1.70W	0	0.0	0.06	0.03
72	TPO	3452.70N	11813.80W	0	0.0	0.32	0.36
73	COY	3321.84N	11618.63W	0	0.0	0.0	0.0
74	HOT	3318.84N	11634.89W	0	0.0	0.0	0.0
75	PEM	3410.04N	11752.18W	0	0.0	-0.21	-0.25
76	ROD	3437.78N	11636.29W	0	0.0	0.0	0.0
77	SMO	3332.15N	11627.70W	8000	0.0	0.0	0.0
78	FTC	3452.25N	11853.51W	0	0.0	-0.04	-0.04
79	DC5	3419.63N	11937.99W	0	0.0	0.29	0.27
80	PKM	35 3.00N	120 2.40W	0	0.0	0.0	0.0
81	DC1	3420.82N	11935.09W	0	0.0	-0.18	-0.18
82	BCH	3511.10N	120 5.05W	0	0.0	0.0	0.0
83	VST	33 9.40N	11713.90W	1129	0.00	0.00	0.00
84	SNS	3325.90N	11732.90W	19	0.0	-0.14	-0.16
85	RMR	3412.77N	11634.52W	17020	0.00	0.00	0.00
86	ADL	3433.38N	11725.02W	90	0.0	0.31	0.39
87	LTC	3329.34N	115 4.20W	4580	0.00	0.00	0.00
88	CRR	3253.18N	11558.10W	0	0.0	0.0	0.0
89	COA	3251.81N	115 7.36W	0	0.0	0.0	0.0
90	COK	3250.95N	11543.61W	0	0.0	0.0	0.0
91	DAH	3244.07N	11533.47W	-6	0.0	0.0	0.0
92	ING	3259.30N	11518.61W	0	0.0	0.0	0.0
93	PLT	3243.87N	11443.76W	0	0.0	0.0	0.0
94	RUN	3258.33N	11458.63W	0	0.0	0.0	0.0
95	SGL	3238.95N	11543.52W	0	0.0	0.0	0.0
96	SUP	3257.31N	11549.43W	0	0.0	0.0	0.0
97	MDA	3354.78N	11659.97W	845	0.0	0.45	0.59
98	THR	3433.19N	11743.10W	1025	0.0	0.0	0.0

99	SIL	3420.87N	11649.60W	1730	0.0	0.0	0.0
100	SSK	3412.97N	11741.32W	1765	0.0	0.0	0.0
101	PCF	34 3.19N	11747.44W	162	0.0	-0.05	-0.12
102	RAY	34 2.18N	11648.67W	2342	0.0	0.0	0.0
103	VRG	3350.25N	11648.53W	1500	0.0	0.0	0.0
104	PIC	3254.85N	11438.59W	263	0.0	0.0	0.0
105	LGA	3245.58N	11429.57W	68	0.0	0.0	0.0
106	YMD	3233.28N	11432.68W	76	0.0	0.0	0.0
107	HDG	3425.73N	11618.30W	1347	0.0	0.0	0.0
108	SNR	3251.71N	11526.21W	0	0.0	0.0	0.0
109	BON	3241.67N	11516.11W	0	0.0	0.0	0.0
110	YEG	3426.18N	11957.56W	0	0.0	0.0	0.0
111	CPEZ	3252.80N	117 6.00W	0	0.0	0.59	0.63
112	SBCZ	3426.50N	11942.80W	0	0.0	0.62	0.76
113	GSCZ	3518.10N	11648.30W	0	0.0	0.0	0.0
114	RVRZ	3359.60N	11722.50W	0	0.0	-0.06	-0.09
115	PLMZ	3321.20N	11651.70W	0	0.0	0.24	0.41
116	SCIZ	3258.80N	11832.80W	219	0.0	0.02	0.08
117	SBBZ	3441.30N	11749.50W	850	0.0	0.0	0.02
118	MWCZ	3413.40N	118 3.50W	1730	0.0	-0.03	-0.07
119	PASZ	34 8.95N	11810.29W	308	0.0	-0.15	-0.18
120	SYPZ	3431.63N	11958.67W	1305	0.0	-0.10	-0.12
121	TPCZ	34 6.45N	116 2.92W	761	0.0	0.0	0.0
122	ISAZ	3539.80N	11828.40W	835	0.0	0.0	0.0
123	CWCZ	3626.35N	118 4.68W	1620	0.0	0.0	0.0
124	CLCZ	3549.00N	11735.80W	766	0.0	0.0	0.0
125	CISZ	3324.40N	11824.20W	485	0.0	-0.13	-0.20
126	GLAZ	33 3.10N	11449.60W	627	0.0	0.0	0.0
127	HAYZ	3342.40N	11538.20W	439	0.0	0.0	0.0
128	BARZ	3240.80M	11640.30W	510	0.0	0.0	0.0
129	MLL	34 5.48N	11656.18W	1513	0.0	0.0	0.0
130	WWR	3359.51N	11639.36W	702	0.0	0.0	0.0
131	PNM	3358.64N	11548.05W	1147	0.0	0.0	0.0
132	CPM	34 9.24N	11611.80W	937	0.0	0.0	0.0
133	CPTZ	3318.20N	11720.40W	61	0.0	0.05	0.10
134	VGR	3350.25N	11648.53W	1500	0.0	0.0	0.0
135	GAV	34 1.35N	11730.34W	0	0.0	-0.13	-0.18
136	SSV	3413.02N	11729.34W	1594	0.0	0.0	0.0
137	LED	3428.06N	11556.19W	853	0.0	0.0	0.0
138	COQ	3351.63N	11730.58W	0	0.0	0.37	0.35
139	CPE	3252.80N	117 6.00W	0	0.0	0.0	0.0
140	BMT	35 8.15N	11835.01W	1237	0.0	0.0	0.0

APPENDIX B: Improvement in earthquake relocations by applying three successive iterations of the station delay constant to seismic station data.

Note: Improvement in the quality of earthquake relocations is noted by the shift in the class "B" relocations to class "A" relocations. Quality rating for earthquake relocations is explained in Table 3 which is presented in the text.

1973-1975 Data

Iteration 1

Quality of relocation:	A	B	C	D	Total no. of
Number of earthquakes:	1	38	2	0	Earthquakes
Percentage:	2.4	92.7	4.9	0.0	41

Iteration 2

Quality of relocation:	A	B	C	D	Total no. of
Number of earthquakes:	5	33	1	0	Earthquakes
Percentage:	12.8	84.6	2.6	0.0	39

Iteration 3

Quality of relocation:	A	B	C	D	Total no. of
Number of earthquakes:	7	31	1	0	Earthquakes
Percentage:	17.9	79.5	2.6	0.0	39

1976 Data

Iteration 1

Quality of relocation:	A	B	C	D	Total no. of
Number of earthquakes:	2	27	1	1	Earthquakes
Percentage:	6.5	87.1	3.2	3.2	31

Iteration 2

Quality of relocation:	A	B	C	D	Total no. of
Number of earthquakes:	6	24	0	1	Earthquakes
Percentage:	19.4	77.4	0.0	3.2	31

Iteration 3

Quality of relocation:	A	B	C	D	Total no. of
Number of earthquakes:	6	24	0	1	Earthquakes
Percentage:	19.4	77.4	0.0	3.2	31

APPENDIX C: HYPO71 (REVISED) data output summary for three typical earthquakes.

Note:

1. Iterative step-wise locational procedure
2. Statistical information describing the earthquake relocation
3. Phase-card list
4. First-motion plot of P-wave readings from the phase list.

①

I	ORIG	LAT N	LONG W	DEPTH	DM	RMS	AVRPS	SKD	CF	ADJUSTMENTS (KM) DLAT	DLON	DZ	PARTIAL F-VALUES DLAT	DLON	DZ	STANDARD ERRORS DLAT	DLON	DZ	ADJUSTMENTS DLAT	DLON
1	23.72	34- 6.67	119- 3.95	0.00	0	0.99	0.00	D0A	0.50	-5.95	-6.17	7.34	64.04	111.08	49.26	0.74	0.59	1.05	-5.95	-6.17
2	23.53	34- 3.45	118-59.93	11.67	8	0.21	-0.01	B0A	0.50	-2.47	-0.62	1.11	44.94	5.86	12.52	0.37	0.26	0.31	-2.47	-0.62
*	23.37	34- 2.12	118-59.52	12.78	11	0.08	-0.00	A4A	0.50	0.0	-0.13	0.0	-1.00	0.46	-1.00	0.0	0.20	0.0	0.0	0.0
1	23.37	34- 2.12	118-59.52	12.78	11	0.08	-0.00	A2A	0.50	0.03	-0.17	0.11	0.01	0.56	0.19	0.29	0.22	0.25	0.0	0.0

②

DATE	ORIGIN	LAT N	LONG W	DEPTH	MAG	NO	DM	GAP	M	RMS	ERH	ERZ	Q	SQD	ADJ	IN	NR	AVR	AAR	NM	AVXM	SDXM	NF	AVFM
761213	1910 23.37	34- 2.12	118-59.52	12.78	3.00	23	11	67	1	0.08	0.4	0.2	A	A|A	2.78	50	37	-0.00	0.07	0	0.0	0.0	16	3.1

③

STN	DIST	AZM	AIN	PHWK	HRMN	P-SEC	TPOBS	TPCAL	DLY/RI	P-RES	P-WT	AMX	PRX	CALK	K	XMAG	RMK	FMP	FMAG	SRMK	S-SEC	TSOBS	S-RES	S-WT
SBLG	10.6	321	137	IP 1	1838	26.36	2.99	3.22	-0.11	-0.12	1.22	0	0	0.0	0									
KVP	12.7	55	131	IP 0	1838	26.87	3.50	3.40	-0.12	0.15	1.54	0	0	0.0	0			60	2.7					
PTD	17.5	101	122	IP 0	1838	27.62	4.25	4.11	0.12	0.02	1.69	0	0	0.0	0			55	2.7					
CAM	24.6	151	114	IPD1	1838	28.74	5.37	5.14	0.21	0.02	1.26	0	0	0.0	0									
SID	27.0	46	112	IPD1	1838	28.78	5.41	5.50	-0.11	0.02	1.26	0	0	0.0	0									
SAD	30.6	90	109	IP 1	1838	29.30	5.93	6.06	0.01	-0.13	1.20	0	0	0.0	0			65	2.9					
IWL	45.5	54	101	EP-2	1838	31.75	8.38	8.40	0.02	-0.04	0.04	0	0	0.0	0									
SHCD	49.2	319	102	IPD1	1838	32.58	9.21	8.99	0.19	0.03	1.26	0	0	0.0	0									
SHSC	53.4	266	100	EP 3	1838	33.41	10.04	10.64	-0.17	-0.43	**0.0	0	0	0.0	0									
PYR	53.4	21	99	IPC0	1838	34.90	11.53	11.29	0.22	0.02	1.57	0	0	0.0	0			101	3.4					
IRC	67.1	54	61	EP 2	1838	35.10	11.73	11.84	0.03	-0.14	0.73	0	0	0.0	0			80	3.2					
HYS	75.1	114	61	IP 0	1838	36.65	13.28	12.96	0.32	-0.00	1.47	0	0	0.0	0									
SHC	83.8	308	61	IPC1	1838	37.56	14.19	14.21	0.0	-0.02	1.05	0	0	0.0	0			80	3.2					
SWY	83.6	26	61	IPD1	1838	37.60	14.23	14.32	-0.16	0.07	1.03	0	0	0.0	0			108	3.5					
LOJ	88.4	37	61	IPD0	1838	38.00	14.63	14.87	-0.11	-0.13	1.30	0	0	0.0	0			36	2.6*					
CIS	88.6	142	61	EP-2	1838	38.29	14.92	14.88	0.0	0.04	0.68	0	0	0.0	0			73	3.2					
MWC	88.7	76	61	EP 2	1838	38.28	14.91	14.91	-0.02	0.02	0.68	0	0	0.0	0			78	3.2					
AIL	92.3	347	61	IPD0	1838	38.90	15.53	15.50	-0.03	0.06	1.31	0	0	0.0	0									
FIC	91.1	6	61	EP 2	1838	38.80	15.43	15.54	-0.04	-0.06	0.65	0	0	0.0	0									
SHSN	93.9	209	48	EP 2	1838	39.51	16.14	16.35	-0.13	-0.08	0.63	0	0	0.0	0			55	3.0					
LRR	104.0	59	48	EP 3	1838	40.15	16.78	16.87	0.0	-0.08	0.30	0	0	0.0	0									
SVPZ	105.9	301	48	EP 2	1838	40.50	17.13	17.09	-0.12	0.16	0.54	10	0	0.0	0			68	3.2	ES	54.20	30.83	0.62	0.0
SVP	105.9	301	48	EP 3	1838	40.50	17.13	17.09	0.05	-0.01	0.30	0	0	0.0	0									
MLO	121.8	71	48	EP 4	1838	43.00	20.43	19.27	-0.18	1.34	0.0	0	0	0.0	0									
SCIZ	124.2	161	48	EP 4	1838	43.50	20.13	19.32	0.08	0.73	0.0	6	0	0.0	0			51	3.0		0.0	-23.37	-57.90	0.0
SHSM	125.4	270	48	EP+2	1838	43.18	19.81	19.48	0.16	0.18	0.44	0	0	0.0	0									
TMO	126.9	117	48	EP 4	1838	44.60	21.23	19.65	0.0	1.58	0.0	0	0	0.0	0									
DMI	127.7	17	48	IPD4	1838	44.10	20.73	19.75	0.0	0.98	0.0	0	0	0.0	0									
SHDZ	129.5	56	48	IP 4	1838	44.50	21.13	19.97	0.0	1.16	0.0	14	0	0.0	0			61	3.2	ES	60.00	36.63	1.09	0.0
SHCC	147.9	313	48	EP 4	1838	46.97	23.60	22.20	0.0	1.40	0.0	0	0	0.0	0			59	3.2					
PKM	148.1	319	48	EP-4	1838	43.35	19.98	22.24	0.0	-2.26	0.0	0	0	0.0	0									
ISAZ	186.7	15	48	EP 4	1838	53.00	29.63	26.95	0.0	2.68	0.0	1	0	0.0	0			58	3.3	ES	74.10	50.73	2.76	0.0
SBL	202.6	80	48	EP 4	1838	41.40	18.03	28.88	0.0	-10.85	0.0	0	0	0.0	0									

DATE	ORIGIN	LAT N	LONG W	DEPTH	MAG	NO	GAP	DMIN	RMS	ERH	ERZ	Q	M
761213	1838 23.37	34- 2.12	118-59.52	12.78	3.08	23	67	10.6	0.08	0.4	0.2	A	1

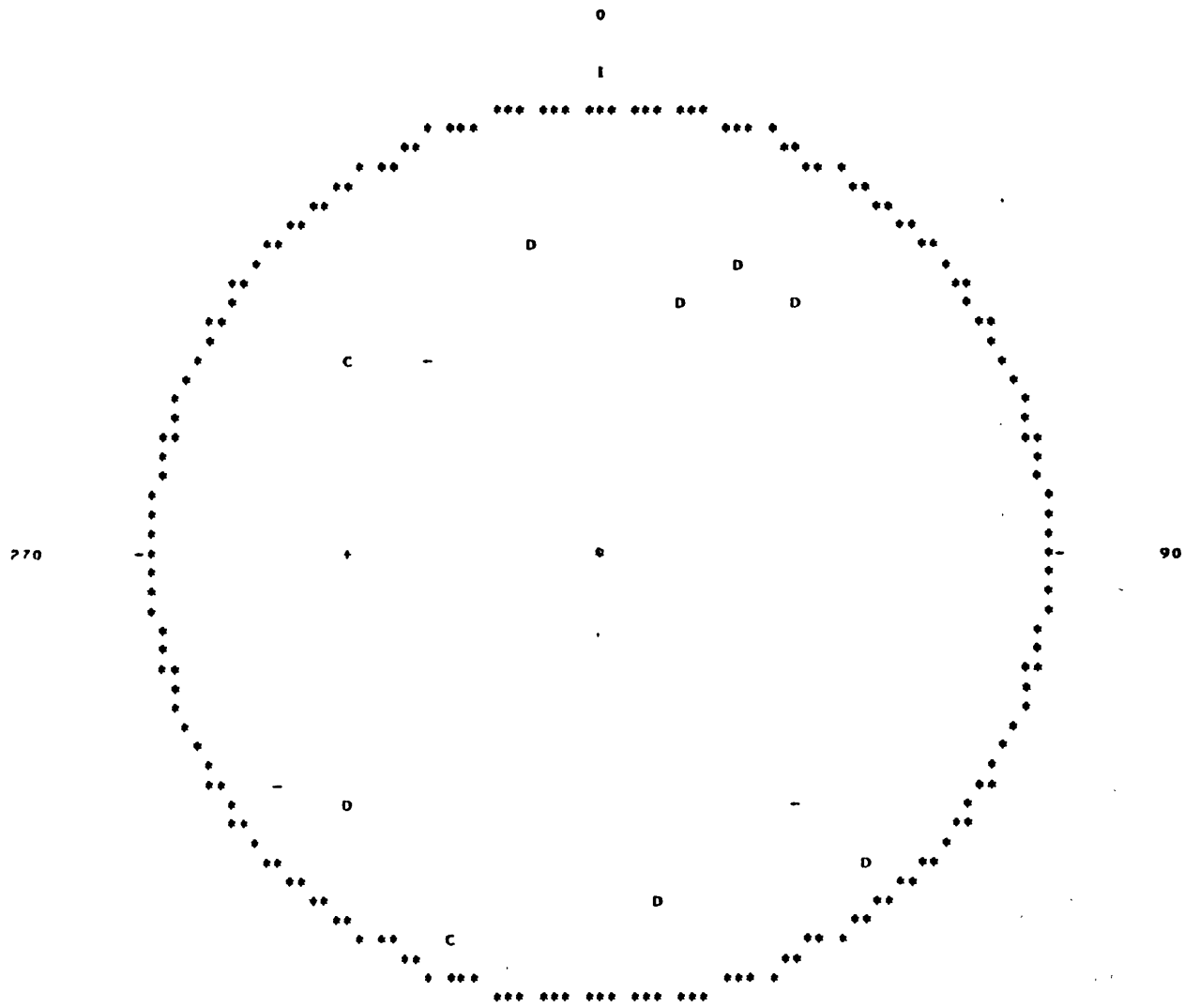

④

I	ORIG	LAT N	LONG W	DEPTH	OM	RMS	AVRES	SKD	CF	ADJUSTMENTS (KM) DLAT	DLON	DZ	PARTIAL F-VALUES DLAT	DLON	DZ	STANDARD ERRORS DLAT	DLON	DZ	ADJUSTMENTS TAKEN DLAT	DLON	DZ
1	19.30	33-30.42	110-11.64	0.00	0	0.67	0.00	000	0.50	2.01	-5.26	0.0	25.02	22.60	0.00	0.56	0.47	0.0	2.01	-5.26	0.0
2	19.50	33-31.24	110- 0.24	0.00	0	0.19	-0.04	040	0.00	0.0	0.0	-0.39	-1.00	-1.00	0.19	0.0	0.0	1.07	0.0	0.0	0.0
3	19.94	33-31.24	110- 0.24	0.00	0	0.19	0.00	020	0.50	-0.04	-0.01	-0.40	0.01	0.00	0.12	0.48	0.48	1.16	0.0	0.0	0.0

DATE	ORIGIN	LAT N	LONG W	DEPTH	MAG	NO	DM	GAP	M	RMS	ERH	ERZ	Q	SOD	ADJ	IN	NR	AVR	AAR	NN	AVRN	SDXN	NF	AVFM	SDFM	I
760715	227 19.94	33-31.24	110- 0.24	0.00	3.19	22	0	90	1	0.19	0.6	1.2	B	010	5.98	50	46	0.00	0.16	0	0.0	0.0	13	3.2	0.3	2

STN	DIST	AZM	AIN	PRMK	ORMN	P-SEC	IPUBS	IPCAL	OLY-PUB	P-RES	P-WT	AMX	PMX	CALX	K	XMAG	AMK	PMP	PMAG	SMMK	S-SEC	ISUBS	S-RES	S-WT	DT
LCL	5.4	240	137	IPC1	227	42.11	2.57	2.13	0.14	0.30	0.40	0	0	0.0	0		XP0	60	2.7						
ICC	10.4	39	100	IPD1	227	44.05	4.51	3.90	0.17	0.43	0.29	0	0	0.0	0										
EMA	21.5	219	105	IPD1	227	43.90	4.36	4.41	-0.12	0.07	1.31	0	0	0.0	0										
PAS2	31.6	334	100	IPD	227	45.60	6.06	6.01	-0.10	0.22	1.69	16	0	0.0	0			67	2.9	IS	50.10	10.56	0.17	0.0	
VPD	35.2	99	99	EP02	227	45.75	6.21	6.59	-0.08	-0.31	0.70	0	0	0.0	0										
PCF	38.2	57	98	EP 2	227	46.50	6.96	7.05	-0.12	-0.00	0.87	0	0	0.0	0		SYM								
SCV	39.6	112	98	IPD0	227	46.70	7.24	7.31	-0.04	-0.03	1.75	0	0	0.0	0										
HWCZ	40.3	18	98	IPD	227	47.00	7.46	7.43	-0.07	0.10	1.75	34	0	0.0	0			67	3.2	IS	52.00	12.46	-0.64	0.0	
PEW	41.5	36	98	EP-2	227	47.17	7.63	7.64	-0.25	0.24	0.04	0	0	0.0	0		SYM								
SAD	54.3	296	96	IPD0	227	49.09	9.54	9.70	0.01	-0.18	1.67	0	0	0.0	0										
CISZ	56.6	206	96	IPD	227	49.50	9.96	10.07	-0.20	0.00	1.69	61	0	0.0	0			70	3.0	ES	59.00	19.46	1.00	0.0	
SSC	56.6	47	96	EP-2	227	49.69	10.14	10.12	-0.11	0.13	0.03	0	0	0.0	0		SYM	100	3.3						
GAV	61.6	73	95	EP 2	227	50.12	10.50	10.70	-0.10	-0.03	0.03	0	0	0.0	0										
INC	67.0	137	95	EP04	227	50.30	10.84	11.12	0.03	-0.32	0.0	0	0	0.0	0		XP2	60	2.9						
PID	61.7	294	93	EP-2	227	50.69	11.15	11.24	-0.12	-0.22	0.79	0	0	0.0	0										
SIP	70.4	302	94	IPD1	227	51.56	12.02	12.33	-0.11	-0.21	1.14	0	0	0.0	0										
NLU	70.3	32	94	EP 2	227	51.53	11.99	12.41	-0.10	-0.25	0.74	0	0	0.0	0			100	3.4						
NVPZ	71.9	79	94	IP	227	51.90	12.26	12.50	-0.09	-0.23	1.49	10	0	0.0	0			65	3.0	IS	59.70	20.16	-2.07	0.0	
SME	72.6	94	94	EP 4	227	51.61	12.07	12.69	-0.12	-0.50	0.0	0	0	0.0	0			100	3.4						
KVP	73.4	291	94	EP 4	227	51.82	12.29	12.82	-0.12	-0.42	0.0	0	0	0.0	0										
CDP	86.9	36	94	IPC1	227	54.40	14.86	14.96	-0.05	-0.08	1.07	0	0	0.0	0										
PEC	90.4	88	61	EP 4	227	54.90	15.26	15.53	0.11	-0.30	0.0	0	0	0.0	0		XP2								
SHD	93.7	17	61	EP 3	227	55.60	16.06	16.28	0.10	-0.33	0.29	0	0	0.0	0										
CFT	96.7	72	61	EP 1	227	56.00	16.46	16.43	0.14	-0.11	0.33	0	0	0.0	0										
DHT	100.6	78	60	EP 4	227	56.80	16.94	16.98	0.00	-0.52	0.0	0	0	0.0	0		XP2								
SWE	103.0	337	60	EP12	227	57.10	17.56	17.27	-0.16	0.45	0.45	0	0	0.0	0		REV	60	3.0						
PLMZ	131.1	116	48	IP	228	0.90	21.36	20.72	0.41	0.23	1.00	21	0	0.0	0			90	3.6	IS	17.20	37.66	0.05	0.0	
KEE	131.7	100	48	EP 4	227	62.30	22.76	21.74	0.0	1.01	0.0	0	0	0.0	0										
RMM	142.4	75	48	EP 4	227	64.30	24.76	23.92	0.0	1.04	0.0	0	0	0.0	0		XP2								
INI	172.1	90	48	EP 4	227	68.40	29.06	26.64	0.0	2.22	0.0	0	0	0.0	0		XP3								
IPCZ	194.0	82	48	EP 4	228	11.10	31.86	28.46	0.0	3.18	0.0	1	0	0.0	0			69	3.8	ES	33.10	53.56	2.90	0.0	
GSCZ	200.0	37	48	EP 4	228	11.40	31.86	29.19	0.0	2.67	0.0	11	0	0.0	0					IS	37.50	57.96	6.00	0.0	
IMAZ	201.5	351	48	EP 4	228	13.10	33.56	29.31	0.0	4.24	0.0	3	0	0.0	0			70	3.5	IS	38.20	58.66	6.40	0.0	
LEW	211.6	12	48	EP 4	227	16.00	37.26	30.75	0.0	6.51	0.0	0	0	0.0	0		XP3								
PNI	216.9	07	48	EP 4	227	75.55	36.01	31.10	0.0	4.90	0.0	0	0	0.0	0		XP3								
ELCZ	222.0	13	48	IPD4	228	10.00	38.46	31.70	0.0	6.69	0.0	0	0	0.0	0					IS	44.50	64.96	8.39	0.0	
SHM	232.1	01	48	EP 4	227	79.25	39.71	33.01	0.0	6.69	0.0	0	0	0.0	0		XP3								

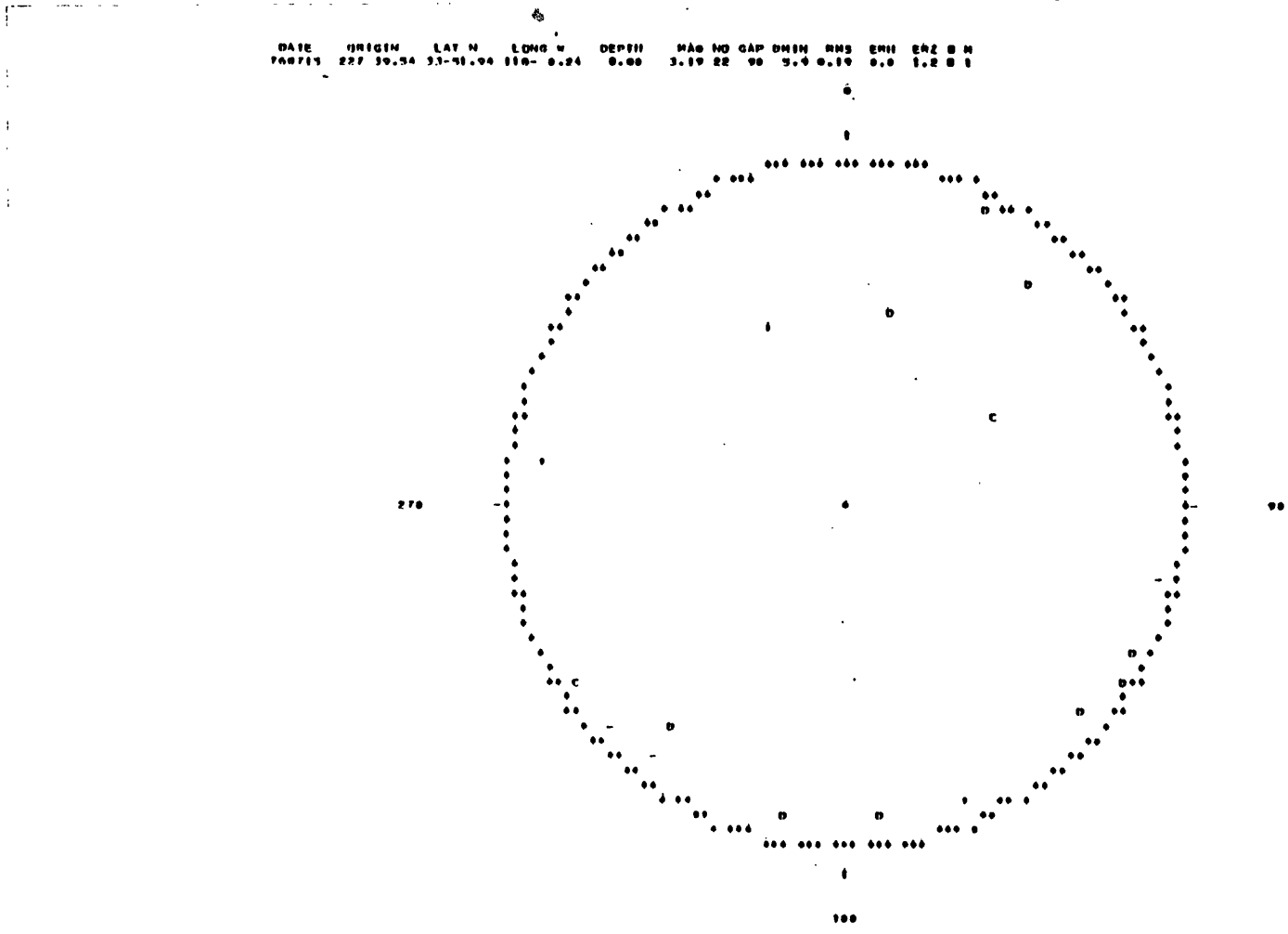
DATE ORIGIN LAT N LONG W DEPTH MAG NO GAP DMIN RMS ERH ERZ B N
760715 227 39.54 33-51.04 118- 0.24 0.00 3.19 22 90 5.4 0.19 0.0 1.2 0 1
0
90
180
270

I	ORIG	LAT N	LONG W	DEPTH	DM	RMS	AVRPS	SKD	CF	ADJUSTMENTS OLAT	ADJUSTMENTS OLON	ADJUSTMENTS OZ	PARTIAL F-VALUES OLAT	PARTIAL F-VALUES OLON	PARTIAL F-VALUES OZ	STANDARD ERRORS OLAT	STANDARD ERRORS OLON	STANDARD ERRORS OZ	ADJUSTMENTS TAKEN OLAT	ADJUSTMENTS TAKEN OLON	ADJUSTMENTS TAKEN OZ
1	44.91	34- 6.20	118-32.87	6.00	0	0.73	0.00	D00	0.50	-9.03	2.18	5.51	65.35	15.34	16.59	0.70	0.56	1.35	-9.03	2.18	2.75
2	44.39	34- 1.11	118-34.29	10.75	9	0.20	-0.26	B0D	0.50	-2.82	1.09	0.0	10.43	3.82	0.21	0.87	0.86	0.0	-2.82	1.09	0.0
3	43.81	33-59.79	118-34.98	10.75	10	0.13	-0.02	A4D	0.50	0.0	0.0	-0.50	-1.00	-1.00	0.44	0.0	0.0	0.75	0.0	0.0	0.0
7	43.81	33-59.79	118-34.98	10.75	10	0.13	-0.00	B2D	0.50	-0.20	0.06	-0.43	0.02	0.01	0.20	1.31	0.69	0.97	0.0	0.0	0.0

DATE	ORIGIN	LAT N	LONG W	DEPTH	MAG	NO	DM	GAP	M	RMS	ERH	ERZ	Q	SOD	ADJ	IN	NR	AVR	AAR	NN	AVXM	SDXM	NF	AVFM	SDFM	I
760910	713	43.81	33-59.79	118-34.98	10.75	2.40	11	10	227	1	0.13	1.5	1.0	C	BID	3.02	50	15-0.00	0.12	0	0.0	0.0	6	2.4	0.1	3

STN	DIST	AZM	AIN	PRMK	IRPH	P-SEC	TPOBS	TPCAL	OLY/HI	P-RES	P-WT	ANK	PRK	CALK	K	XMAG	RMK	FMP	FMAG	SRMK	S-SEC	ISOBS	S-RES	S-WT	DI
PFO	10.2	95	132	IPD0	713	46.98	3.17	2.95	0.12	0.18	1.61	0	0	0.0	0			40	2.4						
KVP	12.7	16	126	IPC0	713	46.71	2.92	3.19	-0.12	-0.15	1.56	0	0	0.0	0			40	2.4						
SULG	19.5	313	115	IPD0	713	47.71	3.92	4.09	-0.11	-0.06	1.63	0	0	0.0	0					IS-I	80.10	6.37	-0.72	0.0	
SAD	25.1	68	101	IPD0	713	48.79	4.98	5.09	0.01	-0.12	1.59	0	0	0.0	0			30	2.6						
SIP	26.2	28	100	EP 3	713	48.84	5.03	5.26	-0.11	-0.12	0.40	0	0	0.0	0										
CAM	30.6	339	106	EP-2	713	50.11	6.30	5.95	0.21	0.14	0.79	0	0	0.0	0										
SCV	44.4	74	101	EP 3	713	51.76	7.97	8.15	-0.04	-0.14	0.39	0	0	0.0	0										
ECP	51.7	143	99	IPD4	713	54.32	10.51	9.65	0.31	0.55	0.0	0	0	0.0	0										
IMC	64.6	47	97	EP 2	713	55.51	11.70	11.43	0.03	0.24	0.61	0	0	0.0	0			30	2.3						
PYM	65.4	14	97	IPD1	713	55.76	11.95	11.56	0.22	0.17	1.07	0	0	0.0	0			30	2.3						
MWC	83.2	72	61	EP 3	713	57.99	14.18	14.28	-0.02	-0.08	0.34	0	0	0.0	0										
ICC	83.5	90	61	EP 4	713	58.18	14.37	14.32	0.17	1.88	0.0	0	0	0.0	0		XP3								
SMM	83.9	21	61	IPD1	713	58.35	14.54	14.65	-0.16	0.05	1.00	0	0	0.0	0			30	2.4						
SNC	92.0	307	61	EP 4	713	60.30	16.49	15.84	0.0	0.95	0.0	0	0	0.0	0										

MISSING STATION	DELTA	AZIM	EX-GAP	RD-GAP
PMA	64.2	118.1	227.4	32.9
SCI	117.9	163.0	227.4	77.8
CIS	80.9	144.0	227.4	80.8
SMSN	99.7	213.3	227.4	99.3
SMSM	132.5	272.9	227.4	40.6
SMSC	66.2	269.8	227.4	42.8
SNS	141.5	116.1	227.4	31.1
SCIZ	117.9	163.0	227.4	77.8
CISZ	80.9	144.0	227.4	80.8

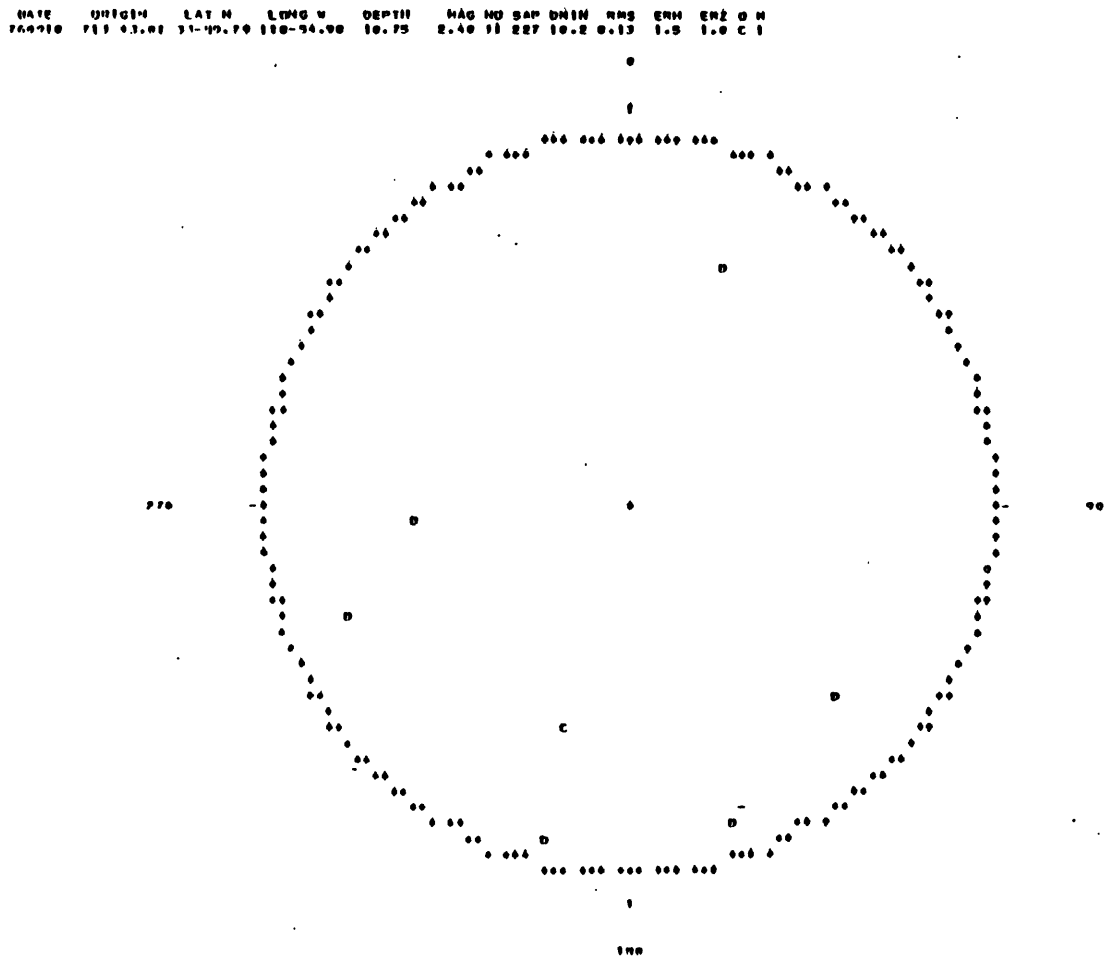
DATE ORIGIN LAT N LONG W DEPTH MAG NO GAP DMIN RMS ERH ERZ Q M
760910 713 43.81 31-49.79 118-54.98 10.75 2.48 11 227 10.2 0.13 1.5 1.0 C 1
270
90
180

APPENDIX D: Summary list of 423 earthquakes relocated in the study area which have occurred between January 1, 1973 and December 31, 1976.

Note: Table 3 (in text) explains the legend for this output summary list.

NO	YRMODY	HRMIN	SEC	LAT	LONG	DEPTH	MAG	NC	GAP	DMIN	RMS	ERH	ERZ	Q	
1	730107	351	39.00	33-52.66	118-40.39	8.00	2.05	10	151	32.4	0.18	1.4	8.5	C1	***
2	730208	1639	15.34	33-59.21	118-42.55	4.96	2.71	16	66	27.0	0.23	1.2	1.8	C1	***
3	730214	19 8	33.27	34- 5.45	119- 3.23	14.00	2.18	6	176	2.3	0.17	2.3	1.1	C1	***
4	730221	1445	57.16	34- 4.72	119- 2.28	12.24	5.90	16	62	4.2	0.26	1.2	1.1	B1	***
5	730221	1452	15.54	34- 1.09	118-57.68	8.00	2.88	10	159	13.9	0.19	1.5	1.6	C1	***
6	730221	1455	7.86	34- 1.66	118-58.40	8.00	3.39	16	67	12.4	0.21	0.9	1.4	B1	***
7	730221	1456	44.68	34- 1.85	118-58.89	8.00	3.31	12	91	11.6	0.16	0.9	1.6	B1	***
8	730221	15 7	8.03	34- 3.03	118-59.75	11.27	2.09	9	66	9.1	0.22	1.5	1.6	B1	***
9	730221	1510	16.95	34- 2.41	118-59.71	11.52	1.96	8	66	10.0	0.19	1.6	2.0	B1	***
10	730221	1516	6.53	34- 1.77	119- 0.61	10.92	2.87	11	86	47.2	0.14	0.9	1.2	B1	***
11	730221	1532	14.86	34- 3.27	118-58.96	11.08	2.85	8	88	9.7	0.11	0.9	1.0	A1	***
12	730221	1548	15.90	34- 5.43	118-59.67	12.98	2.11	7	144	6.8	0.22	2.3	1.8	C1	***
13	730221	1548	29.73	34- 5.35	119- 0.20	11.46	2.59	9	83	6.0	0.12	0.9	0.8	A1	***
14	730221	1559	26.93	34- 4.35	119- 2.67	10.96	3.37	11	64	4.5	0.15	0.9	1.1	B1	***
15	730221	1612	24.57	34- 4.95	118-57.39	12.62	2.22	8	89	10.4	0.10	0.9	1.0	A1	***
16	730221	1618	30.92	34- 3.15	118-57.17	12.65	2.85	10	91	12.1	0.08	0.6	0.5	B1	***
17	730221	17 1	4.57	34- 4.67	118-57.61	11.72	2.05	6	104	10.2	0.09	1.3	1.4	B1	***
18	730221	17 4	32.38	34- 2.64	118-58.16	12.16	2.47	7	97	11.4	0.20	2.1	2.2	B1	***
19	730221	1837	13.58	34- 3.24	118-57.93	14.43	2.56	7	95	11.0	0.16	1.4	1.1	B1	***
20	730221	1854	9.12	34- 2.82	118-58.34	12.35	2.65	10	89	10.9	0.10	0.7	0.7	A1	***
21	730221	1923	22.63	34- 2.92	118-59.70	14.95	2.27	8	66	9.3	0.15	1.3	0.9	B1	***
22	730221	1928	59.63	34- 5.89	119- 1.00	15.27	2.74	8	81	4.5	0.09	0.8	0.5	A1	***
23	730221	2041	38.73	34- 4.40	118-59.18	12.15	2.43	8	91	8.2	0.08	0.7	0.7	B1	***
24	730221	2355	2.58	34- 4.53	118-58.22	13.46	3.08	13	68	9.4	0.13	0.7	0.6	A1	***
25	730222	014	42.04	34- 4.59	118-58.47	12.13	3.19	14	68	8.6	0.16	0.8	0.7	B1	***
26	730222	050	2.74	34- 5.18	118-58.71	14.90	2.50	12	79	7.9	0.09	0.6	0.3	A1	***
27	730222	1 0	30.91	34- 4.35	118-59.37	11.87	2.40	12	64	8.0	0.15	0.9	0.8	B1	***
28	730222	3 8	46.45	34- 2.04	119- 3.04	10.80	2.44	14	67	8.5	0.20	1.1	1.2	B1	***
29	730222	416	46.42	34- 2.73	118-58.98	11.42	2.76	14	73	10.1	0.17	0.9	0.8	B1	***
30	730222	420	43.16	34- 3.35	118-57.54	14.09	2.55	11	72	7.7	0.14	0.9	0.6	A1	***
31	730222	440	3.47	34- 3.24	119- 0.11	13.58	2.19	9	86	8.4	0.07	0.5	0.4	A1	***
32	730222	529	6.30	34- 2.14	118-59.24	11.62	2.51	13	77	10.8	0.20	1.2	1.1	B1	***
33	730222	629	24.13	34- 3.13	118-59.15	11.04	2.53	13	69	9.6	0.20	1.3	1.2	B1	***
34	730222	633	23.64	34- 1.42	119- 1.61	11.40	2.16	9	85	10.1	0.23	1.6	1.7	B1	***
35	730222	721	39.79	34- 3.48	118-59.42	12.91	2.37	13	65	8.9	0.20	1.2	1.0	B1	***
36	730222	930	15.84	34- 5.01	119- 1.89	14.43	3.69	20	69	0.5	0.08	0.4	0.2	A1	***
37	730222	947	31.13	34- 4.21	118-58.46	12.89	2.31	14	64	4.2	0.09	0.5	0.3	A1	***
38	730222	10 6	41.04	34- 3.47	118-58.23	13.76	2.25	11	65	3.5	0.13	0.8	0.5	A1	***
39	730222	1122	52.79	34- 2.18	118-59.72	12.03	1.96	8	124	6.2	0.09	0.9	0.6	B1	***
40	730222	1156	27.93	34- 1.76	119- 0.04	12.28	2.51	16	77	7.0	0.19	1.1	0.8	B1	***
41	730222	1335	59.57	33-59.00	118-57.42	3.20	2.11	6	124	8.4	0.18	0.5	6.8	C1	***
42	730222	1522	47.31	34- 4.23	119- 0.31	11.85	2.76	12	67	6.9	0.27	1.5	1.2	B1	***
43	730222	2124	33.17	34- 3.26	118-58.36	15.04	1.59	7	177	3.7	0.12	1.9	1.3	C1	***
44	730222	2135	31.50	34- 3.29	118-58.70	13.27	1.86	8	159	4.2	0.12	1.3	0.8	C1	***
45	730222	2220	17.04	34- 2.85	118-58.75	13.30	2.03	10	98	4.4	0.08	0.6	0.4	B1	***

NO	YRMODY	HRMIN	SEC	LAT	LONG	DEPTH	MAG	NC	GAP	DMIN	RMS	ERH	ERZ	Q	
46	730223	244	24.44	34- 4.09	118-58.50	12.62	1.07	6	174	4.2	0.03	0.5	1.1	B1	***
47	730223	640	56.42	34- 5.29	118-58.76	13.77	1.57	8	71	2.4	0.05	0.6	1.4	A1	***
48	730223	817	18.77	34- 2.94	118-58.43	12.45	2.87	22	66	2.3	0.09	0.4	0.3	A1	***
49	730223	1152	11.91	34- 4.91	119- 0.58	11.20	1.41	6	165	2.5	0.01	0.3	0.6	B1	***
50	730223	1330	20.59	34- 4.08	118-58.09	12.48	1.09	6	172	3.6	0.05	0.9	1.7	B1	***
51	730223	2117	26.09	34- 2.95	119- 0.09	13.40	1.61	11	159	2.4	0.15	1.3	1.0	C1	***
52	730223	2315	55.04	34- 4.12	118-58.55	12.83	1.53	10	145	1.0	0.09	0.9	0.8	B1	***
53	730223	2330	3.19	34- 5.15	119- 2.08	14.85	1.53	9	145	0.2	0.17	1.8	2.0	C1	***
54	730224	125	1.89	34- 3.82	119- 3.42	9.28	2.09	12	168	3.1	0.20	1.6	1.1	C1	***
55	730224	349	36.22	34- 4.29	118-58.11	10.82	1.55	15	137	1.8	0.06	0.3	0.3	B1	***
56	730224	537	57.40	34- 4.82	119- 0.27	12.65	1.73	13	150	2.2	0.08	0.5	0.8	B1	***
57	730224	752	19.12	34- 2.85	118-59.30	15.68	1.52	13	159	2.2	0.07	0.6	0.8	B1	***
58	730224	9 7	4.35	34- 4.12	118-58.50	15.61	2.14	22	64	1.1	0.12	0.6	0.3	A1	***
59	730224	1055	4.90	34- 3.59	118-59.41	14.98	1.69	15	189	0.9	0.09	0.7	0.6	C1	***
60	730224	1258	58.05	34- 3.44	119- 2.92	17.33	1.76	13	158	3.4	0.09	0.7	0.7	B1	***
61	730224	1312	30.63	34- 4.33	118-57.05	13.65	1.90	17	64	2.5	0.05	0.3	0.2	A1	***
62	730224	1326	31.25	34- 3.19	118-58.34	12.00	2.19	21	65	2.0	0.13	0.6	0.5	A1	***
63	730224	1348	33.79	34- 4.93	118-57.32	11.76	1.72	10	96	3.3	0.05	0.4	0.4	B1	***
64	730224	1839	17.98	34- 5.02	119- 0.61	17.67	1.50	8	146	2.5	0.02	0.3	0.5	B1	***
65	730224	2024	48.15	34- 4.12	118-58.50	10.36	1.68	13	146	1.1	0.11	0.7	1.0	B1	***
66	730224	2248	37.65	34- 3.78	118-58.45	10.84	1.58	13	193	3.9	0.09	0.5	0.6	C1	***
67	730225	644	37.28	34- 4.74	118-59.68	15.15	1.10	12	130	1.5	0.08	1.0	1.6	B1	***
68	730225	1010	37.61	34- 4.12	118-58.68	9.63	1.19	14	149	0.8	0.16	1.4	1.9	C1	***
69	730226	550	39.59	34- 4.12	118-59.81	14.41	2.73	21	64	1.0	0.12	0.5	0.4	A1	***
70	730226	1130	21.10	34- 2.96	118-58.86	14.07	1.69	19	66	2.0	0.17	0.8	0.6	B1	***
71	730226	1557	57.26	34- 6.35	118-58.16	8.00	1.47	11	76	3.7	0.28	2.3	3.9	B1	***
72	730227	210	22.53	34- 2.22	118-59.71	15.74	2.34	22	67	3.4	0.17	0.7	0.5	B1	***
73	730227	419	4.83	34- 4.54	118-58.34	13.76	2.48	26	64	1.6	0.17	0.7	0.5	B1	***
74	730227	845	39.85	34- 3.31	118-58.37	13.73	1.90	17	99	1.8	0.15	0.8	0.7	B1	***
75	730227	1149	16.21	34- 1.66	118-59.66	11.62	1.84	15	126	6.5	0.13	0.9	1.0	B1	***
76	730228	1236	10.59	34- 2.09	118-59.69	15.46	2.71	27	67	3.7	0.18	0.7	0.4	B1	***
77	730301	1041	41.52	34- 3.36	118-59.90	13.47	2.36	20	88	1.6	0.18	0.8	0.6	B1	***
78	730302	735	50.98	34- 4.12	119- 1.44	15.33	1.88	15	157	3.5	0.17	1.1	0.8	C1	***
79	730302	1431	21.04	34- 4.38	118-58.41	14.15	1.32	12	125	1.4	0.12	1.2	1.8	B1	***
80	730305	1255	59.67	34- 2.06	118-58.92	14.86	3.00	27	67	3.6	0.19	0.7	0.5	B1	***
81	730306	627	37.40	33-55.46	118-32.02	12.53	2.53	12	174	15.9	0.12	1.1	1.1	C1	***
82	730307	039	1.99	34- 2.61	118-59.69	15.64	2.53	23	66	5.9	0.21	0.9	0.5	B1	***
83	730307	1256	22.52	34- 4.53	119- 1.79	13.19	1.93	18	158	4.9	0.16	1.0	0.7	C1	***
84	730307	2349	51.81	33-49.58	118-40.57	12.61	2.44	13	160	23.1	0.13	0.9	4.1	C1	***
85	730310	140	52.12	34- 3.68	118-57.78	12.88	2.01	22	119	2.3	0.19	0.8	0.8	B1	***
86	730316	2238	20.49	34- 3.47	118-59.32	12.22	3.03	19	65	5.2	0.20	0.9	0.7	B1	***
87	730317	054	35.71	34- 3.75	118-58.66	12.63	3.28	22	65	1.0	0.13	0.5	0.3	A1	***
88	730321	411	49.20	33-50.50	118-25.00	2.39	3.18	26	58	13.0	0.18	0.5	7.7	C1	***
89	730321	927	19.66	34- 5.16	118-59.49	16.19	1.25	8	121	2.2	0.02	0.3	0.6	B1	***
90	730322	349	17.58	34- 4.45	119- 1.75	16.64	1.63	10	157	4.0	0.12	1.3	0.8	C1	***

NO	YRMODY	HRMIN	SEC	LAT	LONG	DEPTH	MAG	NC	GAP	DMIN	RMS	ERH	ERZ	Q	
91	730323	832	21.19	34- 4.46	118-58.89	12.62	1.94	9	95	0.9	0.03	0.4	0.4	B1	***
92	730326	127	44.92	33-54.11	118-41.00	8.00	2.61	19	72	16.1	0.13	0.6	0.9	B1	***
93	730326	930	37.28	34- 3.63	118-57.72	11.86	1.68	10	174	2.4	0.07	0.7	1.0	B1	***
94	730326	930	41.22	34- 4.12	118-57.72	11.25	2.05	15	149	2.3	0.10	0.5	0.5	B1	***
95	730326	1513	25.51	34- 3.43	118-59.06	12.57	2.58	18	65	1.1	0.16	0.8	0.6	B1	***
96	730326	1526	26.60	34- 4.12	118-59.30	11.64	1.67	13	67	0.2	0.17	1.1	1.0	B1	***
97	730327	039	18.98	34- 4.01	119- 1.13	11.34	2.01	10	112	3.0	0.26	2.1	1.9	B1	***
98	730328	020	11.29	34-10.61	118-59.47	1.39	1.39	6	200	3.2	0.01	0.2	0.0	C1	***
99	730328	629	39.83	34- 3.93	118-56.93	10.71	1.01	6	149	1.8	0.02	0.7	1.2	B1	***
100	730328	1843	53.70	34- 4.74	118-58.39	10.03	1.55	8	99	1.8	0.03	0.4	0.6	B1	***
101	730329	2135	33.96	34- 0.67	118-32.23	6.36	2.73	21	102	13.0	0.15	1.0	1.5	C1	***
102	730331	533	49.82	34- 2.25	118-46.29	8.00	1.59	7	172	4.2	0.21	2.6	5.0	C1	***
103	730331	953	26.67	34- 3.66	118-57.55	11.38	1.54	14	171	2.5	0.14	1.0	0.7	B1	***
104	730402	1735	9.10	34- 4.61	118-58.67	10.48	1.29	7	98	1.4	0.04	0.5	0.8	B1	***
105	730404	2325	4.35	34- 8.32	118-59.30	10.90	1.35	6	81	1.9	0.26	4.3	4.2	B1	***
106	730405	840	2.21	34- 2.35	118-59.60	12.03	1.96	13	120	2.2	0.08	0.6	0.5	B1	***
107	730405	1435	45.79	34- 4.48	118-58.96	11.75	1.58	9	93	0.9	0.07	0.8	1.3	B1	***
108	730407	21 0	28.28	34- 5.45	118-58.07	11.89	1.74	12	70	3.2	0.04	0.2	0.2	A1	***
109	730408	136	29.98	33-57.30	119-14.28	4.84	1.74	9	161	19.5	0.15	1.1	12.9	C1	***
110	730408	226	30.51	34- 2.30	119- 4.02	10.60	1.75	15	263	7.9	0.11	0.7	1.0	C1	***
111	730411	6 0	19.59	34- 5.51	119- 0.88	14.31	1.20	8	156	3.8	0.03	0.6	1.2	B1	***
112	730412	1952	1.36	34- 5.63	119- 1.07	12.00	1.59	7	156	4.1	0.05	0.8	0.9	B1	***
113	730417	1015	14.23	33-55.88	119-12.98	4.95	2.00	6	164	22.3	0.14	1.3	16.6	C1	***
114	730417	1227	4.49	34- 9.26	119-10.17	8.00	1.95	5	151	10.9	0.17	9.0	42.0	D1	***
115	730419	1929	43.31	33-56.91	118-44.50	10.99	1.98	10	208	31.8	0.10	1.1	1.2	C1	***
116	730420	2114	6.39	33-59.94	118-55.93	7.34	2.15	7	254	17.3	0.17	2.6	2.6	D1	***
117	730424	1454	57.87	34- 0.24	118-19.80	3.15	2.11	7	136	1.8	0.08	1.0	1.8	B1	***
118	730427	1757	41.99	34- 0.32	119- 6.73	3.51	2.16	9	240	12.4	0.19	1.6	18.9	D1	***
119	730511	235	36.25	33-58.94	118-32.76	3.99	2.61	17	128	15.1	0.09	0.4	0.8	B1	***
120	730511	1630	38.37	34- 9.40	119-11.29	8.00	2.21	5	146	12.6	0.06	1.3	5.3	D1	***
121	730512	2155	23.25	34- 0.79	119- 1.88	6.39	3.06	14	91	11.1	0.19	1.0	1.5	B1	***
122	730513	152	34.15	33-59.68	118-21.16	8.00	2.57	14	84	0.8	0.16	1.1	0.9	B1	***
123	730514	0 5	40.89	34- 1.91	119- 2.54	10.73	2.17	8	107	8.8	0.15	1.3	1.2	B1	***
124	730520	18 8	42.47	33-56.51	118-20.91	10.13	1.67	9	144	3.4	0.10	1.4	0.8	C1	***
125	730524	830	22.28	33-58.79	118-59.24	0.95	1.97	8	161	16.0	0.11	0.9	129.3	C1	***
126	730615	527	13.64	33-59.82	119- 9.63	8.00	2.35	7	143	15.3	0.06	0.8	1.6	B1	***
127	730621	7 9	5.97	34- 3.16	118-50.10	3.55	1.36	6	137	6.0	0.11	0.6	6.1	C1	***
128	730622	2147	14.95	34- 3.31	118-48.27	1.54	1.67	6	174	5.7	0.11	3.3	2.9	C1	***
129	730627	720	50.58	34- 3.00	118-59.50	1.98	1.94	9	131	2.7	0.10	0.8	0.5	B1	***
130	730703	431	58.99	34- 6.47	118-27.35	23.52		6	331	0.2	9.24	33.1	70.4	D1	***
131	730705	2153	43.95	34- 3.48	119- 1.10	13.30	2.15	9	121	2.4	0.11	1.0	0.6	B1	***
132	730706	518	38.00	34- 3.55	118-59.39	12.17	2.03	12	84	3.5	0.11	0.7	0.6	A1	***
133	730714	548	6.71	34- 0.74	118-49.16	13.54	1.98	13	91	1.5	0.14	1.0	0.8	B1	***
134	730714	8 6	57.62	34- 2.09	119- 1.96	13.07	1.98	13	166	1.5	0.15	1.0	1.0	C1	***
135	730715	1219	24.30	34- 3.99	119- 3.79	17.65	1.63	10	133	4.8	0.08	0.7	0.7	B1	***

NO	YRMODY	HRMIN	SEC	LAT	LONG	DEPTH	MAG	NC	GAP	DMIN	RMS	ERH	ERZ	Q	
136	730718	6 9	30.27	33-59.23	118-43.74	11.25	1.31	8	219	7.4	0.08	1.5	1.6	C1	***
137	730724	657	25.86	34- 2.30	119- 1.10	12.54	2.52	21	66	0.2	0.22	0.9	0.7	B1	***
138	730726	2217	48.41	33-58.87	118-44.36	1.96	1.09	8	293	6.7	0.11	5.9	3.3	D1	***
139	730729	757	12.68	34- 3.21	118-57.57	11.82	2.30	15	98	3.9	0.17	0.9	0.8	B1	***
140	730803	2332	55.07	34- 3.69	119- 4.97	16.24	1.59	12	146	5.6	0.12	1.0	0.7	B1	***
141	730810	1930	38.29	34-11.27	118-58.36	1.65	1.15	7	121	1.5	0.14	1.2	0.5	B1	***
142	730813	23 2	39.51	34- 2.81	118-58.75	15.82	1.92	14	145	3.6	0.19	1.3	0.6	C1	***
143	730816	2324	6.92	34- 3.68	118-48.84	2.63	1.42	9	163	6.4	0.16	1.1	216.0	C1	***
144	730819	922	50.50	34- 3.93	119- 2.25	7.48	1.84	11	159	3.7	0.11	0.9	1.2	B1	***
145	730820	1332	57.78	33-57.19	119-10.23	9.90	1.81	11	143	17.0	0.11	1.0	2.0	C1	***
146	730820	14 1	49.31	33-57.45	119-10.55	8.00	2.52	21	73	17.1	0.12	0.5	0.7	B1	***
147	730921	529	23.30	34- 4.38	118-59.77	11.68	1.27	7	132	3.4	0.07	1.0	0.7	B1	***
148	730923	8 8	17.47	34- 4.47	119- 4.25	17.79	1.77	8	129	3.9	0.08	0.9	0.9	B1	***
149	730923	820	8.28	34- 3.14	118-57.95	12.54	1.80	8	140	4.0	0.11	1.1	1.1	C1	***
150	730926	2028	14.15	34- 1.12	118-20.54	11.09	1.80	6	138	2.9	0.04	0.9	1.3	B1	***
151	730927	1956	19.86	34- 2.82	118-59.39	3.59	2.04	10	159	5.2	0.15	1.3	4.5	C1	***
152	730927	20 5	43.97	34- 2.50	118-59.23	2.55	1.86	9	213	5.7	0.20	1.9	1.7	C1	***
153	730928	2157	30.23	34- 2.66	118-47.43	5.98	1.48	8	128	4.7	0.12	1.1	3.3	B1	***
154	730929	1027	23.53	34- 3.11	118-59.88	2.42	1.77	9	119	2.4	0.07	0.7	0.4	B1	***
155	730930	1151	49.91	33-52.42	118-27.97	0.38	2.26	18	61	15.4	0.19	0.7	57.1	C1	***
156	730 30	14 3	22.33	34-11.19	119- 7.31	2.16	1.45	10	171	10.1	0.17	1.2	1.4	C1	***
157	730902	628	3.87	34- 1.06	118-44.89	13.86	2.32	17	100	5.6	0.16	0.9	0.6	B1	***
158	730903	1221	51.43	34- 1.99	118-50.39	13.66	1.16	9	135	4.5	0.08	0.8	1.4	B1	***
159	730904	2216	52.97	34- 2.24	118-48.05	6.12	1.67	7	119	3.7	0.10	1.4	3.0	B1	***
160	730920	22 7	45.12	34- 0.68	119- 0.11	9.89	2.30	15	68	3.1	0.13	0.7	0.7	A1	***
161	731004	22 6	3.12	34-10.73	119- 7.75	12.78	1.45	10	95	9.8	0.12	0.9	1.1	B1	***
162	731006	16 4	47.92	34- 2.02	119- 0.57	8.00	1.82	17	185	0.7	0.14	0.7	0.9	C1	***
163	731010	22 3	13.75	34- 3.18	118-47.84	1.08	1.29	6	113	5.5	0.05	0.9	1.0	B1	***
164	731012	425	18.10	34- 3.20	118-53.95	10.69	2.24	17	113	5.7	0.14	0.7	0.7	B1	***
165	731015	2157	6.26	34- 2.96	118-47.71	2.17	1.14	7	118	5.1	0.06	0.5	91.0	C1	***
166	731016	2337	31.23	34-10.64	119- 0.41	1.16	1.34	7	129	1.9	0.06	0.5	0.3	B1	***
167	731118	729	59.73	33-58.34	118-22.26	6.88	2.87	20	92	2.6	0.13	0.5	0.9	B1	***
168	731118	733	47.62	33-57.88	118-23.23	4.72	1.92	5	281	3.3	0.27	0.3	0.1	C1	***
169	731021	345	43.37	34- 4.68	118-57.95	14.62	1.14	9	136	1.2	0.12	1.2	1.1	C1	*** TIME
170	731024	2145	14.89	34- 2.55	118-47.88	5.98	1.11	6	119	4.3	0.07	1.2	3.2	B1	***
171	731025	1924	43.28	34-10.61	119- 0.37	1.13	1.32	8	128	1.9	0.06	0.4	0.3	B1	***
172	731026	1645	11.66	34- 1.92	118-53.94	4.50	1.92	8	163	7.9	0.03	0.3	1.4	B1	***
173	731030	1451	5.14	34- 2.54	118-58.81	14.13	1.33	9	155	3.4	0.07	1.0	1.5	B1	***
174	731106	1616	1.77	34- 2.37	119- 1.17	16.41	1.42	9	125	0.4	0.05	0.6	0.4	B1	***
175	731108	2315	15.38	34- 2.93	118-47.91	4.86	1.04	7	114	5.0	0.05	0.7	2.4	B1	***
176	731115	1 4	29.47	34-10.64	119- 0.50	1.14	1.01	7	131	2.0	0.03	0.3	0.2	B1	***
177	731125	1542	52.33	34-11.42	119- 6.49	18.47	1.58	11	92	9.8	0.10	0.8	1.0	B1	***
178	731127	7 9	30.98	33-59.04	119-14.18	2.67	1.68	12	123	18.8	0.13	0.8	154.8	C1	***
179	731129	1125	19.87	34- 0.27	118-25.54	14.50	1.49	17	92	4.1	0.08	0.4	0.3	B1	***
180	731205	1929	53.24	34- 1.73	119- 2.48	7.94	1.38	12	120	3.6	0.11	0.7	0.8	B1	***

NO	YRMODY	HRMIN	SEC	LAT	LONG	DEPTH	MAG	NC	GAP	DMIN	RMS	ERH	ERZ	Q	
181	731209	1536	13.69	34- 0.33	118-25.48	15.02	1.33	16	102	3.9	0.13	0.7	0.5	B1	***
182	731212	10 1	37.86	34- 4.15	118-58.82	12.30	1.79	11	136	2.6	0.15	1.2	0.7	C1	***
183	731220	1423	21.38	34- 4.44	118-56.01	13.28	2.11	18	64	3.3	0.18	0.8	0.7	B1	***
184	731228	2315	15.34	34- 3.16	118-47.77	2.45	1.33	7	114	5.5	0.08	0.7	120.9	C1	***
185	731230	1934	20.65	33-58.29	118-46.28	16.25	1.68	9	249	15.7	0.10	1.5	1.7	C1	***
186	740109	20 2	34.56	34-10.58	119- 0.08	1.35	1.52	6	123	1.5	0.03	0.4	0.2	B1	***
187	740110	1841	59.78	34- 3.60	119- 3.29	13.71	2.13	12	117	4.4	0.20	1.6	1.0	B1	***
188	740110	2226	17.78	34- 5.48	119- 0.76	11.32	1.52	8	109	4.5	0.06	0.6	0.9	B1	***
189	740112	224	9.57	34- 3.78	118-57.89	15.66	2.17	9	154	10.5	0.20	1.5	0.9	C1	***
190	740117	8 0	15.32	34- 5.68	119- 2.69	13.79	1.47	8	155	2.4	0.07	1.4	2.1	C1	***
191	740117	930	51.05	33-51.99	118-19.97	10.47	2.47	22	75	11.8	0.13	0.5	1.4	B1	***
192	740118	17 8	16.48	34- 5.07	118-51.80	17.22	1.54	8	100	2.4	0.05	0.6	1.1	B1	***
193	740125	5 2	25.30	34- 3.56	118-54.16	12.71	1.22	8	132	5.2	0.04	0.4	0.8	B1	***
194	740125	727	21.63	33-55.92	118-42.53	8.00	1.22	15	217	12.0	0.13	0.9	2.6	C1	***
195	740201	1857	32.71	34- 3.73	119- 0.30	2.30	1.28	8	166	3.0	0.09	1.7	1.2	C1	***
196	740201	2358	35.50	34- 2.30	119- 0.31	8.00	1.53	10	158	1.1	0.13	1.2	1.4	C1	***
197	740218	1013	50.83	33-47.45	118-30.97	7.07	1.69	17	139	17.5	0.15	0.7	1.5	C1	***
198	740223	834	36.24	34- 3.34	118-56.29	14.85	1.25	7	139	4.4	0.14	2.0	2.2	C1	***
199	740227	541	17.93	34- 4.77	118- 5.99	10.82	3.29	16	57	12.4	0.15	0.7	0.8	B1	***
200	740303	1632	35.08	34- 1.96	118-59.64	9.24	2.31	14	129	2.1	0.17	1.0	0.8	B1	***
201	740303	1659	23.38	34- 3.25	119- 0.32	8.86	2.27	14	93	2.3	0.25	1.5	1.1	B1	***
202	740306	152	34.01	34- 6.89	118-15.34	11.29	2.86	15	80	8.6	0.11	0.5	0.5	A1	***
203	740307	629	8.62	33-56.76	118-42.95	8.31	1.11	9	246	10.5	0.05	0.9	1.0	C1	***
204	740309	341	16.88	34- 8.32	118-19.48	2.55	2.25	10	83	12.5	0.16	0.9	184.7	C1	***
205	740312	735	45.26	34- 6.18	118-13.75	7.62	3.52	17	72	7.3	0.15	0.5	1.2	A1	***
206	740312	738	43.35	34- 5.31	118-14.49	5.70	2.98	11	84	8.9	0.12	0.6	2.5	B1	***
207	740317	312	44.31	34- 3.50	118-59.76	1.94	1.54	8	110	3.1	0.06	0.4	0.2	B1	***
208	740318	237	25.82	34- 2.82	118-54.66	12.74	2.04	15	96	6.7	0.12	0.7	0.6	B1	***
209	740330	112	36.19	34- 5.05	118-50.81	13.11	1.80	11	94	3.6	0.13	1.0	1.0	B1	***
210	740331	1120	47.76	34- 1.06	118-44.63	5.12	1.66	17	80	5.9	0.11	0.5	0.8	B1	***
211	740401	1956	13.27	34- 4.09	118-59.53	14.50	2.23	17	64	3.5	0.14	0.7	0.4	A1	***
212	740402	946	39.20	34- 3.07	118-57.95	13.72	1.49	8	168	4.2	0.09	1.5	1.0	C1	***
213	740403	1046	21.67	34- 3.30	118-53.75	11.26	2.47	14	88	5.4	0.13	0.7	0.7	A1	***
214	740405	139	37.76	34- 2.75	118-56.32	11.41	2.51	14	100	5.3	0.09	0.5	0.5	B1	***
215	740411	8 0	58.03	34- 4.21	119- 0.60	15.72	1.37	6	122	3.8	0.02	0.5	0.9	B1	***
216	740414	1029	15.22	34- 5.70	119- 2.37	19.17	1.62	10	94	2.8	0.08	0.8	0.6	B1	***
217	740424	0 9	16.18	34- 5.71	118-51.68	1.74	1.23	8	92	1.8	0.11	0.6	0.3	B1	***
218	740425	823	53.53	34- 1.50	119- 5.84	8.86	2.79	14	159	7.6	0.11	0.7	0.8	B1	***
219	740425	928	42.30	34- 1.81	119- 4.99	9.91	1.87	16	190	6.2	0.15	0.9	0.7	C1	***
220	740510	2221	29.54	34- 3.80	118-54.25	13.84	1.10	8	128	6.2	0.06	0.6	1.1	B1	***
221	740522	1946	44.01	34- 3.13	118-58.59	14.07	1.54	11	137	4.1	0.15	1.0	1.5	C1	***
222	740522	2339	48.43	34- 2.30	119- 0.00	8.97	1.37	8	161	1.5	0.10	1.0	1.5	B1	***
223	740521	2 5	18.11	34- 5.50	119- 1.06	15.77	2.27	17	89	4.7	0.11	0.7	0.3	A1	***
224	740706	2136	59.11	34- 2.83	119- 1.76	16.42	1.83	12	129	1.6	0.08	0.6	0.4	B1	***
225	740712	627	44.19	34- 0.35	118-48.86	9.78	1.88	16	177	0.8	0.23	1.6	1.3	C1	***

NO	YRMODY	HRMIN	SEC	LAT	LONG	DEPTH	MAG	NC	GAP	DMIN	RMS	ERH	ERZ	Q	
226	740723	531	30.84	34- 3.79	118-58.79	14.22	1.46	9	117	3.2	0.07	0.9	1.5	B1	***
227	740725	1613	41.78	33-56.16	118-51.74	7.21	2.30	12	226	9.2	0.13	1.5	1.7	C1	***
228	740726	2327	51.69	34-10.41	119- 0.42	1.14	1.01	6	128	2.1	0.03	0.3	0.2	B1	***
229	740805	1117	29.90	33-50.76	118- 6.01	4.68	1.85	10	100	7.6	0.27	1.7	3.2	B1	***
230	740825	046	30.47	33-55.29	118-39.68	9.42	1.91	10	235	16.2	0.07	1.2	1.9	C1	***
231	741008	056	4.38	34- 2.30	118-59.02	2.14	3.41	14	106	3.1	0.27	1.3	0.8	B1	***
232	741008	1 2	39.95	34- 3.45	119- 0.03	1.68	1.42	6	105	2.8	0.04	0.3	0.1	B1	***
233	741008	1 7	49.81	34- 3.43	118-59.79	1.89	1.42	7	111	2.9	0.04	0.3	0.1	B1	***
234	741008	1 8	53.38	34- 3.55	118-59.95	1.88	1.73	7	104	3.0	0.04	0.3	0.1	B1	***
235	741008	111	10.10	34- 3.69	119- 0.05	1.59	1.23	6	105	3.1	0.06	0.5	0.2	B1	***
236	741008	117	9.51	34- 3.39	118-59.75	2.05	1.66	7	111	2.9	0.04	0.6	0.4	B1	***
237	741008	134	54.91	34- 3.56	119- 0.04	1.87	1.64	7	103	2.9	0.05	0.3	0.1	B1	***
238	741008	150	7.41	34- 3.40	118-59.90	1.83	1.46	7	109	2.8	0.06	0.3	0.1	B1	***
239	741008	230	21.10	34- 3.41	118-59.47	1.98	1.66	7	118	3.2	0.03	0.2	0.1	B1	***
240	741008	3 0	16.89	34- 3.52	118-59.62	2.01	1.73	7	112	3.2	0.06	0.4	0.2	B1	***
241	741008	559	5.95	34- 3.49	118-59.41	2.04	1.46	5	116	3.4	0.01	0.0	0.0	C1	***
242	741008	1135	58.15	34- 3.27	118-59.80	2.54	1.47	7	115	2.7	0.05	0.4	78.5	C1	***
243	741009	925	57.41	34- 3.21	118-59.86	2.07	1.06	6	116	2.6	0.06	0.9	0.6	B1	***
244	741009	926	57.31	34- 3.48	118-59.94	1.74	1.07	7	106	2.9	0.03	0.2	0.1	B1	***
245	741009	928	9.54	34- 3.27	118-59.65	2.02	1.15	6	119	2.9	0.06	1.0	0.7	B1	***
246	741009	2142	40.96	34- 3.47	118-59.82	2.23	1.72	8	109	3.0	0.06	0.6	0.5	B1	***
247	741010	18 9	50.67	34- 3.60	118-59.71	1.89	1.26	7	132	3.3	0.05	0.4	0.1	B1	***
248	741012	954	57.35	34- 3.33	118-59.27	3.25	2.94	17	68	3.4	0.14	0.6	1.7	A1	***
249	741012	10 9	39.90	34- 4.50	118-59.26	4.40	1.55	9	97	2.7	0.15	1.0	2.0	B1	***
250	741012	1011	19.41	34- 3.52	118-59.76	1.87	1.82	8	109	3.1	0.05	0.3	0.1	B1	***
251	741012	1025	8.05	34- 2.90	119- 0.34	1.21	1.00	7	113	1.6	0.08	0.5	0.2	B1	***
252	741015	2240	30.15	34-10.24	118-59.92	1.15	1.59	9	149	1.7	0.04	0.5	0.3	B1	***
253	741018	2325	24.65	34- 3.50	119- 0.16	1.72	1.16	7	107	2.7	0.04	0.3	0.1	B1	***
254	741022	0 6	24.15	34- 3.44	119- 0.45	2.33	1.11	7	118	2.4	0.05	0.8	0.5	B1	***
255	741022	1213	38.69	33-58.57	118-24.57	7.11	3.02	22	52	3.2	0.16	0.6	0.8	B1	***
256	741106	031	2.23	34- 3.31	118-59.93	3.86	1.14	7	111	2.6	0.05	0.5	1.3	B1	***
257	741106	038	27.55	34-13.16	118-10.40	3.59	2.94	16	79	10.7	0.12	0.5	1.3	B1	***
258	741111	547	56.57	34- 3.89	118-59.56	14.92	1.59	10	104	3.7	0.06	0.6	0.5	B1	***
259	741114	941	1.38	34- 3.56	118-59.86	1.89	1.33	7	106	3.1	0.04	0.3	0.1	B1	***
260	741114	951	5.22	34- 3.49	118-59.93	1.88	1.01	7	106	2.9	0.06	0.4	0.2	B1	***
261	741114	11 4	48.30	34- 3.62	118-59.86	1.86	1.04	7	105	3.2	0.05	0.3	0.1	B1	***
262	741115	625	32.00	34- 3.28	119- 0.16	2.11	1.17	7	106	2.4	0.03	0.4	0.3	B1	***
263	741127	1913	50.37	33-50.98	118-16.60	6.97	2.32	7	207	7.9	0.16	2.7	4.6	D1	***
264	741204	2012	23.03	34- 3.96	119- 0.05	14.71	1.17	6	134	3.6	0.04	0.9	1.5	B1	***
265	741206	1345	13.08	34- 7.10	118-15.83	10.09	4.36	30	55	9.1	0.13	0.4	0.4	A1	***
266	741207	712	7.74	34- 5.43	119- 0.45	8.00	1.02	6	104	4.0	0.34	4.4	9.9	C1	***
267	741209	2229	25.31	34-10.40	119- 0.74	0.71	1.15	9	134	2.5	0.09	0.6	0.5	B1	***
268	741219	757	2.95	34- 3.81	118-44.46	4.04	1.33	8	148	7.3	0.17	1.1	10.1	C1	***
269	741219	1236	16.56	34- 4.57	118- 6.27	8.00	4.39	28	50	10.1	0.16	0.4	0.8	B1	***
270	741219	1239	50.13	34- 4.44	118- 6.07	7.67	3.81	24	56	10.5	0.09	0.3	0.5	B1	***

NO	YRMODY	IRMIN	SEC	LAT	LONG	DEPTH	MAG	NC	GAP	DMIN	RMS	ERH	ERZ	Q	
271	741220	1423	18.99	34- 5.47	118-51.97	12.48	2.10	12	72	1.7	0.13	0.8	0.8	A1	***
272	741222	2242	42.00	33-59.16	118-21.56	8.00	2.02	5	121	2.3	0.18	3.9	3.8	D1	***
273	741225	1116	38.22	34- 2.30	119- 0.53	8.74	1.80	7	196	0.8	0.09	1.7	1.7	C1	***
274	750107	444	53.05	34- 6.76	119- 1.49	17.26	1.23	9	139	6.2	0.05	0.6	0.4	B1	***
275	750110	1022	26.69	34- 1.29	118-23.04	2.48	1.74	4	128	0.5	0.00			C1	***
276	750111	1444	18.35	33-59.41	118-51.74	13.04	2.54	14	157	5.4	0.12	0.8	0.5	B1	***
277	750113	1121	49.44	33-47.75	118- 6.16	14.09	3.45	13	84	3.5	0.16	1.0	0.8	B1	***
278	750114	750	40.88	33-47.79	118- 6.38	13.65	3.10	13	84	3.3	0.12	0.7	0.5	A1	***
279	750115	738	2.65	33-48.41	118- 5.72	11.24	3.27	11	81	4.3	0.12	0.9	0.8	A1	***
280	750123	148	42.42	33-54.09	118-42.08	8.84	2.70	26	54	15.0	0.10	0.4	0.5	B1	***
281	750124	11 1	53.66	34- 1.37	119- 1.10	10.92	2.05	13	112	1.5	0.11	0.8	0.7	B1	***
282	750128	522	22.85	34-11.77	118-39.07	5.55	2.31	21	101	10.5	0.20	0.7	1.5	B1	***
283	750130	1218	52.77	33-59.82	119-10.20	8.12	1.44	14	191	15.8	0.12	1.0	1.8	C1	***
284	750204	1527	23.35	34- 3.88	118-47.65	8.27	1.44	9	108	6.8	0.13	1.1	2.7	B1	***
285	750208	1736	34.47	34- 4.00	118-47.20	6.98	1.78	12	113	7.2	0.15	0.9	1.9	B1	***
286	750210	1254	28.26	34- 7.58	118-16.00	12.21	2.12	19	83	9.1	0.12	0.5	0.7	A1	***
287	750216	5 0	45.07	33-49.75	118-49.93	8.00	1.81	12	280	19.6	0.12	1.9	2.2	C1	***
288	750223	1021	59.96	34- 3.79	118-59.09	13.27	2.68	21	54	3.4	0.20	0.8	0.6	B1	***
289	750301	545	4.19	34- 1.20	118-43.24	6.60	2.00	13	85	8.1	0.14	0.7	1.1	B1	***
290	750303	1534	44.57	33-54.61	118-21.82	8.00	2.98	15	101	9.5	0.20	1.0	2.4	B1	***
291	750307	1629	33.80	34- 0.56	118-30.95	1.65	3.72	4	217	12.2	0.50			D1	***
292	750317	947	10.55	33-47.73	118- 6.42	10.75	1.39	6	114	3.1	0.04	0.5	0.6	B1	***
293	750327	652	49.40	33-58.34	118-20.77	8.00	1.84	9	120	1.1	0.13	1.1	1.2	B1	***
294	750411	21 6	5.52	34- 3.14	118-59.81	9.58	3.11	22	47	2.5	0.18	0.6	0.6	B1	***
295	750412	637	5.91	34- 3.24	118-59.54	11.86	2.07	13	100	3.0	0.17	1.0	1.0	B1	***
296	750414	455	9.23	34- 2.01	119- 1.52	16.61	1.66	12	166	0.9	0.21	1.5	0.8	C1	***
297	750424	7 2	26.72	34- 2.94	118-59.48	1.88	2.02	8	133	2.7	0.11	1.2	0.9	B1	***
298	750425	0 1	25.78	34- 2.88	118-59.33	16.50	1.40	9	138	2.9	0.12	1.6	1.2	C1	***
299	750427	13 2	8.55	34- 5.43	119- 0.36	14.32	1.42	8	160	3.9	0.10	1.1	0.8	C1	***
300	750502	8 9	47.01	33-59.13	118-23.07	16.98	2.51	5	153	1.0	0.15	3.5	3.3	D1	***
301	750504	2016	31.42	33-57.17	118-25.34	9.54	2.06	8	108	5.8	0.10	1.0	1.8	B1	***
302	750504	2027	16.71	33-58.72	118-23.82	8.73	1.80	9	114	2.1	0.08	0.7	0.9	B1	***
303	750504	2045	5.99	34- 0.27	118-24.30	12.48	1.41	5	158	2.4	0.08	1.5	1.1	C1	***
304	750512	021	52.02	34- 3.51	118-27.35	8.00	4.83	12	185	5.3	1.12	7.5	12.9	D1	***
305	750517	814	8.33	33-57.32	118-21.38	21.20	2.22	10	112	4.9	0.19	1.8	2.4	B1	***
306	750526	312	16.67	34- 4.73	118-58.79	16.79	1.46	8	99	1.8	0.03	0.4	0.6	B1	***
307	750528	1259	48.81	34- 2.13	118-59.63	12.52	2.08	14	107	2.1	0.14	0.9	0.7	B1	***
308	750601	053	23.28	34- 2.85	118-16.98	3.83	1.41	6	118	3.3	0.08	0.8	2.4	B1	***
309	750608	22 3	22.11	33-59.74	118-23.07	8.00	1.83	5	192	0.2	0.24	13.3	16.7	D1	***
310	750609	16 5	11.80	34- 2.30	119- 1.86	13.32	1.47	10	165	1.3	0.17	1.6	1.8	C1	***
311	750610	1143	14.56	34- 0.93	118-45.05	8.66	2.14	11	123	5.3	0.14	1.0	1.1	B1	***
312	750621	20 3	41.85	34- 1.61	119- 1.10	4.63	1.86	10	212	1.1	0.21	2.0	2.1	C1	***
313	750706	219	40.82	34- 3.74	118-53.11	9.86	2.25	8	162	17.3	0.16	1.9	1.8	C1	***
314	750707	1159	8.24	33-58.46	118-25.80	9.72	2.76	11	99	4.9	0.12	0.8	0.5	B1	***
315	750712	2216	22.47	34- 4.60	118-58.53	10.93	1.43	9	132	5.8	0.16	1.3	1.6	B1	***

NO	YRMODY	HRMIN	SEC	LAT	LONG	DEPTH	MAG	NC	GAP	DMIN	RMS	ERH	ERZ	Q	
316	750713	039	42.24	34- 4.38	118-58.14	11.33	1.55	10	111	6.0	0.18	1.4	2.5	B1	***
317	750721	241	24.32	33-49.98	118-17.64	1.30	1.43	7	142	9.4	0.16	1.2	244.0	C1	***
318	750722	618	17.76	33-57.67	118-32.24	8.00	2.25	5	267	14.7	0.19	13.5	23.7	D1	***
319	750722	1224	33.68	33-59.88	118-24.54	9.96	2.08	16	142	2.5	0.31	1.6	1.3	C1	***
320	750724	7 2	11.02	33-54.25	118-43.70	8.00	1.13	13	154	13.2	0.10	0.9	1.1	B1	***
321	750724	7 8	24.17	33-52.26	118-42.67	0.62	1.04	20	132	17.2	0.15	0.5	11.2	C1	***
322	750804	716	15.20	34- 1.36	118-23.61	10.53	2.48	9	130	3.3	0.07	0.6	0.7	B1	***
323	750902	7 8	37.96	34- 2.80	118-58.36	6.93	1.37	9	148	4.2	0.11	1.1	1.9	C1	***
324	750903	129	48.08	33-59.74	118-22.21	13.70	2.16	4	241	1.2	0.09			C1	***
325	750925	1136	16.73	33-56.12	118-55.54	13.00	1.54	9	267	13.4	0.12	1.4	3.0	C1	***
326	750926	6 6	34.70	34- 2.80	119- 1.10	8.00	1.33	8	157	1.1	0.08	0.8	1.1	B1	***
327	750927	1247	33.72	33-59.76	118-31.63	9.99	2.38	16	100	11.7	0.13	0.8	1.2	B1	***
328	751002	2236	40.72	34-12.89	119- 6.00	8.19	1.30	10	135	7.6	0.14	1.0	2.0	B1	***
329	751003	859	17.11	34-11.71	119- 7.48	5.18	2.15	12	95	10.7	0.16	0.9	4.8	C1	***
330	751005	1510	10.52	34- 2.49	118-57.11	13.42	1.98	13	158	5.4	0.16	1.3	1.0	C1	***
331	751006	1238	34.50	34- 0.15	118-21.45	8.66	2.99	9	205	14.6	0.10	1.1	0.8	C1	***
332	751006	1255	38.30	33-51.11	118-27.13	9.96	3.01	17	162	17.9	0.14	0.8	0.7	B1	***
333	751007	2323	26.69	33-52.55	118-29.03	3.90	2.69	15	112	16.1	0.21	1.2	2.4	C1	***
334	751011	1655	0.59	34- 6.72	118- 4.86	0.96	3.22	26	53	9.3	0.21	0.6	11.2	C1	***
335	751024	1420	40.85	33-48.33	118-50.75	8.00	1.82	10	196	22.3	0.16	2.1	2.4	C1	***
336	751027	2 7	15.92	33-58.21	118-21.09	13.13	3.19	5	253	3.9	0.10	5.1	5.7	D1	***
337	751103	342	17.69	33-51.42	118-34.42	1.83	2.32	13	139	23.3	0.17	0.9	147.3	C1	***
338	751125	236	57.35	33-56.91	118-20.56	10.51	2.01	5	271	6.3	0.09	4.7	3.8	D1	***
339	751203	110	26.35	33-54.81	118- 4.66	8.00	2.24	9	77	10.8	0.14	0.9	3.0	B1	***
340	751225	1435	19.32	33-59.48	119- 6.59	8.00	2.92	16	136	28.1	0.20	1.4	2.0	C1	***
341	751225	1441	23.54	34- 1.09	119- 4.48	9.93	2.08	11	190	10.2	0.15	1.4	1.4	C1	***
342	751229	1035	23.10	34- 1.95	119- 6.23	1.80	2.40	7	167	25.5	0.26	2.6	400.9	C1	***
343	760111	1118	18.58	34- 7.02	118-32.47	13.42	2.19	8	170	8.1	0.09	0.9	0.9	B1	***
344	760117	1254	50.62	34- 5.24	118-56.43	10.55	2.40	5	136	11.7	0.12	1.8	2.1	C1	***
345	760121	355	30.72	33-49.62	118-46.09	8.00	2.37	8	175	20.0	0.16	1.4	3.3	C1	***
346	760203	340	17.21	34- 5.72	118-18.17	1.93	2.36	9	80	13.5	0.22	1.2	278.5	C1	***
347	760204	1943	56.26	33-59.80	118-21.18	8.00	2.29	8	104	15.3	0.11	1.0	4.1	B1	***
348	760206	1844	56.33	34- 2.29	118-21.51	1.53	1.97	4	158	5.4	0.02			C1	***
349	760207	2018	12.48	33-59.06	118-20.36	10.18	2.14	6	133	4.2	0.15	2.0	2.6	B1	***
350	760210	254	2.76	34-10.91	118- 3.03	13.48	2.33	9	92	4.7	0.13	0.9	0.8	B1	***
351	760212	2212	8.42	33-59.78	118-51.55	9.82	2.67	12	138	11.8	0.20	1.8	1.2	C1	***
352	760222	1425	41.91	33-51.21	118-56.00	8.00	2.55	7	248	41.3	0.63	18.6	8.9	D1	***
353	760222	1426	27.81	33-50.40	118-50.09	3.72	3.22	20	142	35.9	0.15	0.9	1.2	C1	***
354	760319	9 7	48.34	33-51.78	118-38.18	6.70	3.42	28	75	25.5	0.23	0.9	0.9	C1	***
355	760409	739	53.60	33-53.34	118-37.73	0.28	1.86	5	157	29.0	0.02	0.3	43.4	D1	***
356	760413	1333	5.63	33-50.47	118-23.36	6.56	2.58	21	106	17.0	0.16	0.6	1.2	C1	***
357	760426	22 4	12.71	34-10.30	118-21.17	10.02	2.13	4	253	6.1	0.02			C1	***
358	760504	955	29.71	34- 6.22	119- 1.53	13.43	3.07	21	72	3.6	0.23	1.0	0.6	B1	***
359	760520	232	40.48	34- 5.01	119- 1.40	11.00	2.13	6	194	4.7	0.05	1.0	1.2	C1	***
360	760603	5 4	24.75	34- 6.71	118-13.64	11.73	1.72	8	142	6.5	0.31	3.8	4.4	C1	***

NO	YRMODY	HRMIN	SEC	LAT	LONG	DEPTH	MAG	NO	GAP	DMIN	RMS	ERH	ERZ	Q		
361	760609	1610	24.58	34- 2.39	118-59.18	8.36	2.99	20	66	10.5	0.17	0.7	0.7	B1	***	
362	760610	1619	28.90	33-52.45	118-43.26	4.09	2.17	5	263	34.9	0.34	7.7	126.3	D1	***	
363	760616	557	58.13	34- 4.28	118-57.97	10.81	2.15	5	178	8.7	0.07	1.7	2.6	C1	***	
364	760619	824	59.62	34- 2.78	119- 4.27	1.36	2.20	5	257	18.7	0.06	2.6	128.4	D1	***	
365	760620	051	28.91	33-59.88	118-49.07	8.00	3.81	26	68	35.6	0.23	0.8	0.8	C1	***	
366	760621	051	32.47	34- 2.77	118-36.38	8.00	2.78	8	240	5.1	0.13	5.0	7.9	D1	***	
367	760627	2211	36.17	34- 3.01	118-18.09	9.29	3.37	34	33	3.8	0.17	0.4	0.5	B1	***	
368	760715	327	39.54	33-51.94	118- 8.24	8.00	3.19	22	90	5.9	0.19	0.6	1.2	B1	***	
369	760716	327	39.61	33-51.68	118- 9.24	11.91	2.35	9	74	4.4	0.08	0.5	0.9	A1	***	
370	760722	14 8	15.40	33-55.29	118-16.50	8.89	2.18	5	250	25.5	0.04	1.3	1.3	C1	***	
371	760722	1141	31.59	33-56.52	118-15.90	1.87	2.90	20	84	13.3	0.74	1.2	36.5	D1	***	TIME
372	760723	2053	55.41	33-51.77	118-10.47	12.61	3.56	28	73	3.2	0.14	0.4	0.4	A1	***	
373	760727	9 0	50.92	33-55.03	118-31.61	8.00	2.33	14	122	15.8	0.16	1.1	1.5	B1	***	
374	760728	323	36.87	34- 8.68	119-10.46	14.98	2.92	19	103	10.9	0.17	0.8	0.5	B1	***	
375	760801	11 8	40.61	34- 3.23	118-59.75	8.87	1.93	10	172	8.8	0.21	1.6	1.1	C1	***	
376	760803	1622	35.35	34- 4.01	118-20.18	2.29	2.41	5	165	6.9	0.32	5.0	709.6	D1	***	
377	760806	1742	59.14	34- 6.71	118-35.30	8.14	2.36	4	269	2.6	0.02			C1	***	
378	760818	1718	57.60	34- 0.47	118-22.19	8.00	1.89	6	119	1.8	0.07	1.2	1.8	B1	***	
379	760822	953	47.24	33-54.98	118-32.87	8.00	1.93	5	290	18.7	0.35	39.1	74.2	D1	***	
380	760824	1043	52.99	33-55.90	118-17.17	16.74	2.62	31	98	6.2	0.16	0.5	0.8	B1	***	
381	760825	2311	23.96	33-54.03	118-53.50	6.65	2.50	13	185	13.9	0.21	1.3	1.3	C1	***	
382	760901	2210	44.21	34- 6.67	119- 3.95	12.17	1.86	4	216	0.2	0.66			D1	***	
383	760902	256	46.94	33-55.79	118-18.84	4.67	2.31	9	287	23.5	0.16	4.3	13.9	D1	***	
384	760903	1516	51.16	33-52.26	118-40.79	8.00	2.29	9	153	18.8	0.10	0.7	2.1	C1	***	
385	760906	1022	50.49	34-12.22	118-51.09	16.94	1.99	4	200	11.6	0.00			C1	***	
386	760910	713	43.81	33-59.79	118-54.98	10.75	2.40	11	227	10.2	0.13	1.5	1.0	C1	***	
387	760914	19 9	35.52	34- 8.74	118-57.96	6.82	2.34	11	128	9.4	0.16	1.1	1.7	B1	***	
388	760915	436	30.74	34-11.55	118- 1.02	12.46	2.28	5	289	13.9	0.09	5.4	1.7	D1	***	
389	760915	1949	52.33	34-10.62	119- 0.88	8.15	1.96	4	137	8.8	0.10			C1	***	
390	760915	2313	20.73	33-51.31	118- 9.46	10.91	2.88	11	117	3.7	0.12	1.3	1.1	B1	***	
391	760916	2154	5.46	34- 6.19	118-19.25	2.40	1.94	4	186	3.1	0.13			C1	***	
392	760924	14 2	15.98	34- 0.80	118-14.86	11.22	2.51	15	80	3.7	0.11	0.6	0.6	A1	***	
393	760924	2222	22.19	34-10.65	119- 2.46	16.77	2.15	5	169	7.8	0.12	5.1	6.5	D1	***	
394	760926	556	50.94	34- 3.06	119- 0.74	15.60	1.79	4	218	8.1	0.00			C1	***	
395	760928	1816	2.29	34- 9.71	119- 2.43	8.00	2.09	4	250	10.3	0.01			C1	***	
396	760929	7 0	51.09	34- 6.00	118-18.18	11.81	2.17	19	91	3.3	0.12	0.6	0.5	B1	***	
397	761005	2224	15.48	34- 1.15	118-25.37	8.00	1.99	5	170	3.5	0.20	5.1	8.6	D1	***	
398	761011	711	50.39	34- 1.28	118-10.29	13.85	2.16	7	96	14.1	0.10	1.0	0.9	B1	***	
399	761013	112	25.87	33-59.82	118-21.09	6.71	1.68	5	249	2.9	0.14	6.8	6.1	D1	***	
400	761014	12 1	17.01	33-58.50	118-24.80	9.20	1.78	4	279	5.4	0.00			C1	***	
401	761018	551	15.25	33-56.32	118-31.96	3.81	2.26	13	118	16.2	0.23	1.3	28.2	C1	***	
402	761018	811	6.16	33-49.29	118-30.13	2.95	2.10	4	318	24.3	0.07			C1	***	
403	761019	5 4	16.90	33-60.00	118-20.38	6.54	2.00	6	193	4.0	0.16	3.4	3.9	D1	***	
404	761103	1054	2.79	33-52.56	118-14.00	2.63	2.57	5	186	54.4	0.09	1.7	209.7	D1	***	
405	761107	1010	49.74	33-52.44	118- 9.96	2.02	2.11	9	89	4.6	0.10	0.8	136.5	B1	***	

NO	YRMODY	HRMIN	SEC	LAT	LONG	DEPTH	MAG	NC	GAP	DMIN	RMS	ERH	ERZ	Q	
406	761115	12 8	3.77	33-56.49	118-20.75	15.95	2.92	35	94	6.8	0.14	0.5	0.3	BI	***
407	761121	0 9	46.17	33-59.79	119- 9.98	9.02	2.76	19	137	15.7	0.12	0.7	0.6	BI	***
408	761121	1939	44.91	34- 0.11	119-10.11	0.04	2.43	19	185	15.3	0.20	1.4	6.8	DI	***
409	761122	1753	10.96	33-58.59	118-38.42	16.87	4.09	12	221	13.4	0.15	3.0	3.7	DI	***
410	761122	1755	11.05	33-56.24	118-37.54	8.00	4.24	37	51	18.3	0.17	0.5	0.5	CI	***
411	761122	18 6	12.94	33-56.95	118-38.17	14.91	2.33	9	213	16.2	0.08	1.1	1.8	CI	***
412	761122	1932	36.49	33-57.44	118-37.98	8.00	3.20	35	97	15.2	0.19	0.5	0.6	BI	***
413	761125	1533	14.61	33-53.47	118-11.27	13.11	2.52	21	91	5.8	0.15	0.6	0.6	BI	***
414	761128	18 1	30.60	33-58.43	118-36.39	8.00	1.67	4	284	12.9	0.06			CI	***
415	761129	040	1.81	33-56.05	118-30.08	10.45	2.85	27	103	12.8	0.14	0.7	0.5	BI	***
416	761130	2155	18.87	34- 6.04	118-17.72	9.38	2.78	23	53	3.5	0.14	0.5	0.5	AI	***
417	761207	730	2.85	33-56.82	118-41.11	5.30	2.87	20	141	12.9	0.15	0.6	0.9	CI	***
418	761211	1145	30.57	33-56.15	118-41.78	8.00	2.63	28	75	12.7	0.20	0.8	0.8	BI	***
419	761211	1150	40.01	33-55.30	118-42.15	8.00	3.15	29	77	13.2	0.16	0.6	0.6	BI	***
420	761212	2214	20.39	33-56.57	118-42.27	10.06	2.62	23	75	11.6	0.17	0.7	0.8	BI	***
421	761213	1838	23.37	34- 2.12	118-59.52	12.78	3.08	23	67	10.6	0.08	0.4	0.2	AI	***
422	761213	1843	41.79	34- 2.20	118-59.43	12.98	3.00	22	67	10.6	0.09	0.4	0.3	AI	***
423	761223	349	28.84	33-55.85	118-42.99	9.96	2.66	14	148	11.6	0.10	0.6	0.7	BI	***

APPENDIX E: Epicenter, magnitude, and focal depth plots for the study area.

Note: Scale is 1:250,000. Plotting symbols are described in Figures 13, 14, and 15.

81-295


MAGNITUDE PLOT
1973 - 1976
34°15'
34°00'
119°00'
118°30'
N
0 5
km
0 5
miles

81-295


EPICENTER PLOT
1973 - 1976
34°15'
34°00'
119°00'
118°30'
N
0 5
km
0 5
miles
P. 172


1973 - 1976 A AND B
QUALITY LOCATIONS
34°15'
34°00'
119°00'
118°30'
N
0 5
km
0 5
miles
P. 175

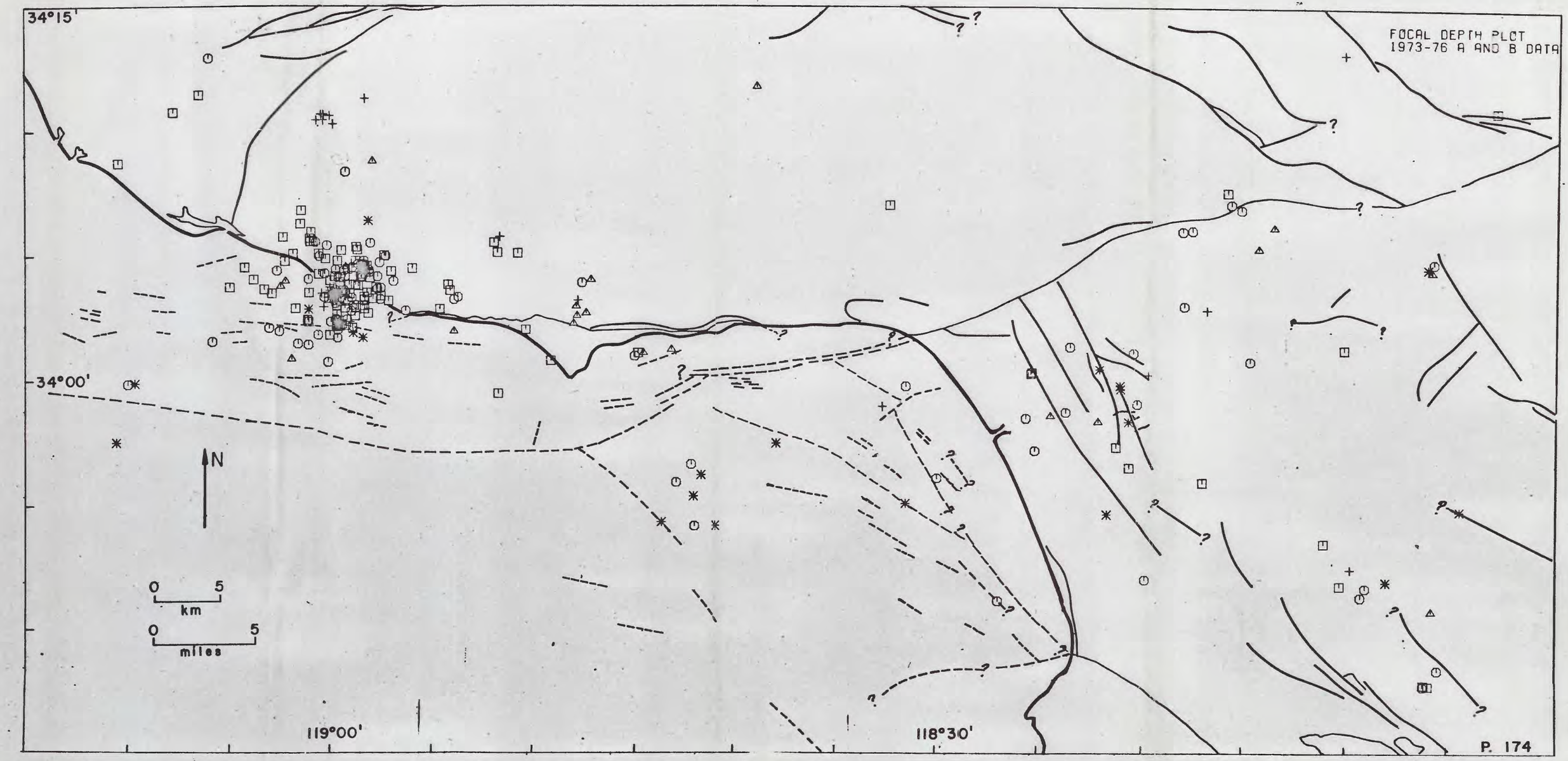
FOCAL DEPTH PLOT
1973-76 A AND B DATA
34°15'
34°00'
119°00'
118°30'
N
0 5
km
0 5
miles
P. 174

APPENDIX F: Epicenter, magnitude, and focal depth plots for Point Mugu area.

Note: Scale is 1:83,333. Plotting symbols described in Figures 13, 14, and 15.

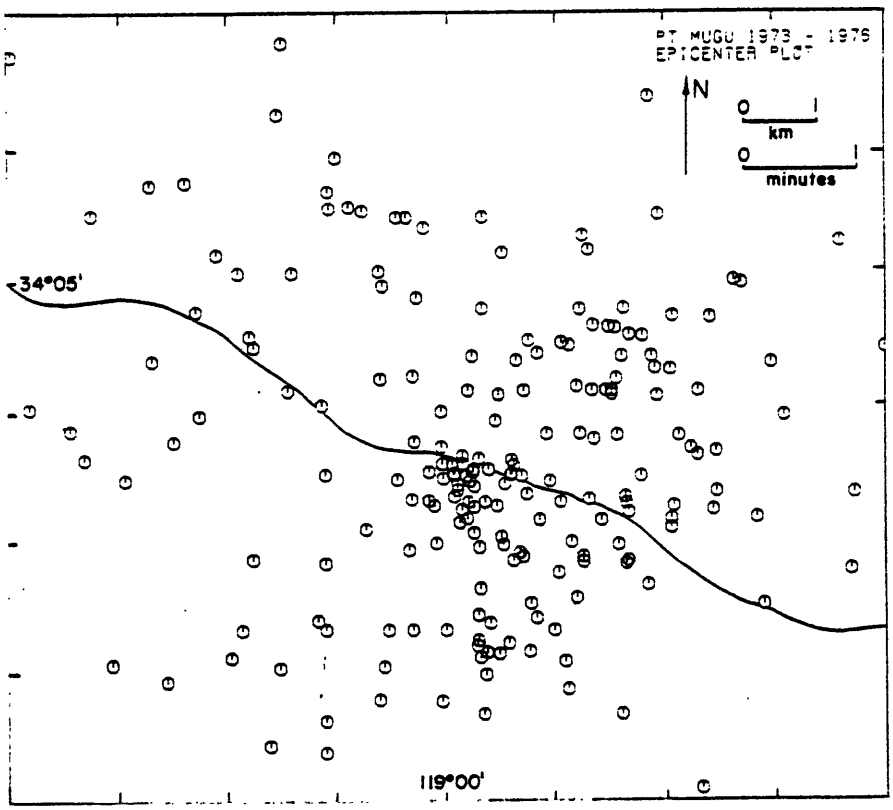
PT MUGU 1973 - 1979
EPICENTER PLOT
N
0 1
km
0 1
minutes
34°05'
119°00'

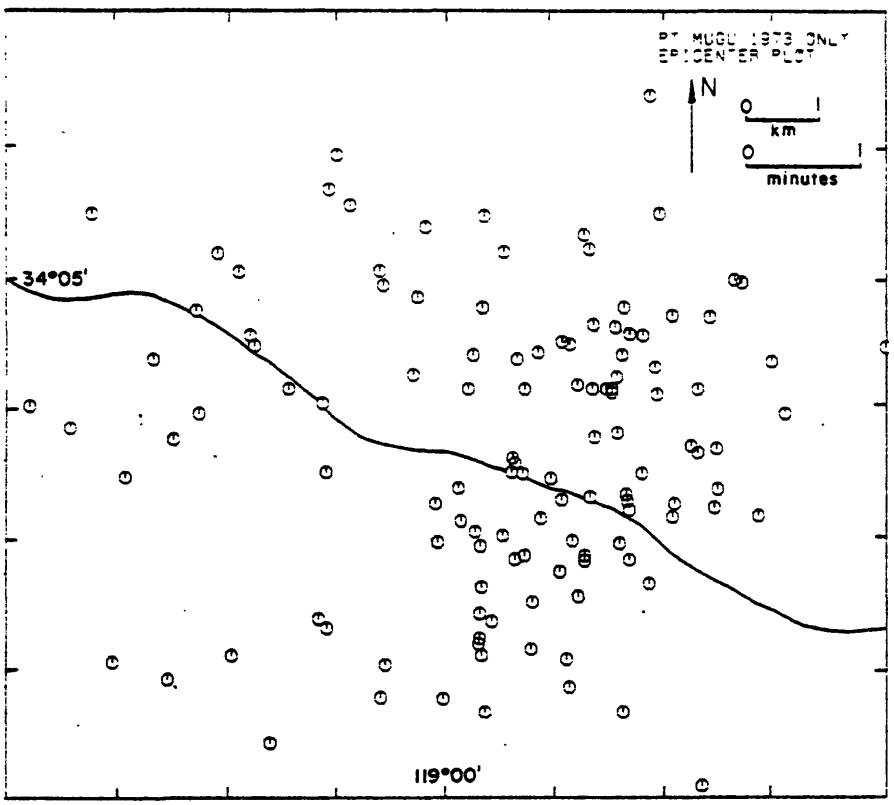
N
0 1
km
0 1
minutes
34°05'
119°00'

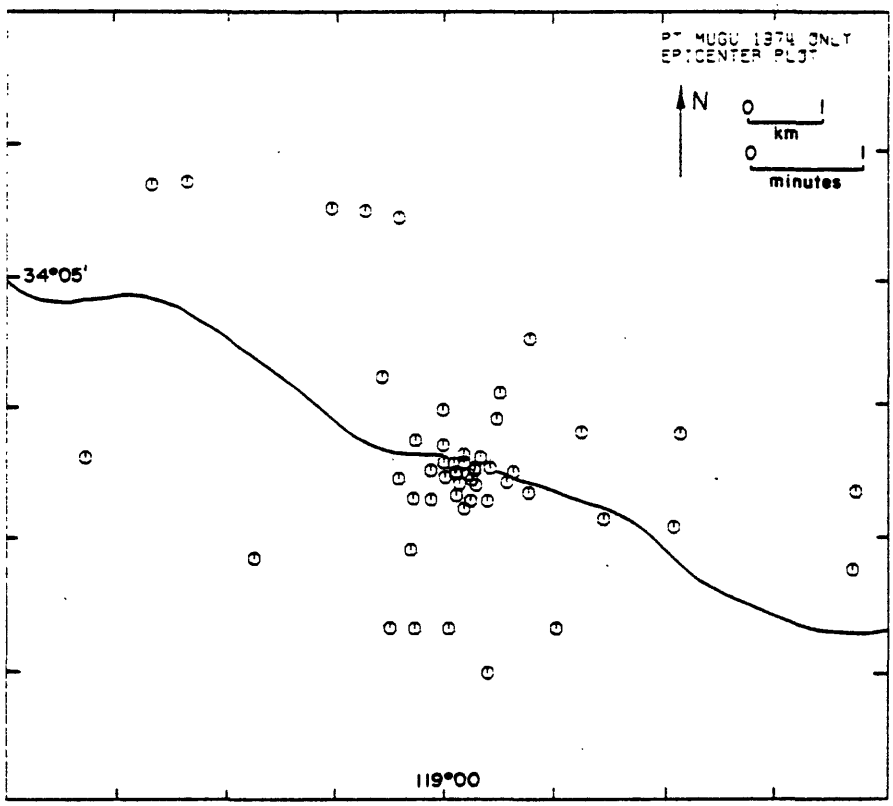
PT MUGU 1974 ONLY
EPICENTER PLOT
N
0 1
km
0 1
minutes
34°05'
119°00

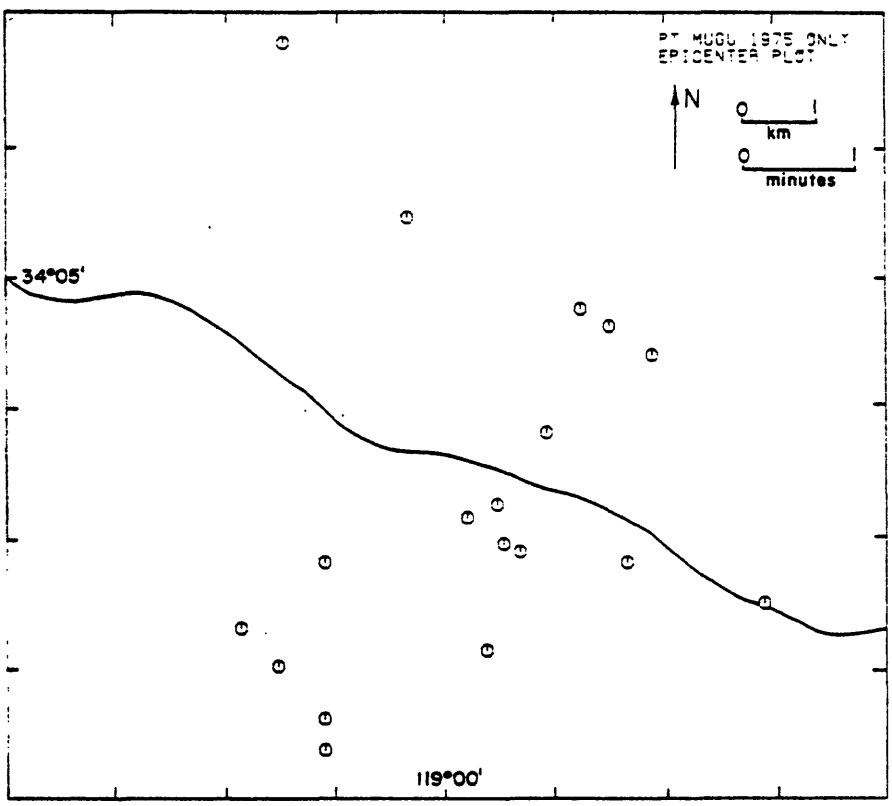
PT MUGU 1975 ONLY
EPICENTER PLOT
N
0 1
km
0 1
minutes
34°05'
119°00'

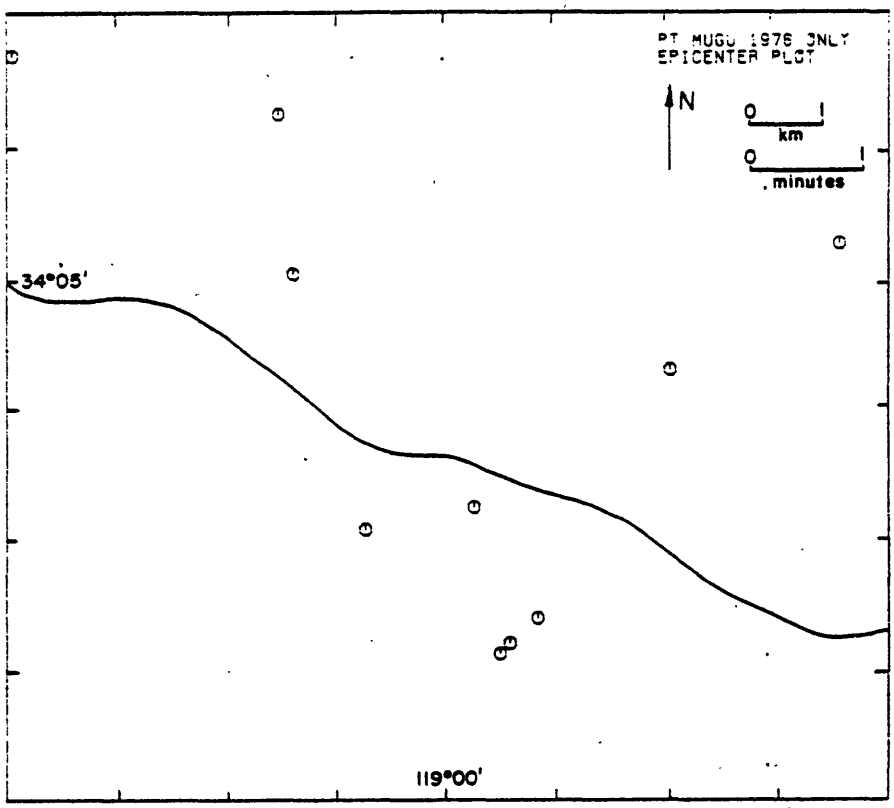
PT MUGU 1976 ONLY
EPICENTER PLOT
N
0 1
km
0 1
minutes
34°05'
119°00'

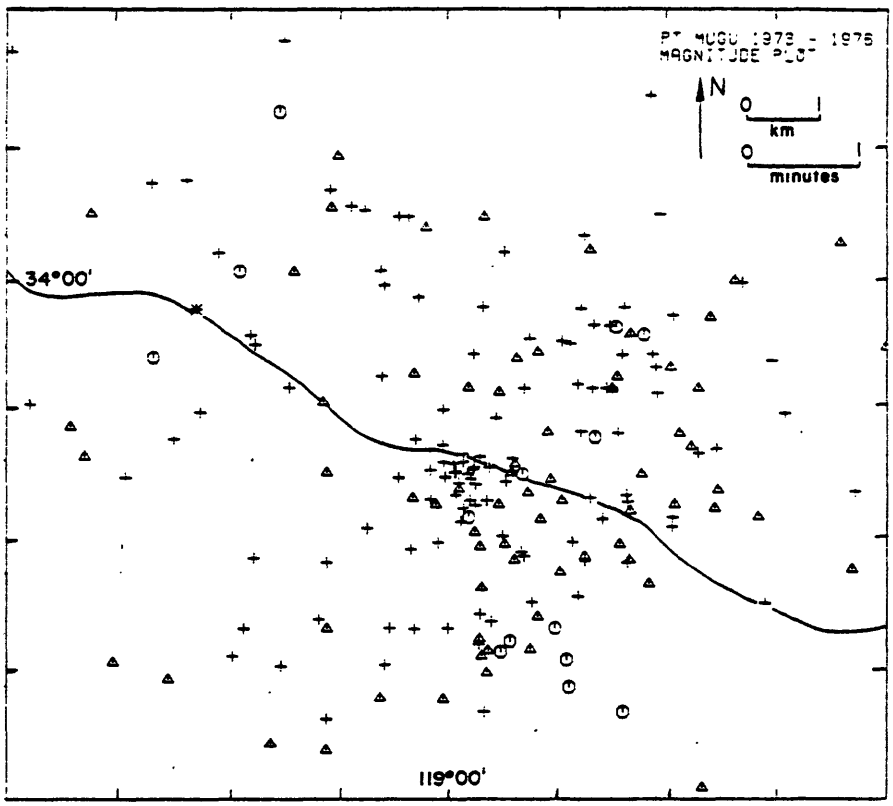
PT MUGU 1973 - 1976
MAGNITUDE PLOT
N
0
km
0
minutes
34°00'
119°00'

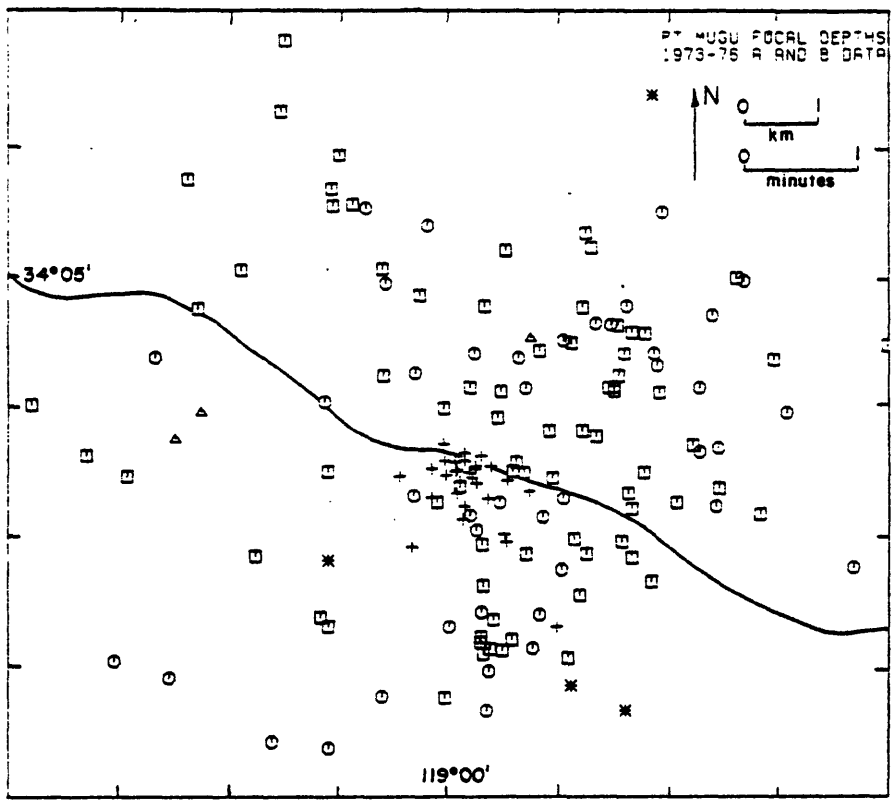
PT MUGU FOCAL DEPTHS
1973-75 A AND B DATA
N
km
minutes
34°05'
119°00'

APPENDIX G: Problems limiting the precision of a fault-plane solution

Three possible problems are capable of limiting the precision of a fault-plane solution. The first is the interpretation of the P-wave signal, which is often ill-defined at its onset in terms of both origin time and polarity. Presently, the USGS, CIT, and USC all use one seismogram-record reader to reduce these inconsistencies, although various readers have been employed since 1973. Scheduled quarry blasts set off at Corona, Jensen, and Eagle Mountain in the Mojave Desert, located east of approximately $118^{\circ}20'$W longitude, send a compressional blast wavefront throughout southern California which is regularly recorded at seismic stations. These blasts served as checks on station polarities.

Second, ambiguity exists in the selection of either one of the two orthogonal nodal planes as the proper fault plane for any particular earthquake--the alternative nodal plane becomes the auxiliary fault plane. S-wave data does not help to distinguish between the two possible fault planes in the case of a double-couple source mechanism since the shear-wave radiation pattern is also composed of four symmetrical lobes. Structural lineaments and seismicity trends paralleling a nodal plane are criteria often used to distinguish between the fault plane and the auxiliary fault plane.

The final problem is the sensitivity of the fault-plane solution to the crustal velocity model. In order

to establish the variance in the fault-plane solution as a function of the crustal velocity model, the first-motion plots and corresponding fault-plane solutions for five well-located earthquakes have been compared with respect to the six crustal velocity models suggested above for southern California. For each of these earthquakes, located in the central Los Angeles basin, a P-wave first-motion plot has been produced using the six different crustal velocity models. The poles to each fault plane have been plotted in this Appendix. The variation in the orientation of the fault planes due to a changing crustal velocity model is tabulated in Table 8. The change in strike and dip for a fault plane, as a function of the crustal velocity models considered, is 36.5^{o} and 27.0^{o}, respectively. Thus, the velocity data is a limiting factor in the precision of the fault-plane solutions.

Variation in fault-plane orientation versus crustal velocity model. Poles to each possible fault plane are plotted for the six crustal velocity models discussed in the text.

U = USGS/Healy model
L = Los Angeles basin model
M - Pt. Mugu model
K = Kanamori and Hadley (Mojave Desert) model
T = Transverse Ranges model

See Table 8.

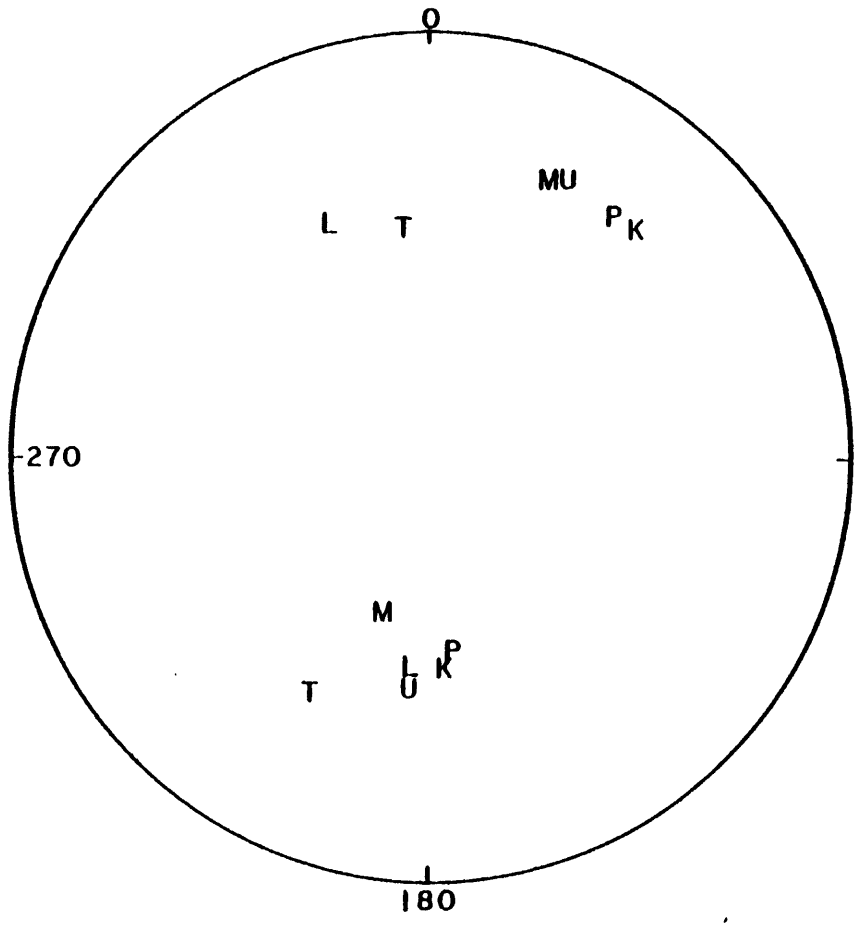

event
740227

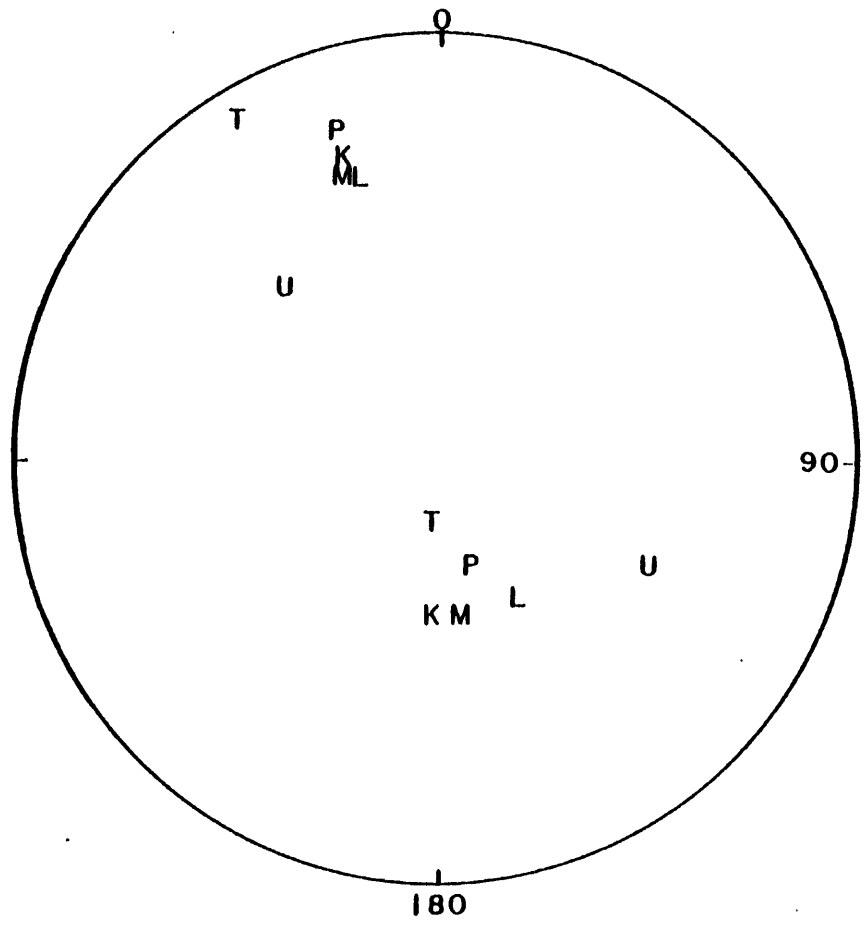

event
740306

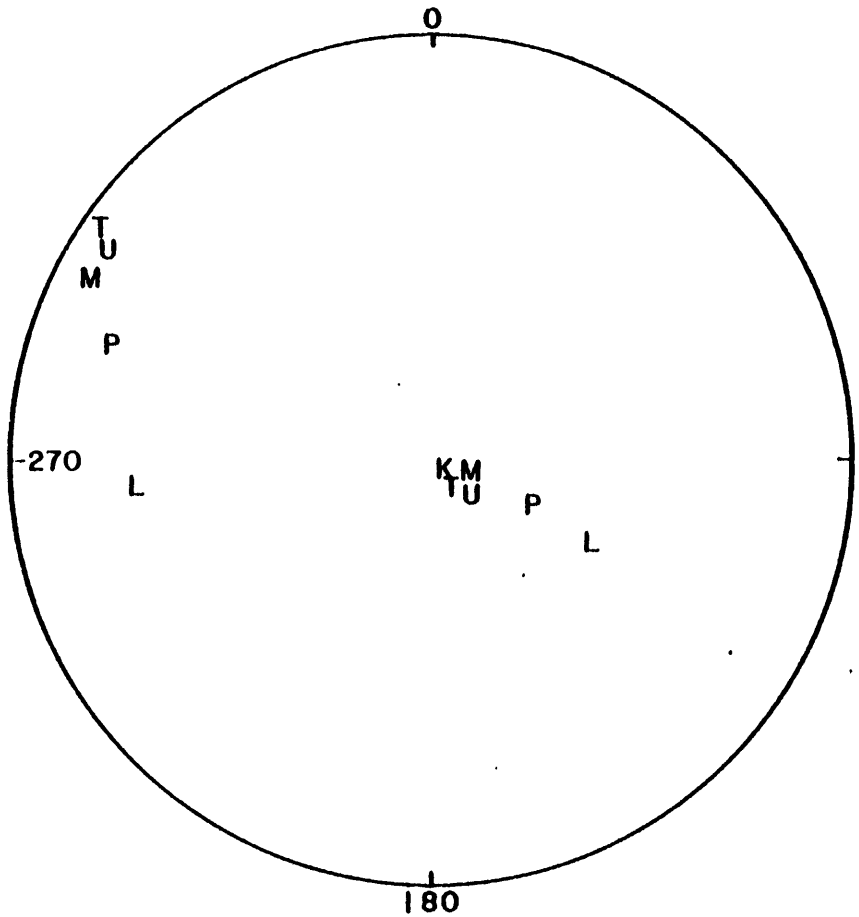

event
740312

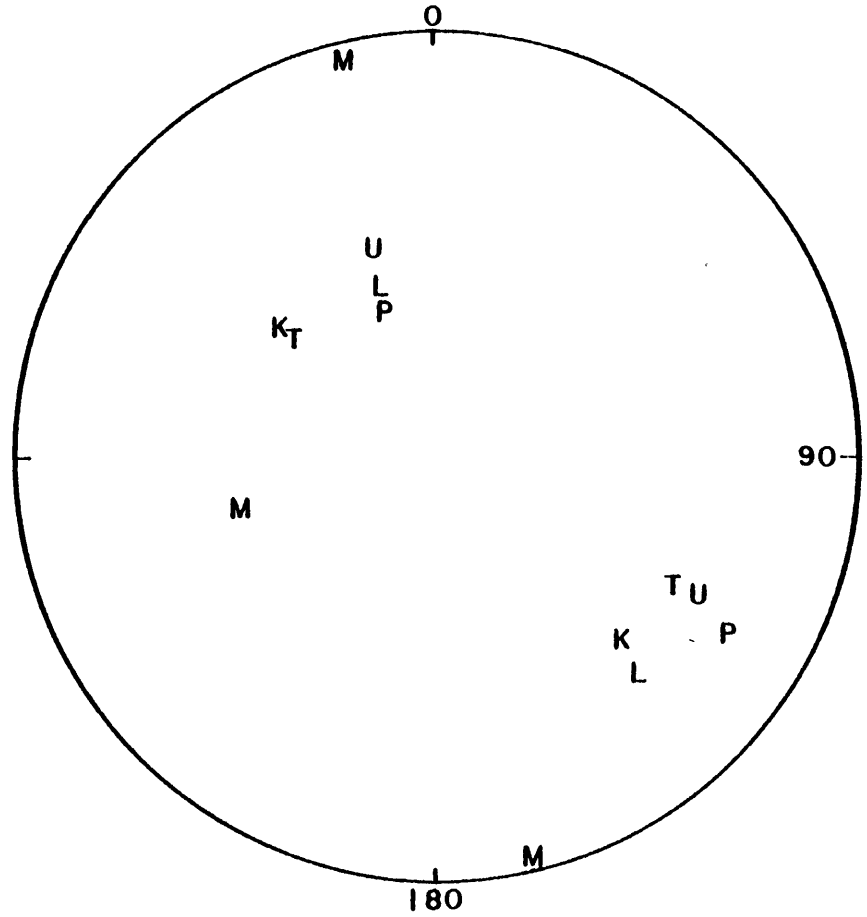

event
741106

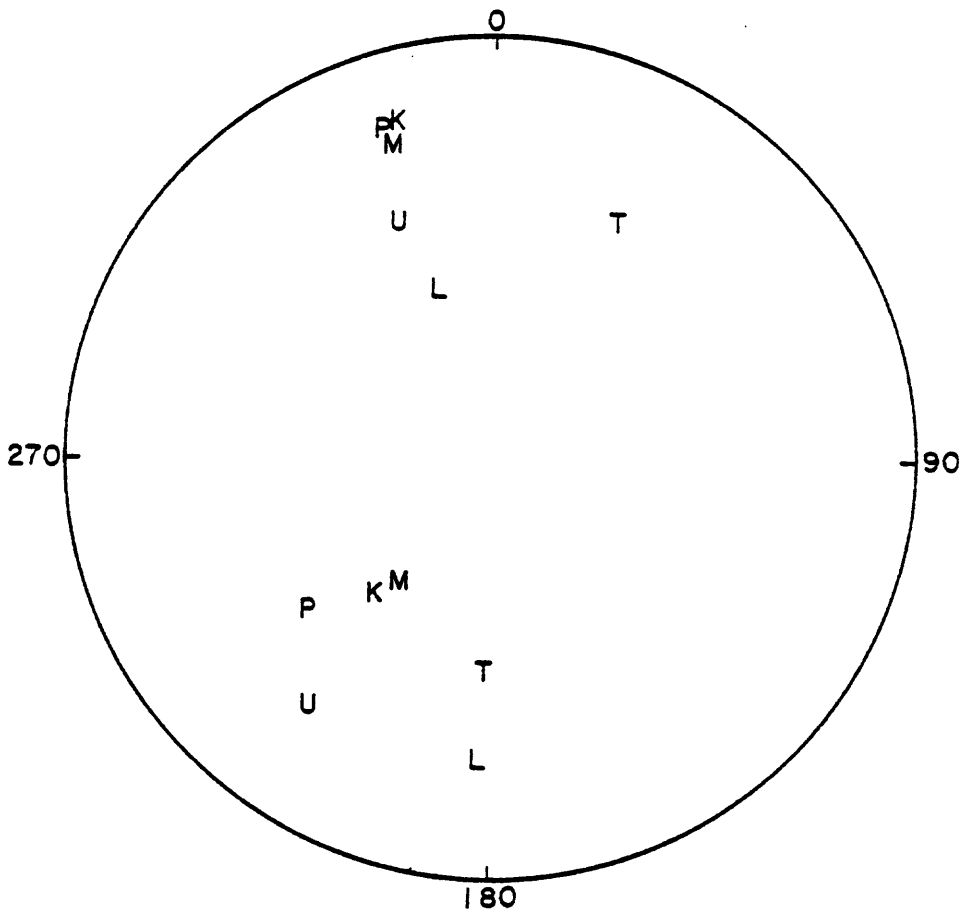

event
741219

TABLE 8

Maximum variation between the strike and dip of possible fault planes due to changes in crustal velocity models

Event	Strike (°)	Dip (°)	Quality of Earthquake Location
740277	69	14	B
	34	30	
740306	14	38	A
	30	20	
740311	10	34	A
	42	30	
741106	23	16	B
	40	16	
741219	53	40	B
	50	32	

Standard deviation in strike = 36.5°; in dip = 27.0°